PLASMA ENHANCED CHEMICAL VAPOR DEPOSITION COATING AMORPHOUS SILICA BASED IMPLANTS ENHANCING ANGIOGENESIS AND MITIGATING TOXIC OXIDATIVE STRESS IN CRITICAL SIZE BONE DEFECTS

By

FELIPE ALVES DO MONTE

DISSERTATION

Submitted in partial fulfillment of the requirements
for the degree of Doctor of Philosophy at
The University of Texas at Arlington
December, 2017
Arlington, Texas

Supervising Committee:

Dr. Pranesh B. Aswath, Supervising Professor and Committee Chair
Dr. Harry K W Kim
Dr. Kytai Nguyen
Dr. Christopher Chen

ACKNOWLEDGMENTS

Initially, I would like to equally thank Dr. Pranesh Aswath, Dr. Harry Kim and Dr. Venu Varanasi for their advising and time spent with me and my research projects. I also would like thank Dr. Kytai Nguyen for advising me since the first semester of my PhD course, giving me orientation about the courses and track that I should follow.

I would like to thank all professors from the Biomedical Engineering and Material Science and Engineering Departments at the University of Texas at Arlington, especially Dr. Limping Tang, Dr. Christopher Chen, Dr. Michael Cho, Dr. George Alexandrakis, Dr Young-tae Kim, Dr. Chi-Chum Tsai and Dr. Yi Hong.

I am grateful to have had excellent friends during my PhD course journey, whom I could establish a truthful and strong bond. I would like to thank all my partners from study groups and students that worked with me in multiple research projects. Thank you, Dr. Olumide Aruwajoye, Dr. Vinay Sharma, Kamal Awad, Dr. Vibhu Sharma, Ami Shah, Neelam Ahuja, Annabelle Yao, David Wang, Dr. Natascia Cozza, Dr. Megan Maginot, Dr. Azhar Ilyas, Taha Azimaie and Kimaya Vyavhare.

One of the great things that happened during my PhD building process was the opportunity to learn from people from different countries, cultures, research and academic institutions. I would like to especially thank Ila Oxendine, Amanda McLaren, Ruel Cornelia, Yang Lee, Richard Banlaygas, Melody Fletcher, Lisa Gardner, Dr. Suresh Adapala, Dr. Ryosuke Yamaguchi, Dr. Gen Kuroyanagi and Dr.Thomas Park from Texas Scotish Rite Hospital for Children.

I am thankful for having three great persons,Julie Rochow, Beth Robinson and Jennifer Standlee, who helped me handle all the logistics, school paper work and managing courses.

I would like to thank Dr. Chi Ma and Dr. Liu Xiaohua from Texas A & M College of Dentistry for research collaboration in other projects not presented on my PhD dissertation.

Although we only have had a few moments together, it was an honor to have met Dr Aswath's wife, Shobha Aswath and Dr Kim's wife, Dr Anna Kim and daughters, Audrey ans Sophia. Thank you for making our lives less difficult here, especially during the first years.

Thanks Dr. Marco Brotto and Dr. Leticia Brotto for the great support and open doors and future research opportunities.

Lastly, I would like to thank the most important, my family, starting with Fernanda Monte, my strong, patient and proactive wife, and Joana, my happy, genuine and unique daughter. I would like to thank my father, Dr. Antonio do Monte, one of the inspirations of my career and my supportive mother, Dr. Laudicea Monte. I am thankful to my father-in-law and mother-in-law, Josenildo Oliveira and Maria do Carmo Oliveira. Finally, I would like to thank my brother, Henrique Monte and his wife and daughter, Andrea Monte and Maria Antonio Monte. Also, I thank my brother-in-law, Ricardo Oliveira.

Thanks God for giving me this great opportune to improve my knowledge and contribute to development of my country and my community.

December 7, 2017

DEDICATION

This work is dedicated to the memory

of my father,

Dr. Antonio do Monte Filho

and

my father-in-law,

Mr. Josenildo Rodrigues de Oliveira

ABSTRACT

PLASMA ENHANCED CHEMICAL VAPOR DEPOSITION COATING AMORPHOUS SILICA BASED IMPLANTS ENHANCING ANGIOGENESIS AND MITIGATING TOXIC OXIDATIVE STRESS IN CRITICAL SIZE BONE DEFECTS

Felipe Alves do Monte, PhD

University of Texas at Arlington, 2017

Supervising Professor: Pranesh B. Aswath

The advances in bone tissue engineering search for a biomaterial that could efficiently and gradually replace the bone while the new tissue grows through the implanted structure. However, due to limitations mainly related to mechanical properties and challenges, such as the balance between tissue regeneration and material degradation, the coating of well-known inert materials still has been used in orthopedics and dental clinical practices. Bone defects are commonly related to deleterious oxidative stress induced by low oxygen levels and inflammation. Toxic oxidative stress can impair damaged tissue healing due to inhibiting new blood vessels and new bone formation. The interaction between this hostile environment and implanted materials have been neglected, and the use of materials that can reduce oxidative stress to a physiological levels could enhance new tissue formation, reducing healing time and preventing material's loosening and failure. Based on findings from our group's previous study, we identified that ionic silicon plays a significant role on reduction of reactive oxygen species by upregulating superoxidase dismutase1 (SOD1), which is an important antioxidant enzyme. Another study demonstrated that mesoporous silica could enhance angiogenesis by upregulating hypoxic inducible

growth factor (HIF-1α). For present research, we hypothesized that implants coated with amorphous silica by plasma enhanced chemical vapor deposition (PECVD) method could enhance endothelial cells angiogenesis under toxic oxidative stress condition. Moreover, we tested the hypothesis that the PECVD coating implants could enhance angiogenesis and reduce oxidative stress in an adult rat's critical size calvarial defects. In order to test our hypothesis, we investigated (*in vitro*), and under normal condition, the effect of the ionic silicon and/or the amorphous silica PECVD coating materials on the endothelial cells viability, proliferation, migration, capillary tubule formation, matrix deposition, angiogenic markers and antioxidant enzymes. An *In vivo* experiment was also conducted in a rat's critical size calvarial defect. And angiogenic and oxidative markers were measured in histological sections and serum. Firstly, we demonstrated that ionic silicon can recover the HUVECs' viability under toxic oxidative stress conditions by reducing cell death and upregulating HIF-1α, VEGFA, and vascular endothelial growth factor receptor 2 (VEGFR-2). Secondly, we showed that PECVD coating amorphous silica based implants incorporated with nitrogen and phosphorus enhanced endothelial cells angiogenesis, increasing matrix deposition, cell migration, capillary tube formation, and gene expression of angiogenic markers and antioxidant enzymes. Third, we verified angiogenesis improvement on HUVECs under oxidative stress by preventing cell death, enhancing matrix deposition and upregulating the expression of angiopoietin-1 and antioxidant enzymes. Lastly, *in vivo* experiment corroborated with these findings and demonstrated enhancement in angiogenesis and reduction of oxidative stress. In conclusion, our findings support the use of PECVD coating amorphous silica-based implants applied in large bone defects due to its antioxidant and proangiogenic effect.

TABLE OF CONTENTS

LIST OF ILLUSTRATIONS

Chapter 2

Chapter 3

Chapter 4

Chapter 5

LIST OF TABLES

Chapter 3

Chapter 4

Chapter 5

CHAPTER 1

GENERAL INTRODUCTION

1.1 Introduction

Large and complex bone defects are injuries usually correlated with high energy trauma and can lead to functional and cosmetic disability associated with bone loss, poor vascularization and neural damage. Despite the advances in bone tissue engineering, the implants used on reconstruction of these injuries are still associated with complications such as loosening and failure results from foreign bone response and lack of osteointegration. Therefore, there is a necessity to engineer a device with improved biocompatibility that can enhance new blood vessels and bone formation, and accordingly improve osteointegration. Large bone defects are associated with relevant soft tissue and vascular injury, followed by consequent oxygen deprivation. The hypoxic environment tends to form overwhelmed levels of reactive oxygen species and reduce endothelial cells and osteoblast activity. The biomaterials used on a hypoxic environment are not designed to stimulate healing despite the unfavorable conditions, and therefore lead to extended healing times and poor outcomes. It is a relevant approach to synthesize biomaterials that can enrich angiogenesis and osteogenesis in hypoxic environment. Recently, our group has been studying a plasma enhanced chemical vapor deposition (PECVD) based amorphous silica materials. The results showed that surface coating with SiON composition increased mineralization and osteoblast activity. Moreover, these studies demonstrated that the presence of ionic silicon can enhances superoxidase dismutase-1, an important antioxidant enzyme. New blood vessel formation is a crucial event in the early stage

of the bone healing which will bring cells, growth factors and remove the toxins and the dead tissue. Ionic silicon released from microcarriers can upregulated hypoxia inducible factor (HIF-1α) and induces angiogenesis on human umbilcal vein endothelial cells (HUVECS). Phosphorus has been associated with upregulation of angiogenic markers. Thus, coating implants with amorphous silica incorporated with nitrogen and phosphorus could enhance new blood vessel formation and mitigate oxidative stress. These conditions can facilitate the osteointegration of implants used in bone replacement.

1.2 Hypothesis

Therefore, we hypothesize that ionic silicon and PECVD coating amorphous silica based materials can enhance angiogenesis and reduce oxidative stress on HUVECs under normal condition and harmful oxidative stress. The present study brings the attention of biomaterials and tissue engineering research to a situation that mimics more realistically what happens in surgical practice, using in vivo and vitro models to understand the interaction between the amorphous silica based implants and the unfavorable environment formed by elevated levels of reactive oxygen species induced by toxic concentration of hydrogen peroxide (*in vitro*) and critical size bone defects (*in vivo*).

The present study addresses the following aims:

1- Study the effect of ionic silicon on HUVECs under harmful hydrogen peroxide environment (in vitro).

2- Comprehend the role of PECVD coating amorphous silica base materials formed by Si, O, N and P on HUVECS angiogenesis (*in vitro*)

3- Appreciate the role of PECVD based amorphous silica materials formed by Si, O, N and P on angiogenesis under toxic levels of oxidative stress (*in vitro* and *in vivo*).

1.3- Specific aims

Our overall purpose was to investigate the effect of amorphous silica based materials on angiogenesis in the hostile environment of large bone defects. As well as to understand the role of silicon ion released by these materials on angiogenesis under a harmful oxidative stress environment. The complex and high energy fractures are commonly associated with large bone loss and significant vascular damage, leading to hypoxia and consequently harmful levels of reactive oxygen species. This unfavorable environment contribute to an inappropriate healing, which can result in delayed and nonunion. This hostile environment will be the home of biomaterials used as bone filler. Therefore, it seems reasonable use materials based on elements that can reduce oxidative stress and/or enhance angiogenesis and osteogenesis. An analogue situation can be observed in bone losses caused by other conditions, for instance, bone removal due to tumor and infection, and congenital bone mal-formations.

1.3.1 Specific aim 1: Study the effect of ionic silicon on HUVECs under harmful hydrogen peroxide environment (in vitro).

This aim studied the effect of hydrogen peroxide, a common reactive oxygen species found in hypoxic environments, on human umbilical vein endothelial cells (HUVECs). These cells are a well-established model for studying angiogenesis *in vitro* The present aim was to study HUVECs viability and proliferation to evaluate cytotoxicity and cells growth under specific silicon ion concentration, respectively. Moreover, it was tested the cells' capacity to migrate and form a capillary like-tube structure, two important cells properties essential for a successful defect healing.

Lastly, in order to verify the effect of silicon ion on HUVECs under deleterious oxidative stress and guide a possible mechanism, the cells were exposed at the same time to preselected hydrogen peroxide and silicon ion concentrations, and cell viability and gene expression were studied.

1.3.2 Specific aim 2: Understand the role of PECVD coating amorphous silica based materials formed by Si, O, N and P on endothelial cells angiogenesis (in vitro).

The initial aim was to manufacture PECVD coating amorphous silica based implants and incorporate nitrogen and phosphorus changing the surface elemental composition.

In vitro: HUVECS were tested on PECVD based amorphous silica implants. First, the wettability of different implants was tested. Following, the effect of implants and ions released from the surfaces was tested. The present study tested HUVECS viability, adhesion, morphology, proliferation, matrix deposition, tube formation, and migration. Lastly, the effect of implants on gene expression of angiogenic and antioxidant markers was tested.

1.3.3 Specific aim 3: Understand the role of PECVD coating amorphous silica based materials formed by Si, O, N and P on angiogenesis under toxic oxidative stress (in vitro and in vivo).

In vitro: the cells on implants were exposed to preselected harmful hydrogen peroxide concentration, then it was tested cell viability, matrix deposition, capillary tube formation, angiopoietin-1 and 4-hydrononenal (4-HNE) l in conditioned medium. Gene expression of angiogenic and antioxidant markers were tested to verify the effect of an applied coating on HUVECs and facilitate the understanding of mechanisms involved in probable angiogenic and antioxidant effects induced by the coatings.

In vivo: A rat critical size calvarial defect, which is an orthotopic defect that will not heal without intervention, was used to evaluate the effects of coated materials *in vivo.* This animal model is widely used because it is reproducible, quick, and does not require implant or fracture stabilization. Furthermore, the animal model allows a straight approach to the investigation of biomaterials on intramembranous ossification. Our focus was to analyze the effect of studied materials on new blood vessel formation, and local and system oxidative stress markers. The new blood vessels formation and local oxidative stress were analyzed by immunohistochemistry, and systemic oxidative stress was evaluated by measuring levels of products of lipid peroxidation (4-HNE) in the blood stream.

1.4 Dissertation structure

In following passages, an overview of the six chapters of this dissertation is provided. Moreover, the significance and contribution of each chapter to the central theme is highlighted.

Chapter 1, General Introduction: The problem addressed in this research work is presented while summarizing hypothesis and specific aims. The lack of osteointegration as a major issue in the implants used for bone replacement has been discussed. The unfavorable oxidative stress environment faced by these implants is hypothesized to lead to loosening and failure due a poor attachment between the biomaterial and the host tissue. The angiogenesis and the reduction of oxidative stress have been defined as the main strategies for enhancing osteointegration. Implants coated with amorphous silica by PECVD method were chosen as a potential angiogenic and antioxidant biomaterials. Lastly, the specific aims and in vitro and in vivo experimental design used to prove the hypothesis have been detailed. For a better understanding of the research work flow presented in this dissertation, we

concluded this chapter describing the dissertation structure, which prepare the reader for our findings described in the chapters 3,4, and 5, and summarized in chapter 6.

Chapter 2, Background: This chapter deals with definitions of osteointegration, biocompatibility, angiogenesis, osteogenesis and oxidative stress. Extensive literature review study used to show the importance of the implant osteointegration and its relationship with angiogenesis and oxidative stress is described. In addition, the interaction between angiogenesis and osteogenesis phenomena during the bone healing is explained. A general idea of PECVD coating method and the effect of silica based material in new bone and blood vessel formation is given. At the end this chapter emphasizes on the clinical relevance of this research.

Chapter 3, This chapter discusses the in vitro experiments ran to test the hypothesis that ionic silicon could enhance angiogenesis in HUVECs despite toxic oxidative stress induced by hydrogen peroxide. The results showed that 0.5 mM ionic silicon improved HUVECs migration , capillary tube formation and upregulated VEGFA, VEGFR2 and HIF-1a in HUVECs even under unfavorable conditions of 0.6mM H_2O_2 . Moreover, 0.5 mM ionic silicon solution enhanced cell survival and reduced cell death in HUVECs under toxic oxidative stress conditions. These findings support the use of silica on implants used for bone replacement, once they can potentially enrich angiogenesis even when the materials are under harmful oxidative stress.

Chapter 4, describes *in vitro* experiment using PECVD coated amorphous silica-based implants, incorporated with phosphorus and nitrogen. It demonstrated that the coated surfaces improved HUVECs adhesion, matrix deposition and capillary

tubule formation. Moreover, an upregulation of angiogenic markers (VEGFA, HIF-1a, ang-1 and Nesprin-2), and oxidative stress markers (SOD-1, cat-1 and NOS3) was observed. At the end, it was verified that SiONP2 composition (N_2O flow rate=5) presented the most relevant outcome and could enhance angiogenesis and osteointegration, reducing the possibility of loosening and failure.

Chapter 5, The goal of this chapter was to evaluate the effect of the PECVD coated SiONP implants on HUVECs angiogenesis under toxic oxidative stress. In addition, the implant was tested for oxidative stress and angiogenic markers in vivo, using a rat critical size cavarial defect model. *In vitro* experiment showed a remarkable improvement on angiogenic properties of HUVECs under toxic oxidative stress. *In vivo* study demonstrated the potential benefit of PECVD coated amorphous silica-based implants on reduction of oxidative stress and leverage angiogenesis in large bone defects.

Chapter 6, Conclusion: This section finalizes this dissertation and makes the link among all chapters, demonstrating the importance of this approach and significance of its results. Here, the authors talk about how the researchers have neglected the effect of manufactured materials on host environment during the initial testing, and demonstrated how beneficial PECVD coating amorphous silica-based materials can be for osteointegration by boosting angiogenesis and reducing oxidative stress.

CHAPTER 2

BACKGROUND

One million bone graft procedures occur in the United States every year[1]. The autograft, the bone collected from the same individual, is the gold standard treatment.[2–4] However, the autograft has some disadvantages, such as morbidity of the donor area and the lack of sources from the same individual.[5] Allograft, which is the bone harvested from a different individual from the same species, could be an option but immunogenicity, lack of sources, and unsatisfactory biological properties are drawbacks that make this option unusual.[5]

Based on the previous statements, we can see that inert biomaterials have large applicability in this field. And Polyether ether ketone (PEEK),[6–9] titanium[10–14] and ceramics, such as zirconia[15–20] are some of the materials currently used in bone replacement and supportive implants, such as plates, rods and screws. Nevertheless, the lack of osteointegration observed by implants loosening and failure is a issue that still need to be overcomed. Then, the coating procedures emerge with the aim to improve attachment between implants and the host tissue and to reduce inflammatory response. Initially, implants coated with hydroxyapatite (HA) were developed with the aim to improve osteointegration and biocompatibility of naked metal implants. However, the analysis of multiple clinical trials have demonstrated that after 5 years, HA-coated implants presented the same survival rate as uncoated titanium implants.[21] Today, the advancement of biomaterials and the usage of bioactive glasses provided with enhanced bioactivity and osteoinduction further resulted in improved osteointegration.[22] However, bioactive glasses have certain limitations such as poor

interfacial bonding that facilitates coating delamination and in-addition the high temperature manufacturing processes result in reduced bioactivity.[23]

In recent work, our group demonstrated the use of plasma enhanced vapor deposition (PECVD) coating method for deposition of amorphous silica. This approach allows us to overcome the limitations of bioactive glass coatings process by the use of the low temperature fabrication method, the preservation of silicon bioactivity and enhanced adhesion to underlying surface.[24,25] In addition, we demonstrated that the incorporation of nitrogen in PECVD-based amorphous silica upregulates superoxidase dismutase I (SOD1) which further triggers the downstream gene expression of Runx2 and collagen type I, providing it with enhanced osteogenesis and biomineralization.[25]

Despite the advances in bone tissue engineering and biomaterials, the aseptic implant failure for lack of osteointegration is not unusual.[26] The revision for the replacement of the primary implant is usually required and followed by elevated morbidity, and usually cost at least twice the value of the initial procedure.[27] For example, in 2002 a revision of hip arthroplasty was approximately $ 57,000 in the United States.[28]

Inert biomaterials have been used for replacement of large bone defects, dental implants, and hip and knee replacements. The interaction between these implants and the host tissue has been vastly studied with the aim to enhance the biocompatibility and improve the osteointegration. Biocompatibility was recently defined as "*the ability of a biomaterial to perform its desired function with respect to a medical therapy, without eliciting any undesirable local or systemic effects in the recipient or beneficiary of that therapy, but generating the most appropriate beneficial cellular or tissue response in that specific situation, and optimizing the clinically relevant performance*

of that therapy"[29]. And osteointegration can be defined as a direct connection between the implants and the surrounding living bone without formation of any scar fibrotic tissue between the structures[30,31].

Despite the number of studies[6–9,11–14,32–34], most of the attention is dedicated to the study of the effect of the biomaterials in the host tissue without considering the unfavorable oxidative stress condition present in this environment.[35] Perhaps, the elaboration of materials that could reduce the toxic oxidative stress could improve the biocompatibility and the osteointegration and reduce complications, such as implants loosening and failure.[35]

Such as was mentioned above, we showed in a recent publication that the presence of ionic silicon plays a dominant role in superoxidase dismutase-1 (SOD-1) production.[36] This enzyme has a relevant function in reduction of oxidative stress by converting superoxide in hydrogen peroxide, which will suffer further conversion in H_2O and O_2. Hence, maybe silica based materials can have some antioxidant effect on implants' host environment, facilitate elimination of reactive oxygen species and improve osteointegration.

There is a vast scientific information about the antioxidant effect of ionic silicon and silica on plants and vegetables.[37–39] However, we could not find relevant papers that demonstrated the antioxidant effect of ionic silica and silica based materials in mammals' cells *in vitro* and *in vivo.*

Angiogenesis is defined as the sprouting of new blood vessels from a preexistent one.[40] This phenomena is crucial for adequate bone healing and improvements on angiogenesis could boost the healing process and mitigate delayed and non-fracture union in large bone defects. Furthermore, the angiogenesis

enrichment could facilitate the attachment between the implants and surrounding bone.[40–42] A study found that silica mesoporous can improve angiogenesis in endothelial cells by up-regulating the hypoxia inducible factor 1alfa (HIF-1α).[43] Other studies demonstrated that bioactive glasses can leverage angiogenesis.[44–48] One study demonstrated that ions released from bioactive glasses could stimulate human umbilical vein endothelial cells (HUVECS) proliferation, accelerate cell migration, up-regulated expression of the vascular endothelial growth factor (VEGF), basic fibroblast growth factor (b-FGF) and endothelial nitric oxide synthase (eNOS).[47] Another study showed that human dental pulp stromal cells combined with Bioglass® could up-regulate expression of endothelial cell markers, CD31 and vascular endothelial growth factor, on these cells *in vivo* and *in vitro*.[44]

With the purpose of better understanding our research work, we will describe some physiological and pathological events that happen in a large bone defect healing: angiogenesis, intramembranous ossification and oxidative stress. Moreover, we will describe some considerations about PECVD coating processing.

2.1 Angiogenesis

Angiogenesis and osteogenesis are strongly correlated. Therefore, it is essential to understand both mechanisms to engineer new biomaterials and transpose the hostile hypoxic environment created from a large bone defect after an injury.[42,49,50] Angiogenesis is recognized as the sprouting of a new vessel from the previous one stimulated by inflammatory substances and growth factors, such as the tumor necrosis factor-α (TNF-α), interleukin-1 (IL-1), IL-6, IL-11,IL-18 and VEGF released after tissue injury. Figure 1 explains the process initialization with rupture a of a basal membrane by metalloproteases triggered by an initial overproduction of a growth factor on an injured area (Fig 1A) and migration of endothelial cells (Fig 1B)[50]. The

basal membrane is a thin layer of cells' that lies immediately deep to the endothelial cells monolayer, and in a mature vessel constrain the structure preventing endothelial cells migration and uncontrolled growth[50,51]. The earliest stage of fracture healing is the hematoma formation, environment rich in VEGF[52]. This hormone is a specific mitogen for endothelial cell and by activation of tyrosine kinase receptors induces cells proliferation, migration and new blood vessel formation[53]. VEGF can be upregulated by multiple factors, and one of the most important is hypoxic induced factor 1 alfa (HIF-1a) that is upregulated on na unbalanced hypoxic environment. Studies have shown that the VEGF produced by osteoblast also play an important role on osteogenesis and intramembranous ossification from initial stages, stimulating macrophages infiltration, to final stages, inducing osteoclast production during the remodeling phase [52-54]

2.1.1 Angiogenic markers

- Vascular endothelial growth factor- A (VEGFA) and vascular endothelial growth factor receptor-2 (VEGFR2)

The VEGF-A is a heparin-binding protein that can induces vascular permeability and stimulates endothelial cell survival, proliferation, migration and differentiation.[55–57] The molecule binds and activates the tyrosine kinase receptors, the vascular endothelial cell receptor 1 and 2 (VEGFR-1 and 2).[58] The VEGFR-2 is considered more important in controlling endothelial cell function. (See figure 2). [59,60]

- Hypoxia inducible factor (HIF-1a)

The HIF-1a is a major driver of the close coupling between angiogenesis and osteogenesis, can work as a pro or anti-angiogenic factor. Mostly, the HIF-1a act as a proangiogenic factor under hypoxic conditions by stimulating upregulation of VEGFA

and down streaming angiogenesis by activating VEGFR-2 receptor. We will describe more details about this molecule in the following sections.

- Angiopoietin 1 (Ang-1)

Ang1 is a protein well known for playing a significant role on angiogenesis. The protein has a carboxyl-terminal fibrinogen -like domain that binds to Tie2 receptor and promotes endothelial cell migration, differentiation and survival by activating endothelial-specific receptor tyrosine kinase 2 (Tie-2)[61]. Studies have concluded that Ang-1 inhibit endothelial cell apoptosis[62,63] by multiples pathway, which contain PI-3 kinase/AKT activation and inhibition of Smac with upregulation of Survivin protein[63]. Ang1 can be more beneficial to osteogenesis than the vascular endothelial growth factor. Studies demonstrated that molecule can increase bone mass[64] and induce osteoblast differentiation, mineralization and bone formation.[65]

2.2 Intramembranous ossification

The bone has the peculiar capacity to heal without forming fibrotic tissue. After an injury, the bone can heal by a direct intramembranous or indirect endochondral ossification. The intramembranous occur without previous cartilage tissue formation. In the endochondral ossification there is an initial cartilage production followed by a calcium deposition, collagen type I production and accordingly new mature bone formation.[49,66] On our study, we focus on intramembranous ossification, which is the predominant on healing process of craniomaxillofacial fractures. Initially, after a bone damage there is a hematoma formation, which consists of blood and bone marrow cells. Following the initial stage there is an inflammatory response with a secretion of chemokines tumor necrosis factor-α (TNF-α), interleukin-1 (IL-1), IL-6, IL-11 and IL-18.[49] The chemokines will recruit mesenchymal cells from the inner periosteum layer

and systemically, from other body sites by the homing effect,[49] and induces bone regeneration.[67]

2.3 Oxidative stress

Oxidative stress is the imbalance between prooxidant and antioxidant systems.[68] The injured environment swiftly decreases oxygen site levels. In small injuries, this situation can be efficiently reversed. However, on large bone defects the imbalance remains, with a prolonged elevation of reactive oxygen species (ROS) level.[69] ROS are intermediate products of oxygen reduction produced by the mitochondrial respiratory chain during physiological cell metabolism. Most ROS is formed by superoxide anion, that by action of superoxidase dismutase or spontaneously is rapidly removed by conversion to hydrogen peroxide.[68]

The unbalance in cell metabolism, such as, the hypoxic condition induced by a large bone defect, can induce ROS accumulation, oxidative stress and further cell dysfunction and death. Antioxidant enzymes are proteins whose function is to reduce the ROS levels and maintain physiologic cell metabolism. A small level of oxidative stress is beneficial for regular cell methabolism.[70] However, toxic levels of reactive oxygen species decrease levels of antioxidant enzymes and induces cell malfunction and DNA damage.[71] Therefore, there is a necessity of equilibrium between degradation and ROS formation. (See figure 3). Antioxidant enzymes are a group of proteins responsible for accelerating the ROS degradation . The most important include superoxidase dismutase 1 (SOD-1) that act converting superoxide ion (O_2^-) in hydrogen peroxide (H_2O_2), and Catalase (cat-1) and glutathione peroxidase that degrade hydrogen peroxide in water and oxygen.

HIF-1α is a transcription factor that plays an important role on angiogenesis. During physiological oxygen levels, HIF-1α is raptly oxidized and deactivated. Nevertheless, low oxygen level environments accumulate HIF-1a and can downstream an angiogenesis pathway upregulating VEGF and VEGFR.[72,73] Moreover, an alternative angiogenesis pathway can be activated by lipid and protein oxidation and further nuclear factor kappa-light-chain-enhancer of activated B cells (NF-kB) and toll like receptor 2(TLR2) activation (see Figure 4).[69]

Oxidative stress can have a deleterious effect on osteoblast reducing mineralization and gene expression of osteogenic markers, such as Runt-related transcription factor 2 (Runx2) alkaline phosphatase (ALP) and collagen type I[74,75]. These observations suggest that high levels of reactive oxygen species can aggravate regeneration of large bone defects.

2.3.1 Antioxidant enzymes and endothelial nitric oxide synthase

- Superoxidase dismutase-1 (SOD-1)

There are three human isoforms of SOD: 1- Cu/Zn SOD (SOD1): located predominantly in the cytoplasm, 2- Mn SOD (SOD2): located mainly in the mitochondria, and 3 – Cu/Zn EC-SOD (SOD3): extracellular.[76,77] SOD1 play a major role on the first line of defense against superoxide free radical. Furthermore, studies suggest that SOD1 blocks the release of mitochondrial cytochrome c and could act against cell apoptosis.[78,79] Additionally, this Study shows that SOD1 can have a protective effect on HUVECs under oxidative stress induced by oxygen and glucose deprivation.[79] SOD-1 is important for adequate bone formation, and its presence has shown it to be important for collagen cross-linking and maintenance of bone mineral

density.[80,81] SOD-1 showed it to recover the osteoblast differentiation and the matrix deposition in an oxidative stress environment.[82]

- Catalase-1 (Cat-1)

Catalases, also known as hydroperoxides, can be formed by more than 300 sequences. These enzymes are found in practically all living organisms in contact with oxygen. This function is to protect the cells against oxidative stress induced by reactive oxygen species. The enzyme catalyzes hydrogen peroxide (H_2O_2), breaking down the molecule in water and oxygen**.** (See reaction one below).[83,84]

$2H_2O_2 \longrightarrow 2H_2O + O_2$ (1)

- Glutathione peroxidase 1 (GPx1)

GPx1 is abundant in cell cytoplasm and belongs to a glutathione peroxidase family. GPX-1 is one of the most important human antioxidant enzymes, acting as a catalyst of hydroperoxides and hydrogen peroxides, which protects cells against damage. The catalyzes reaction is the same as catalase-1 showed above. Moreover, GPx1 mediate mitochondrial function, signal transduction and maintenance of thiol redox- balance.[84] GPx contain selenocysteine as its active site. Initially, there is an oxidation of selenol (E-SeOH) and production of selenenic acid (E-SeOH). This acid will react with glutathione (GSH) and produce selenenyl sulfide (E-SeSG). Afterwards, a second molecule of GSH generates an active form of the enzyme. Under higher levels of hydroperoxides, E-SeOH may undergo further oxidation. (See figure 5).[85]

- Endothelial cell Nitric oxide Synthase (eNOS) or Nitric Oxide synthase-3 (NOS3)

NOS3 is an enzyme mostly produced by endothelial cells and its main function is to produce nitric oxide (NO), which is a short-lived free radical gas that play a

significant role on a tissue adequate perfusion by inducing blood vessel dilation and protection. Unbalanced oxidative stress produces abnormal elevated levels of superoxide anion that inactivates NO and produces a potent oxidant peroxynitrite that induced proteins, lipids, and DNA damage. [86]

A study demonstrated that eNOS knockout mice presented a reduction of endothelial cells mobilization by VEGF, and a decreased matrix metalloproteose-9, which is necessary for stem cells mobilization during angiogenesis. Therefore, the study demonstrated the importance of eNOS on angiogenesis and tissue regeneration. [87] Nitric oxide has important roles in angiogenesis, such as the suppression of the angiostatin, which is an inhibitor of angiogenesis[88]. Another study also found that the enzyme can be important for angiogenesis after ischemia.[89]

NOS seems to have a close relationship to fracture healing.[86,89–92] One study observed that NOS inhibition led to an inadequate healing of rat femoral fracture.[90] Another study evaluated the temporal expression of NOS for 21 days and showed a progressive increase during all time points.[91]

2.3.2 Oxidative stress marker, 4-hydrononenal (4-HNE)

The accumulation of free radicals can induce abnormal degradation of cell membrane by phospholipid peroxidation. The process is characterized by electron transfer from the membrane to the free radical, generating many sub products. One of the most commons products of phospholipid peroxidation is the 4-hydroxinonenal (HNE), which mainly results in oxidation of the fatty acyl chain.[93,94] The 4-HNE is metabolized in a water soluble and less toxic molecule, which facilitates its excretion.[94,95] However, toxic levels of oxidative stress induced by acute or chronicle

conditions can induce mitochondrial disfunction[96] and has been used as an indicative of oxidative stress in tissue and fluids[93,96].

The 4-HNE is one of the major products of oxidative stress cell damage. The molecule can be detected systemically in a variety of organs. Nonetheless, analysis of its free form has a limited value because the 4-HNE exists bonded to other molecules, such as, DNA, proteins or amino phospholipids.[94] Therefore, most of the methods target the detection of 4-HNE adducts with protein, and the main approach has been the immunochemical techniques and the mass spectrometric analysis. Among the immunodetection methods, specifics antibodies have been developed for detection of 4-HNE bound to proteins. [96,97]

One study measured 4-HNE levels in rats from broad ages and verified that serum levels can vary from 10 to 20 ng/mL, and no statistical difference was observed among the groups. [98] As mentioned above, the 4HNE- is more accurately measured bound to other biological molecules, such as proteins. Hence, the 4-HNE BCA assay seems to be a feasible and efficient way for measuring its concentration in the blood stream and evaluate the effect of elements, biomaterials and drugs on increased or mitigated oxidative stress in animal models and in vitro studies with human cells.

There are other molecules that are frequently used as an indicator of oxidative stress level. For example, the Malondialdehyde (MDA), which is also a product of lipid peroxidation, also detected as a free stated and covalent bonded to other biological molecules.[99] Another study demonstrated a significant difference on serum levels and half-life of 4-HNE and MDA. On one hand, 4-HNE was detected in significant higher levels and for long period of time, approximately up to 10 days. On the other hand, MDA was detected in lower levels and up to 2 days.[100] Therefore, many studies have

been using 4-HNE in histological and serum samples to detect and quantify oxidative stress.[93–98,100–102]

2.4 Biomaterials, biocompatibility and oxidative stress

As mentioned before in this review, improvement of biomaterials biocompatibility is the major goal in their development. A successful biomaterial implantation requires an equilibrium of oxidant production and elimination. Researchers have shown that pre-existing host tissue condition can affect healing response.[103] Therefore, preexisting conditions, for example, diabetes, cardiovascular diseases, tumors, or high energy trauma, and even the surgical wound, can produce high levels of reactive oxygen species and play a major role on implant fate.(See figure 6).[104–109]

Oxidative stress plays a relevant role in inflammation, fibrosis and wound healing.[110] Additionally, the phases of healing and inflammation are associated with significant alterations of redox equilibrium.[111,112] Studies have shown that inflammation is associated with enhanced oxidant production. Furthermore, oxidative stress is considered a major inflammation amplifier.[113]

The inflammatory response to a material implantation is described as a timely event, beginning with protein absorption (within a few seconds), and followed by , neutrophil invasion (1 day), monocyte/macrophage infiltration (3 days), foreign body giant cell (FBGC) (1-2 weeks), finalizing with collagenous encapsulation (3-4 weeks) (See figure 7).[114] The inflammation is required for an adequate tissue healing. After implantation the healing response starts with fibroblast infiltration, angiogenesis and granulation tissue formation. Finally, there are the maturation and the tissue remodeling phases that can lasts for months or years. [114]

The surgical wound to implant biomaterials into the body by itself can generate a tissue damage that induces a release of intra and extracellular components, which contribute to elevation of oxidative stress. In addition, the oxidative stress induced by the extracellular matrix and cell degradation products triggers H_2O_2 production as a defense mechanism against possible invading organisms and recruit phagocytic leucocytes from distant sites.[115]

In addition to reactive oxygen species released from the damaged cells, other components are released from the cells and extracellular matrix. These components called damage-associated-signals (DAMPs), include molecules, such as S-100 proteins, high mobility groups box-1 (HMGB-1), ATP, DNA, and hyaluronic acid.[116,117] The DAMPs can be the cause or the consequence of oxidative stress and are responsible for activation of innate immune response and exacerbation of inflammation. (See figure 7)[117] Other factors, for instance, hypoxia and time of surgical wound exposure to the air can influence elevation of ROS and interfere with the healing of the host area of implanted materials. (see figure 8).[35,118,119]

Overall, oxidative stress can have influence on multiple stages of the tissue healing and remodeling, acting on the early stages on the cells responsible for the cell debris cleaning, granular tissue formation and angiogenesis. The presence of ROS and its sub products can influence cell viability, adhesion, migration, spreading, differentiation and proliferation.[120–125] In the late stages of the tissue healing, maturation and remodeling, the temporary extracellular matrix is replaced by a mature structure. During these stages new DAMPs are produced and lead to macrophage activation and oxidative attack of the implant.[126,127]

The product of materials degradation also can induce production of reactive oxygen species. Even inert materials, such as metals, can undergo some degree of degradation by electrochemical corrosion and can produce more ROS than degradable materials, such as polymers. (See figure 9).[35,128,129]

Therefore, it is important to manage the oxidative stress either using biomaterials or drug delivery systems with antioxidant enzymes, or managing the oxidative stress in the host tissue.[130] These strategies could reduce inflammatory response, improve the biocompatibility, and promote a heightened implant osteointegration. Currently, researchers have proposed the strategy to target nuclear factor (erythroid-derived 2)-like 2 (Nrf2), a major transcriptional factor activator of antioxidant enzymes, instead of using antioxidant enzymes (cat-1) and molecules (vitamin C).[35,131]

2.5 Inorganic elements playing the role on angiogenesis

Inorganic elements are recognized as essentials for the growth of living organisms. The balance among these elements and new blood vessel formation and maintenance is required for an adequate cells and tissues survival.[132–134] Elements such as Titanium (Ti), Vanadium (Va), Chromium (Cr), and Cooper (Cu) have been used as implants for bone reconstruction and replacement,[135–137] and its interaction with angiogenesis can have pro or anti-angiogenic effects.[132–134] Other inorganic elements, for instance, Si, N, and P also have been incorporated to biomaterials and can play a relevant role in angiogenesis and maintenance of new blood vessel formation.[43,132,138–140]Usually metal implants used in dental and orthopedic surgeries are combined in alloys formed by at least 2 or more compounds, such as TiAlV and CoCrMo alloys used for hip and knee replacement and TiCu used for dental implants.[141–144]

Currently, Ti based materials are largely used in clinical practice. These materials demonstrated an ambiguous effect on endothelial cells angiogenesis.[134] Interestingly, smooth and hydrophilic surfaces showed to elevate VEGFA and cell differentiation improving the vascular network formation.[145] However, another publication correlated TiO_2 nanoparticles with an anti-angiogenic effect by inhibition of VEGF and VEGFR-2.[146]

Va is an element largely use in metal implants. Studies have clearly established the inhibition effect of Va on cell proliferation.[147] Moreover, it has been reported that this can induce cells apoptosis and a cytotoxic effect by DNA interaction.[147–149] Additionally, another study reported that this element can damage endothelial cells by increasing ROS production.[147,150]

Cr is usually combined with Co and other elements as a metal alloy used as orthopedic implants. [137] A study reported that Cr can direct a reaction with biological structures and produce ROS, DNA damage and gene mutations.[133,151] Even a low concentration of Cr can induce OH radicals formation and activation of nuclear factor-kappaB (NF-kB) and stimulate inflammatory processes. Furthermore, Cr can cause apoptosis by inducing p53 activation. [151,152]

P is present in a high amount in the human body mainly concentrated in the bone. Reports indicated that increased P ions can stimulate Akt signaling and increase MMP-2 and bFGF.[153,154] Another research article verified that P can enhance endothelial cells migration and tubule formation.[138] Moreover, this increased the expression of key pro-angiogenic genes, such as the forkhead box protein C2 (FOXC2), Ostpontin (OPN), and VEGFA in pre-osteoblast cells.[138,155] Osteopontin is a well-known osteogenic marker indicator of osteoblast differentiation that can also

has been recently related with angiogenesis.[139,155] In a nutshell, phosphorus has a stimulatory effect on genes with a pro-angiogenic effect and on VEGF production.[132] Recently, our research group reported the effect of nitrogen incorporation to amorphous silica and an enhancement on osteogenesis. However, a better understanding about the effect of this element on angiogenesis is required. Studies have reported the effect of nitrogen coating bisphosphonates (N-BPs) inhibiting angiogenesis through inhibition of farnesyl pyrophosphate synthase (FPPS) in endothelial cells.[140,156] Other researchers have reported the effect of nitrogen on endothelial cells angiogenesis linking the element effect with nitric oxide activity.[132] Previously in this review we have mentioned and described some nitric oxide properties and effects on angiogenesis and oxidative stress. Mainly, the NO can prevent endothelial cells apoptosis and enhance endothelial cell proliferation through the bFGF and VEGF expression.[157,158]

Si is currently known as an element which alone or combined with Mg and Ca plays a major role on osteogenesis by upregulating transcription factors related with osteoblast differentiation, Runx-2 and Osterix.[159–162] Furthermore, the studies observed upregulation of proteins related with bone matrix formation. [159–162]The effect of Si ion on angiogenesis have been indirectly reported by studying products of dissolution and/or degradation of materials such as bioactive glasses.[163,164] The bioactive glasses have been successfully applied in bone tissue engineering due to their capacity to strongly attach to the host tissue.[165] Silicon ion is the main composition of the bioactive glasses, which has the most successful formulation used in dental and orthopedic clinical practice represented by the 45S5 (Bioglass®).[166] However, the Bioactive glasses are also formed by other elements, such as Na, Ca, Mg and Cu.[166–168] In general, it has been reported that these materials can induce

angiogenesis by stimulating secretion of angiogenic factors, which increase endothelial cells migration, proliferation, and capillary tubule formation.[167,169–171] Nonetheless, just recently the recognition of ionic silicon as a pro-angiogenic element started to be elucidated.[43] The authors demonstrated that ionic silicon plays a role in stimulating VEGFA production in endothelial cells through up-regulation of HIF-1a.[43]

2.6 Plasma enhanced chemical vapor deposition (PECVD)

PECVD is a thin film deposition technique that allows for tunable control over the chemical gases making a solid deposit of reacted elemental from the gases on preselected substrate. The most significant advantages of this technique for biomaterials application are as follows: allows the creation of high energy, stable bonding states, allow ionic release of components from the film which is very useful in physiological application; generated a uniform coating of silicon dioxide, silicon nitride, silicon oxynitride, and phosphorous containing silicon oxynitride films at low temperature (250-400^{o}C). Use of an energetic plasma to 'damage' the substrate surface could result in an appreciable surface roughness that aids in cell attachment. (See figure 10).[24,36,172]

Initially, the chemical vapor deposition (CVD) was used for fabrication of electronic semiconductor devices, such as solar cells and batteries; and optical coatings, such as mirrors and antireflection coatings.[173–176]

CVD is a method of coating a substract forming a thin film. The method uses deposition of a solid phase from a gaseous phase, and a volatile precursor gas reacting or decomposing on a heated substract. The system operates on temperatures between 400 and 1200 ^{0}C. First, there is a gas phase decomposition. Second, there is diffusion to surface followed by physical adsorption, diffusion, decomposition and desorption of a reaction by products. (see figure 11). [177]

Afterward, the PECVD emerges. This method applies plasma rather than temperature as a source of energy for the gases reaction. With this method the substrate (wafer) is maintained at a lower temperature created by the radio frequency electromagnetic waves. During this process there is a high free electron content with non-thermal equilibrium, and the plasma becomes positively charged and the particles are accelerated toward the wafer. The wafers rest on a negative charged plate that is heated to lower temperatures (~250-400 ^{0}C) compare to the CVD method.[178–181]

The process uses precursor(s) and carrier gas mix in the chamber. Firstly, The energy is transferred to the system by radio frequency induced plasma. Secondly, there is dissociation with ions and radicals formation and particles move to the substrate. Lastly, the radicals are adsorbed onto the substrate and the film layer starts to form with gradual density increasing. (see figure 12)[182]

The other advantages and the limitations of the method are as follows: Advantages→ a lower operating temperature, a good step coverage, a uniform coating on different surfaces patterns, a high packing density and a stress reduction.[177]

Limitations→ The current toxic precursors, have a limited capacity, sample contamination, to establish stoichiometry and a high equipment cost.[177]

2.7 Conclusion

Therefore, supported by the extensive and broad literature reviews mentioned in this section, we strongly believe that the PECVD coating amorphous silica-based implants recently created by our research group can boost angiogenesis and reduce oxidative stress in large bone defects. In addition, our research work bring a current perspective of testing biomaterials in oxidative stress environment, which mimic the real deleterious environment faced by these implants.

Here, we are testing our hypothesis by verifying the effect of the new synthesized implants in the angiogenic properties of human umbilical vein endothelial cells (HUEVCS) and rat's critical size calvarial defects.

2.8 References

1. Vacan~, J. P. & Langer, R. Tissue engineering: the design and fabrication of living replacement devices for surgical reconstruction and transplantation.

2. Elsalanty, M. E. & Genecov, D. G. Bone Grafts in Craniofacial Surgery. doi:10.1055/s-0029-1215875

3. Szpalski, C., Barr, J., Wetterau, M., Saadeh, P. B. & Warren, S. M. Cranial bone defects: current and future strategies. *Neurosurg. Focus* **29,** E8 (2010).

4. Lethaus, B., Bloebaum, M., Koper, D., Poort-Ter Laak, M. & Kessler, P. Interval cranioplasty with patient-specific implants and autogenous bone grafts e Success and cost analysis. *J. Cranio-Maxillofacial Surg.* **42,** 1948–1951 (2014).

5. Betz, R. R. Limitations of autograft and allograft: new synthetic solutions. *Orthopedics* **25,** s561-70 (2002).

6. Overton, J. A. *et al.* IMPROVED METHODS FOR ACRYLIC-FREE IMPLANTS IN NON-HUMAN PRIMATES FOR NEUROSCIENCE RESEARCH. *J. Neurophysiol.* jn.00191.2017 (2017). doi:10.1152/jn.00191.2017

7. Shuai, C. *et al.* Characterization and Bioactivity Evaluation of (Polyetheretherketone/Polyglycolicacid)-Hydroyapatite Scaffolds for Tissue Regeneration. *Mater. (Basel, Switzerland)* **9,** (2016).

8. Bubik, S. *et al.* Attachment and growth of human osteoblasts on different biomaterial surfaces. *Int. J. Comput. Dent.* **20,** 229–243 (2017).

9. Zoidis, P., Bakiri, E., Papathanasiou, I. & Zappi, A. Modified PEEK as an alternative crown framework material for weak abutment teeth: a case report. *Gen. Dent.* **65,** 37–40 (2017).

10. Vandamme, K. *et al.* In vivo molecular evidence of delayed titanium implant osseointegration in compromised bone. *Biomaterials* **32,** 3547–3554 (2011).

11. Divakar, D. D. *et al.* Enhanced antimicrobial activity of naturally derived bioactive molecule chitosan conjugated silver nanoparticle against dental implant pathogens. *Int. J. Biol. Macromol.* (2017). doi:10.1016/j.ijbiomac.2017.10.166

12. Yu, X. *et al.* Fluorine-free preparation of titanium carbide MXene quantum dots with high near-infrared photothermal performances for cancer therapy. *Nanoscale* (2017). doi:10.1039/c7nr05997c

13. Yuan, N. *et al.* The Incorporation of Strontium in a Sodium Alginate Coating on Titanium Surfaces for Improved Biological Properties. *Biomed Res. Int.* **2017,** 9867819 (2017).

14. Apostu, D., Lucaciu, O., Berce, C., Lucaciu, D. & Cosma, D. Current methods of preventing aseptic loosening and improving osseointegration of titanium implants in cementless total hip arthroplasty: a review. *J. Int. Med. Res.* 300060517732697 (2017). doi:10.1177/0300060517732697

15. Uraba, A. *et al.* Biomechanical behavior of adhesive cement layer and periodontal tissues on the restored teeth with zirconia RBFDPs using three-kinds of framework design: 3D FEA study. *J. Prosthodont. Res.* (2017). doi:10.1016/j.jpor.2017.10.001

16. Kniha, K. *et al.* Evaluation of peri-implant bone levels and soft tissue dimensions

around zirconia implants-a three-year follow-up study. *Int. J. Oral Maxillofac. Surg.* (2017). doi:10.1016/j.ijom.2017.10.013

17. Kretzer, J. P. *et al.* Ion release in ceramic bearings for total hip replacement: Results from an in vitro and an in vivo study. *Int. Orthop.* (2017). doi:10.1007/s00264-017-3568-1

18. Roy, M. E., Whiteside, L. A. & Sebastian, A. M. Retrieved Magnesia-Stabilized Zirconia Femoral Heads Exhibit Minimal Roughening and Abrasive Potential. *J. Arthroplasty* (2017). doi:10.1016/j.arth.2017.07.018

19. Bal, B. S. *et al.* Reconciling in vivo and in vitro kinetics of the polymorphic transformation in zirconia-toughened alumina for hip joints: I. Phenomenology. *Mater. Sci. Eng. C. Mater. Biol. Appl.* **72,** 252–258 (2017).

20. Kwon, Y., Kim, T. Y., Kwon, G., Yi, J. & Lee, H. Selective Activation of Methane on Single-Atom Catalyst of Rhodium Dispersed on Zirconia for Direct Conversion. *J. Am. Chem. Soc.* (2017). doi:10.1021/jacs.7b11010

21. Lee, J. J., Rouhfar, L. & Beirne, O. R. Survival of hydroxyapatite-coated implants: A meta-analytic review. *J. Oral Maxillofac. Surg.* **58,** 1372–1379 (2000).

22. Granito, R. N. *et al.* In vivo biological performance of a novel highly bioactive glass-ceramic (Biosilicate®): A biomechanical and histomorphometric study in rat tibial defects. *J. Biomed. Mater. Res. Part B Appl. Biomater.* **97B,** 139–147 (2011).

23. Gomez-Vega, J. M., Saiz, E. & Tomsia, A. P. Glass-based coatings for titanium implant alloys. *J. Biomed. Mater. Res.* **46,** 549–59 (1999).

24. Ilyas, A., Lavrik, N. V, Kim, H. K. W., Aswath, P. B. & Varanasi, V. G. Enhanced interfacial adhesion and osteogenesis for rapid "bone-like" biomineralization by PECVD-based silicon oxynitride overlays. *ACS Appl. Mater. Interfaces* **7,** 15368–79 (2015).

25. Ilyas, A. *et al.* Amorphous Silica , a New Antioxidant Role for Rapid Critical-Sized Bone Defect Healing.

26. Dixon, T., Shaw, M., Ebrahim, S. & Dieppe, P. Trends in hip and knee joint replacement: socioeconomic inequalities and projections of need. *Ann. Rheum. Dis.* **63,** 825–830 (2004).

27. Lavernia, C., Lee, D. J. & Hernandez, V. H. The increasing financial burden of knee revision surgery in the United States. *Clin. Orthop. Relat. Res.* **446,** 221–226 (2006).

28. Kurtz, S. Prevalence of Primary and Revision Total Hip and Knee Arthroplasty in the United States From 1990 Through 2002. *J. Bone Jt. Surg.* **87,** 1487 (2005).

29. Williams, D. F. On the mechanisms of biocompatibility. *Biomaterials* **29,** 2941–2953 (2008).

30. Parithimarkalaignan, S. & Padmanabhan, T. V. Osseointegration: An update. *J. Indian Prosthodont. Soc.* **13,** 2–6 (2013).

31. Albrektsson, T. & Johansson, C. Osteoinduction, osteoconduction and osseointegration. *Eur. Spine J.* **10,** S96–S101 (2001).

32. Lopez-Lopez, J. A. *et al.* Choice of implant combinations in total hip replacement: systematic review and network meta-analysis. *BMJ* **359,** j4651 (2017).

33. Kiele, P., Cvancara, P., Mueller, M. & Stieglitz, T. Design of experiment evaluation of sputtered thin film platinum surface metallization on alumina substrate for implantable conductive structures. *Conf. Proc. ... Annu. Int. Conf. IEEE Eng. Med. Biol. Soc. IEEE Eng. Med. Biol. Soc. Annu. Conf.* **2017,** 1066–1069 (2017).

34. Pieralli, S., Kohal, R.-J., Lopez Hernandez, E., Doerken, S. & Spies, B. C. Osseointegration of zirconia dental implants in animal investigations: A systematic review and meta-analysis. *Dent. Mater.* (2017). doi:10.1016/j.dental.2017.10.008

35. Mouthuy, P. A. *et al.* Biocompatibility of implantable materials: An oxidative stress viewpoint. *Biomaterials* **109,** 55–68 (2016).

36. Ilyas, A. *et al.* Amorphous Silica: A New Antioxidant Role for Rapid Critical-Sized Bone Defect Healing. *Adv. Healthc. Mater.* (2016). doi:10.1002/adhm.201600203

37. Carneiro, J. M. T. *et al.* Evaluation of silicon influence on the mitigation of cadmium-stress in the development of Arabidopsis thaliana through total metal content, proteomic and enzymatic approaches. *J. Trace Elem. Med. Biol.* **44,** 50–58 (2017).

38. Biju, S., Fuentes, S. & Gupta, D. Silicon improves seed germination and alleviates drought stress in lentil crops by regulating osmolytes, hydrolytic enzymes and antioxidant defense system. *Plant Physiol. Biochem. PPB* **119,** 250–264 (2017).

39. Manivannan, A. & Ahn, Y.-K. Silicon Regulates Potential Genes Involved in Major Physiological Processes in Plants to Combat Stress. *Front. Plant Sci.* **8,**

1346 (2017).

40. Kovacic, J. C. *et al.* Endothelial Progenitor Cells, Angioblasts, and Angiogenesis-Old Terms Reconsidered From a Current Perspective. *Trends Cardiovasc. Med.* **18,** 45–51 (2008).

41. Alt, V. *et al.* Assessment of angiogenesis in osseointegration of a silicaâ€“collagen biomaterial using 3D-nano-CT. *Acta Biomater.* **7,** 3773–3779 (2011).

42. Kanczler, J. M. & Oreffo, R. O. C. Osteogenesis and angiogenesis: The potential for engineering bone. *Eur. Cells Mater.* **15,** 100–114 (2008).

43. Dashnyam, K. *et al.* Promoting angiogenesis with mesoporous microcarriers through a synergistic action of delivered silicon ion and VEGF. *Biomaterials* **116,** 145–157 (2017).

44. El-Gendy, R. *et al.* Investigating the Vascularization of Tissue-Engineered Bone Constructs Using Dental Pulp Cells and 45S5 Bioglass(R) Scaffolds. *Tissue Eng. Part A* **21,** 2034–2043 (2015).

45. Zhang, J. *et al.* Effects of bioactive cements incorporating zinc-bioglass nanoparticles on odontogenic and angiogenic potential of human dental pulp cells. *J. Biomater. Appl.* **29,** 954–964 (2015).

46. Stahli, C., James-Bhasin, M., Hoppe, A., Boccaccini, A. R. & Nazhat, S. N. Effect of ion release from Cu-doped 45S5 Bioglass(R) on 3D endothelial cell morphogenesis. *Acta Biomater.* **19,** 15–22 (2015).

47. Mao, C., Chen, X., Miao, G. & Lin, C. Angiogenesis stimulated by novel nanoscale bioactive glasses. *Biomed. Mater.* **10,** 25005 (2015).

48. Zhang, Y. *et al.* Mesoporous bioactive glass nanolayer-functionalized 3D-printed scaffolds for accelerating osteogenesis and angiogenesis. *Nanoscale* **7,** 19207–19221 (2015).

49. Marsell, R. & Einhorn, T. A. The biology of fracture healing. *Injury* **42,** 551–555 (2011).

50. Stegen, S., van Gastel, N. & Carmeliet, G. Bringing new life to damaged bone: The importance of angiogenesis in bone repair and regeneration. *Bone* **70,** 19–27 (2015).

51. Ucuzian, A. A., Gassman, A. A., East, A. T. & Greisler, P. NIH Public Access. **31,** 1–28 (2011).

52. Street, J. *et al.* Vascular endothelial growth factor stimulates bone repair by promoting angiogenesis and bone turnover. *Proc. Natl. Acad. Sci.* **99,** 9656–9661 (2002).

53. Hu, K. & Olsen, B. R. The roles of vascular endothelial growth factor in bone repair and regeneration. *Bone* **91,** 30–38 (2016).

54. Hu, K. & Olsen, B. R. Osteoblast-derived VEGF regulates osteoblast differentiation and bone formation during bone repair. **126,** 509–526 (2016).

55. Leung, D. W., Cachianes, G., Kuang, W. J., Goeddel, D. V & Ferrara, N. Vascular endothelial growth factor is a secreted angiogenic mitogen. *Science* **246,** 1306–1309 (1989).

56. Gerber, H. P. *et al.* Vascular endothelial growth factor regulates endothelial cell survival through the phosphatidylinositol 3'-kinase/Akt signal transduction pathway. Requirement for Flk-1/KDR activation. *J. Biol. Chem.* **273,** 30336–

30343 (1998).

57. Keck, P. J. *et al.* Vascular permeability factor, an endothelial cell mitogen related to PDGF. *Science* **246,** 1309–1312 (1989).

58. Ferrara, N., Gerber, H.-P. & LeCouter, J. The biology of VEGF and its receptors. *Nat. Med.* **9,** 669–676 (2003).

59. Shibuya, M. Vascular endothelial growth factor and its receptor system: physiological functions in angiogenesis and pathological roles in various diseases. *J. Biochem.* **153,** 13–19 (2013).

60. Johnson, K. E. & Wilgus, T. A. Vascular Endothelial Growth Factor and Angiogenesis in the Regulation of Cutaneous Wound Repair. *Adv. Wound Care* **3,** 647–661 (2014).

61. Harel, S., Mayaki, D., Sanchez, V. & Hussain, S. N. A. NOX2, NOX4, and mitochondrial-derived reactive oxygen species contribute to angiopoietin-1 signaling and angiogenic responses in endothelial cells. (2017). doi:10.1016/j.vph.2017.03.002

62. Jin Kwak, H., So, J.-N., Jae Lee, S., Kim, I. & Young Koh, G. Angiopoietin-1 is an apoptosis survival factor for endothelial cells.

63. Harfouche, R. *et al.* Mechanisms Which Mediate the Antiapoptotic Effects of Angiopoietin-1 on Endothelial Cells. doi:10.1006/mvre.2002.2421

64. Suzuki, T. *et al.* Osteoblast-specific Angiopoietin 1 overexpression increases bone mass. (2007). doi:10.1016/j.bbrc.2007.08.099

65. Park, S.-H. *et al.* Potential of L-thyroxine to differentiate osteoblast-like cells via Angiopoietin1. (2016). doi:10.1016/j.bbrc.2016.08.137

66. Berendsen, A. D. & Olsen, B. R. Bone development. *Bone* **80,** 14–18 (2015).

67. Arvidson, K. *et al.* Bone regeneration and stem cells. *J. Cell. Mol. Med.* **15,** 718–46 (2011).

68. Reuter, S., Gupta, S. C., Chaturvedi, M. M. & Aggarwal, B. B. Oxidative stress, inflammation, and cancer: How are they linked? *Free Radic. Biol. Med.* **49,** 1603–1616 (2010).

69. Kim, Y.-W. & Byzova, T. V. Oxidative stress in angiogenesis and vascular disease. *Blood* **123,** (2014).

70. Babusikova, E., Evinova, A., Hatok, J., Dobrota, D. & Jurecekov, J. Oxidative Changes and Possible Effects of Polymorphism of Antioxidant Enzymes in Neurodegenerative Disease. in *Neurodegenerative Diseases* (InTech, 2013). doi:10.5772/54619

71. Saxena, S. & Jamil, K. Oxidative stress and expression level of Catalase, Glutathione S Tranferase Enzyme in type 2 Diabetes Patients. *Int. J. Sci. Eng. Res.* **5,** (2014).

72. Solaini, G., Baracca, A., Lenaz, G. & Sgarbi, G. Hypoxia and mitochondrial oxidative metabolism. *Biochim. Biophys. Acta - Bioenerg.* **1797,** 1171–1177 (2010).

73. Turrens, J. F. Mitochondrial formation of reactive oxygen species. *J. Physiol.* **552,** 335–44 (2003).

74. Arai, M., Shibata, Y., Pugdee, K., Abiko, Y. & Ogata, Y. Effects of reactive oxygen species (ROS) on antioxidant system and osteoblastic differentiation in MC3T3-E1 cells. *IUBMB Life* **59,** 27–33 (2007).

75. Bai, X. *et al.* Oxidative stress inhibits osteoblastic differentiation of bone cells by ERK and NF-κB. *Biochem. Biophys. Res. Commun.* **314,** 197–207 (2004).

76. Antioxidant enzymes and human diseases. *Clin. Biochem.* **32,** 595–603 (1999).

77. Fukai, T. & Ushio-Fukai, M. Superoxide Dismutases: Role in Redox Signaling, Vascular Function, and Diseases. doi:10.1089/ars.2011.3999

78. Fujimura, M. *et al.* The Cytosolic Antioxidant Copper/Zinc-Superoxide Dismutase Prevents the Early Release of Mitochondrial Cytochrome c in Ischemic Brain after Transient Focal Cerebral Ischemia in Mice.

79. Gabryel, B. *et al.* Superoxide dismutase 1 and glutathione peroxidase 1 are involved in the protective effect of sulodexide on vascular endothelial cells exposed to oxygen–glucose deprivation. *Microvasc. Res.* **103,** 26–35 (2016).

80. Nojiri, H. *et al.* Cytoplasmic superoxide causes bone fragility owing to low-turnover osteoporosis and impaired collagen cross-linking. *J. Bone Miner. Res.* **26,** 2682–94 (2011).

81. Ilyas, A. *et al.* Amorphous Silica: A New Antioxidant Role for Rapid Critical-Sized Bone Defect Healing. *Adv. Healthc. Mater.* **5,** 2199–2213 (2016).

82. Choi, Y. J., Lee, J. Y., Chung, C. P. & Park, Y. J. Cell-penetrating superoxide dismutase attenuates oxidative stress-induced senescence by regulating the p53-p21(Cip1) pathway and restores osteoblastic differentiation in human dental pulp stem cells. *Int. J. Nanomedicine* **7,** 5091–106 (2012).

83. Chelikani, P., Fita, I. & Loewen, P. C. Diversity of structures and properties among catalases. *Cell. Mol. Life Sci.* **61,** 192–208 (2004).

84. Catalase and glutathione peroxidase mimics. *Biochem. Pharmacol.* **77,** 285–

296 (2009).

85. Bhabak, K. P. & Mugesh, G. Functional mimics of glutathione peroxidase: bioinspired synthetic antioxidants. *Acc. Chem. Res.* **43,** 1408–1419 (2010).

86. Förstermann, U. & Sessa, W. C. Nitric oxide synthases: regulation and function. *Eur. Heart J.* **33,** 829–37, 837a–837d (2012).

87. Aicher, A. *et al.* Essential role of endothelial nitric oxide synthase for mobilization of stem and progenitor cells. *Nat. Med.* **9,** 1370–1376 (2003).

88. Matsunaga, T. *et al.* Angiostatin inhibits coronary angiogenesis during impaired production of nitric oxide. *Circulation* **105,** 2185–2191 (2002).

89. Murohara, T. *et al.* Nitric oxide synthase modulates angiogenesis in response to tissue ischemia. *J. Clin. Invest.* **101,** 2567–2578 (1998).

90. Diwan, A. D., Wang, M. I. N. X., Jang, D., Zhu, W. E. I. & Murrell, G. A. C. Nitric Oxide Modulates Fracture Healing. *J. Bone Miner. Res.* **15,** 342–351 (2000).

91. Zhu, W., Diwan, a D., Lin, J. H. & Murrell, G. a. Nitric oxide synthase isoforms during fracture healing. *J. Bone Miner. Res.* **16,** 535–40 (2001).

92. Diwan, A. D., Khan, S. N., Cammisa, F. P., Sandhu, H. S. & Lane, J. M. Nitric oxide modulates recombinant human bone morphogenetic protein-2-induced corticocancellous autograft incorporation: A study in rat intertransverse fusion. *Eur. Spine J.* **19,** 931–939 (2010).

93. Chapple, S. J., Cheng, X. & Mann, G. E. Effects of 4-hydroxynonenal on vascular endothelial and smooth muscle cell redox signaling and function in health and disease. *Redox Biol.* **1,** 319–331 (2013).

94. Spickett, C. M. The lipid peroxidation product 4-hydroxy-2-nonenal: Advances in chemistry and analysis. *Redox Biol.* **1,** 145–152 (2013).

95. Alary, J., Guéraud, F. & Cravedi, J.-P. Fate of 4-hydroxynonenal in vivo: disposition and metabolic pathways. *Mol. Aspects Med.* **24,** 177–87

96. Andringa, K. K., Udoh, U. S., Landar, A. & Bailey, S. M. Proteomic analysis of 4-hydroxynonenal (4-HNE) modified proteins in liver mitochondria from chronic ethanol-fed rats. *Redox Biol.* **2,** 1038–1047 (2014).

97. Hill, B. G. *et al.* Myocardial ischaemia inhibits mitochondrial metabolism of 4-hydroxy-trans-2-nonenal. *Biochem. J.* **417,** 513–24 (2009).

98. Yang, W. *et al.* Age-dependent changes of the antioxidant system in rat livers are accompanied by altered mapk activation and a decline in motor signaling. *EXCLI J.* **14,** 1273–1290 (2015).

99. [43] Malondialdehyde determination as index of lipid Peroxidation. **186,** 421–431 (1990).

100. Dong Hyun Kim, Seung Jun Kwack, Kyung Sik Yoon, J. S. C. & B.-M. & Lee. 4-Hydroxynonenal: A Superior Oxidative Biomarker Compared to Malondialdehyde and Carbonyl Content Induced by Carbon Tetrachloride in Rats.

101. Spickett, C. M. The lipid peroxidation product 4-hydroxy-2-nonenal: Advances in chemistry and analysis. *Redox Biol.* **1,** 145–152 (2013).

102. Journal of Toxicology and Environmental Health, Part A. (2017). doi:10.1080/15287394.2015.1067505

103. Wilson, C. *et al.* HHS Public Access. **347,** 882–886 (2015).

104. Martin-Gallan, P., Carrascosa, A., Gussinye, M. & Dominguez, C. Biomarkers of diabetes-associated oxidative stress and antioxidant status in young diabetic patients with or without subclinical complications. *Free Radic. Biol. Med.* **34,** 1563–1574 (2003).

105. Haidara, M. A., Yassin, H. Z., Rateb, M., Ammar, H. & Zorkani, M. A. Role of oxidative stress in development of cardiovascular complications in diabetes mellitus. *Curr. Vasc. Pharmacol.* **4,** 215–227 (2006).

106. Chung, S. S. M., Ho, E. C. M., Lam, K. S. L. & Chung, S. K. Contribution of polyol pathway to diabetes-induced oxidative stress. *J. Am. Soc. Nephrol.* **14,** S233-6 (2003).

107. Bacevic, M. *et al.* Does Oxidative Stress Play a Role in Altered Characteristics of Diabetic Bone? A Systematic Review. *Calcif. Tissue Int.* **101,** 553–563 (2017).

108. Koloverou, E. *et al.* Moderate physical activity reduces 10-year diabetes incidence: the mediating role of oxidative stress biomarkers. *Int. J. Public Health* (2017). doi:10.1007/s00038-017-1052-8

109. Mancini, F. R. *et al.* Dietary antioxidant capacity and risk of type 2 diabetes in the large prospective E3N-EPIC cohort. *Diabetologia* (2017). doi:10.1007/s00125-017-4489-7

110. Lugrin, J., Rosenblatt-Velin, N., Parapanov, R. & Liaudet, L. The role of oxidative stress during inflammatory processes. *Biol. Chem.* **395,** 203–230 (2014).

111. Mittal, M., Siddiqui, M. R., Tran, K., Reddy, S. P. & Malik, A. B. Reactive oxygen species in inflammation and tissue injury. *Antioxid. Redox Signal.* **20,** 1126–

1167 (2014).

112. Li, X. *et al.* Targeting mitochondrial reactive oxygen species as novel therapy for inflammatory diseases and cancers. *J. Hematol. Oncol.* **6,** 19 (2013).

113. Eming, S. A., Krieg, T. & Davidson, J. M. Inflammation in wound repair: molecular and cellular mechanisms. *J. Invest. Dermatol.* **127,** 514–525 (2007).

114. Franz, S., Rammelt, S., Scharnweber, D. & Simon, J. C. Immune responses to implants - a review of the implications for the design of immunomodulatory biomaterials. *Biomaterials* **32,** 6692–6709 (2011).

115. Niethammer, P., Grabher, C., Look, A. T. & Mitchison, T. J. A tissue-scale gradient of hydrogen peroxide mediates rapid wound detection in zebrafish. *Nature* **459,** 996–999 (2009).

116. Kono, H. & Rock, K. L. How dying cells alert the immune system to danger. *Nat. Rev. Immunol.* **8,** 279–289 (2008).

117. Bryan, N. *et al.* Reactive oxygen species (ROS)--a family of fate deciding molecules pivotal in constructive inflammation and wound healing. *Eur. Cell. Mater.* **24,** 249–265 (2012).

118. Clanton, T. L. Hypoxia-induced reactive oxygen species formation in skeletal muscle. *J. Appl. Physiol.* **102,** 2379–2388 (2007).

119. Tan, S. *et al.* Peritoneal air exposure elicits an intestinal inflammation resulting in postoperative ileus. *Mediators Inflamm.* **2014,** 924296 (2014).

120. Rota, M. *et al.* Diabetes promotes cardiac stem cell aging and heart failure, which are prevented by deletion of the p66shc gene. *Circ. Res.* **99,** 42–52 (2006).

121. Bigarella, C. L., Liang, R. & Ghaffari, S. Stem cells and the impact of ROS signaling. *Development* **141,** 4206–4218 (2014).

122. von Grabowiecki, Y. *et al.* Regulation of a Notch3-Hes1 pathway and protective effect by a tocopherol-omega alkanol chain derivative in muscle atrophy. *J. Pharmacol. Exp. Ther.* **352,** 23–32 (2015).

123. Xavier, J. M., Morgado, A. L., Rodrigues, C. M. & Sola, S. Tauroursodeoxycholic acid increases neural stem cell pool and neuronal conversion by regulating mitochondria-cell cycle retrograde signaling. *Cell Cycle* **13,** 3576–3589 (2014).

124. Jin, R. *et al.* Trx1/TrxR1 system regulates post-selected DP thymocytes survival by modulating ASK1-JNK/p38 MAPK activities. *Immunol. Cell Biol.* **93,** 744–752 (2015).

125. Kim, K.-J., Lee, O.-H. & Lee, B.-Y. Low-molecular-weight fucoidan regulates myogenic differentiation through the mitogen-activated protein kinase pathway in C2C12 cells. *Br. J. Nutr.* **106,** 1836–1844 (2011).

126. Midwood, K. S., Williams, L. V. & Schwarzbauer, J. E. Tissue repair and the dynamics of the extracellular matrix. *Int. J. Biochem. Cell Biol.* **36,** 1031–1037 (2004).

127. Siwik, D. A., Pagano, P. J. & Colucci, W. S. Oxidative stress regulates collagen synthesis and matrix metalloproteinase activity in cardiac fibroblasts. *Am. J. Physiol. Cell Physiol.* **280,** C53-60 (2001).

128. Ozmen, I., Naziroglu, M. & Okutan, R. Comparative study of antioxidant enzymes in tissues surrounding implant in rabbits. *Cell Biochem. Funct.* **24,** 275–281 (2006).

129. Sansone, V., Pagani, D. & Melato, M. The effects on bone cells of metal ions released from orthopaedic implants. A review. *Clin. Cases Miner. Bone Metab.* **10,** 34–40 (2013).

130. Anderson, J. M., Rodriguez, A. & Chang, D. T. Foreign body reaction to biomaterials. *Semin. Immunol.* **20,** 86–100 (2008).

131. Gallorini, M. *et al.* Activation of the Nrf2-regulated antioxidant cell response inhibits HEMA-induced oxidative stress and supports cell viability. *Biomaterials* **56,** 114–128 (2015).

132. Saghiri, M. A., Asatourian, A., Orangi, J., Sorenson, C. M. & Sheibani, N. Functional role of inorganic trace elements in angiogenesis—Part I: N, Fe, Se, P, Au, and Ca. *Crit. Rev. Oncol.* **96,** 129–142 (2015).

133. Saghiri, M. A., Asatourian, A., Orangi, J., Sorenson, C. M. & Sheibani, N. Functional role of inorganic trace elements in angiogenesis—Part II: Cr, Si, Zn, Cu, and S. *Crit. Rev. Oncol. Hematol.* **96,** 143–155 (2015).

134. Saghiri, M. A. *et al.* Functional Role of Inorganic Trace Elements in in Angiogenesis Part III: (Ti, Li, Ce, As, Hg, Va, Nb and Pb) HHS Public Access. *Crit Rev Oncol Hematol* **98,** 290–301 (2016).

135. Kesteven, J., Kannan, M. B., Walter, R., Khakbaz, H. & Choe, H.-C. Low elastic modulus Ti-Ta alloys for load-bearing permanent implants: enhancing the biodegradation resistance by electrochemical surface engineering. *Mater. Sci. Eng. C. Mater. Biol. Appl.* **46,** 226–231 (2015).

136. Cohen, D. J. *et al.* Novel Osteogenic Ti-6Al-4V Device For Restoration Of Dental Function In Patients With Large Bone Deficiencies: Design, Development And

Implementation. *Sci. Rep.* **6,** 20493 (2016).

137. Ogawa, M., Tohma, Y., Ohgushi, H., Takakura, Y. & Tanaka, Y. Early fixation of cobalt-chromium based alloy surgical implants to bone using a tissue-engineering approach. *Int. J. Mol. Sci.* **13,** 5528–5541 (2012).

138. Lin, Y., McKinnon, K. E., Ha, S. W. & Beck, G. R. Inorganic phosphate induces cancer cell mediated angiogenesis dependent on forkhead box protein C2 (FOXC2) regulated osteopontin expression. *Mol. Carcinog.* **54,** 926–934 (2015).

139. Beck, G. R. J. & Knecht, N. Osteopontin regulation by inorganic phosphate is ERK1/2-, protein kinase C-, and proteasome-dependent. *J. Biol. Chem.* **278,** 41921–41929 (2003).

140. Stresing, V. *et al.* Nitrogen-containing bisphosphonates can inhibit angiogenesis in vivo without the involvement of farnesyl pyrophosphate synthase. *Bone* **48,** 259–266 (2011).

141. Liu, X., Chen, S., Tsoi, J. K. H. & Matinlinna, J. P. Binary titanium alloys as dental implant materials-a review. *Regen. Biomater.* **4,** 315–323 (2017).

142. Al-Sayed Ali, S. R. *et al.* Laser Powder Cladding of Ti-6Al-4V alpha/beta Alloy. *Mater. (Basel, Switzerland)* **10,** (2017).

143. Bonisch, M. *et al.* Giant thermal expansion and alpha-precipitation pathways in Ti-alloys. *Nat. Commun.* **8,** 1429 (2017).

144. Antanasova, M., Kocjan, A., Kovac, J., Zuzek, B. & Jevnikar, P. Influence of thermo-mechanical cycling on porcelain bonding to cobalt-chromium and titanium dental alloys fabricated by casting, milling, and selective laser melting. *J. Prosthodont. Res.* (2017). doi:10.1016/j.jpor.2017.08.007

145. An, N. *et al.* Proliferation, behavior, and cytokine gene expression of human umbilical vascular endothelial cells in response to different titanium surfaces. *J. Biomed. Mater. Res. A* **93,** 364–372 (2010).

146. Jo, D. H. *et al.* Anti-angiogenic effect of bare titanium dioxide nanoparticles on pathologic neovascularization without unbearable toxicity. *Nanomedicine* **10,** 1109–1117 (2014).

147. Montiel-Davalos, A. *et al.* Vanadium pentoxide induces activation and death of endothelial cells. *J. Appl. Toxicol.* **32,** 26–33 (2012).

148. Assem, F. L. & Levy, L. S. A review of current toxicological concerns on vanadium pentoxide and other vanadium compounds: gaps in knowledge and directions for future research. *J. Toxicol. Environ. Health. B. Crit. Rev.* **12,** 289–306 (2009).

149. Rodriguez-Mercado, J. J., Alvarez-Barrera, L. & Altamirano-Lozano, M. A. Chromosomal damage induced by vanadium oxides in human peripheral lymphocytes. *Drug Chem. Toxicol.* **33,** 97–102 (2010).

150. Shatos, M. A., Doherty, J. M. & Hoak, J. C. Alterations in human vascular endothelial cell function by oxygen free radicals. Platelet adherence and prostacyclin release. *Arterioscler. Thromb. a J. Vasc. Biol.* **11,** 594–601 (1991).

151. Yao, H., Guo, L., Jiang, B.-H., Luo, J. & Shi, X. Oxidative stress and chromium(VI) carcinogenesis. *J. Environ. Pathol. Toxicol. Oncol.* **27,** 77–88 (2008).

152. Ye, J. *et al.* Role of reactive oxygen species and p53 in chromium(VI)-induced apoptosis. *J. Biol. Chem.* **274,** 34974–34980 (1999).

153. Chang, S.-H. *et al.* Elevated inorganic phosphate stimulates Akt-ERK1/2-Mnk1 signaling in human lung cells. *Am. J. Respir. Cell Mol. Biol.* **35,** 528–539 (2006).

154. Jin, H. *et al.* High dietary inorganic phosphate affects lung through altering protein translation, cell cycle, and angiogenesis in developing mice. *Toxicol. Sci.* **100,** 215–223 (2007).

155. Camalier, C. E. *et al.* An integrated understanding of the physiological response to elevated extracellular phosphate. *J. Cell. Physiol.* **228,** 1536–1550 (2013).

156. Monkkonen, H. *et al.* Bisphosphonate-induced ATP analog formation and its effect on inhibition of cancer cell growth. *Anticancer. Drugs* **19,** 391–399 (2008).

157. Milkiewicz, M., Hudlicka, O., Brown, M. D. & Silgram, H. Nitric oxide, VEGF, and VEGFR-2: interactions in activity-induced angiogenesis in rat skeletal muscle. *Am. J. Physiol. Circ. Physiol.* **289,** H336–H343 (2005).

158. Dimmeler, S., Dernbach, E. & Zeiher, A. M. Phosphorylation of the endothelial nitric oxide synthase at Ser 1177 is required for VEGF-induced endothelial cell migration. *FEBS Lett* **477,** 258–262 (2000).

159. Saffarian Tousi, N. *et al.* Combinatorial effect of Si4 +, Ca2 +, and Mg 2 + released from bioactive glasses on osteoblast osteocalcin expression and biomineralization. *Mater. Sci. Eng. C* **33,** 2757–2765 (2013).

160. Odatsu, T. *et al.* Human periosteum cell osteogenic differentiation enhanced by ionic silicon release from porous amorphous silica fibrous scaffolds. *J. Biomed. Mater. Res. A* **103,** 2797–2806 (2015).

161. Wen, W.-S. *et al.* This article is protected by copyright. All rights reserved. *Int. J. Cancer* 1–23 (2013). doi:10.1002/elsc.201200179

162. Varanasi, V. G. *et al.* Si and Ca Individually and Combinatorially Target Enhanced MC3T3-E1 Subclone 4 Early Osteogenic Marker Expression. *J. Oral Implantol.* **38,** 325–336 (2012).

163. Zhai, W. *et al.* Silicate bioceramics induce angiogenesis during bone regeneration. (2012). doi:10.1016/j.actbio.2011.09.008

164. Haro Durand, L. a. *et al.* Angiogenic effects of ionic dissolution products released from a boron-doped 45S5 bioactive glass. *J. Mater. Chem. B* **3,** 1142–1148 (2015).

165. De Aza, P. N., Luklinska, Z. B., Santos, C., Guitian, F. & De Aza, S. Mechanism of bone-like formation on a bioactive implant in vivo. *Biomaterials* **24,** 1437–1445 (2003).

166. Hench, L. L. The story of Bioglass®. *J. Mater. Sci. Mater. Med.* **17,** 967–978 (2006).

167. Hoppe, A., Güldal, N. S. & Boccaccini, A. R. A review of the biological response to ionic dissolution products from bioactive glasses and glass-ceramics. *Biomaterials* **32,** 2757–74 (2011).

168. Wang, X., Li, X., Ito, A. & Sogo, Y. Synthesis and characterization of hierarchically macroporous and mesoporous CaO-MO-SiO 2-P 2O 5 (M = Mg, Zn, Sr) bioactive glass scaffolds. *Acta Biomater.* **7,** 3638–3644 (2011).

169. Day, R. M. Bioactive glass stimulates the secretion of angiogenic growth factors and angiogenesis in vitro. *Tissue Eng.* **11,** 768–777 (2005).

170. Keshaw, H., Forbes, A. & Day, R. M. Release of angiogenic growth factors from cells encapsulated in alginate beads with bioactive glass. *Biomaterials* **26,**

4171–4179 (2005).

171. Haro Durand, L. A. *et al.* In vitro human umbilical vein endothelial cells response to ionic dissolution products from lithium-containing 45S5 bioactive glass. *Materials (Basel).* **10,** (2017).

172. Vasudev, M. C., Anderson, K. D., Bunning, T. J., Tsukruk, V. V. & Naik, R. R. Exploration of Plasma-Enhanced Chemical Vapor Deposition as a Method for Thin-Film Fabrication with Biological Applications. *ACS Appl. Mater. Interfaces* **5,** 3983–3994 (2013).

173. Preparation of boron nitride thin films by microwave plasma enhanced CVD, for semiconductor applications. *Mater. Sci. Eng. B* **46,** 101–104 (1997).

174. Effect of CVD carbon coatings on Si@CNF composite as anode for lithium-ion batteries. *Nano Energy* **2,** 976–986 (2013).

175. Johnson, C. C., Wydeven, T. & Donohoe, K. Plasma-enhanced CVD silicon nitride antireflection coatings for solar cells. *Sol. Energy* **31,** 355–358 (1983).

176. Brennan, B. W. United States Patent [191 Stenberg [54]. **425,** 1–6 (1976).

177. Campbell, S. A. *Fabrication engineering at the micro- and nanoscale*.

178. Kushner, M. J. A model for the discharge kinetics and plasma chemistry during plasma enhanced chemical vapor deposition of amorphous silicon. *J. Appl. Phys.* **63,** 2532–2551 (1988).

179. Plasma enhanced chemical vapor deposition of amorphous, polymorphous and microcrystalline silicon films. *J. Non. Cryst. Solids* **266–269,** 31–37 (2000).

180. Ilyas, A., Lavrik, N. V., Kim, H. K. W., Aswath, P. B. & Varanasi, V. G. Enhanced

Interfacial Adhesion and Osteogenesis for Rapid ‘bone-like’ Biomineralization by PECVD-Based Silicon Oxynitride Overlays. *ACS Appl. Mater. Interfaces* **7,** 15368–15379 (2015).

181. Ilyas, A. *et al.* Amorphous Silica: A New Antioxidant Role for Rapid Critical-Sized Bone Defect Healing. *Adv. Healthc. Mater.* (2016). doi:10.1002/adhm.201600203

182. Chemical Vapor Deposition. Available at: https://cnx.org/contents/m7vjnKhA@2/Chemical-Vapor-Deposition. (Accessed: 21st November 2017)

183. 270716094_Abstract_682_Design_and_discovery_of_novel_small_molecule_modulators_of_reactive_oxygen_species-mediated_cell_signaling @ www.researchgate.net.

184. Kim, Y.-W. & Byzova, T. V. Oxidative stress in angiogenesis and vascular disease. doi:10.1182/blood

185. Bhabak, K. P. & Mugesh, G. Functional Mimics of Glutathione Peroxidase: Bioinspired Synthetic Antioxidants. *Acc. Chem. Res.* **43,** (1408).

18http://encyclopedia.che.engin.umich.edu/Pages/Reactors/CVDReactors/CVDReactors.html.Availableat:http://encyclopedia.che.engin.umich.edu/Pages/Reactors/CVDReactors/CVDReactors.html.

Illustrations

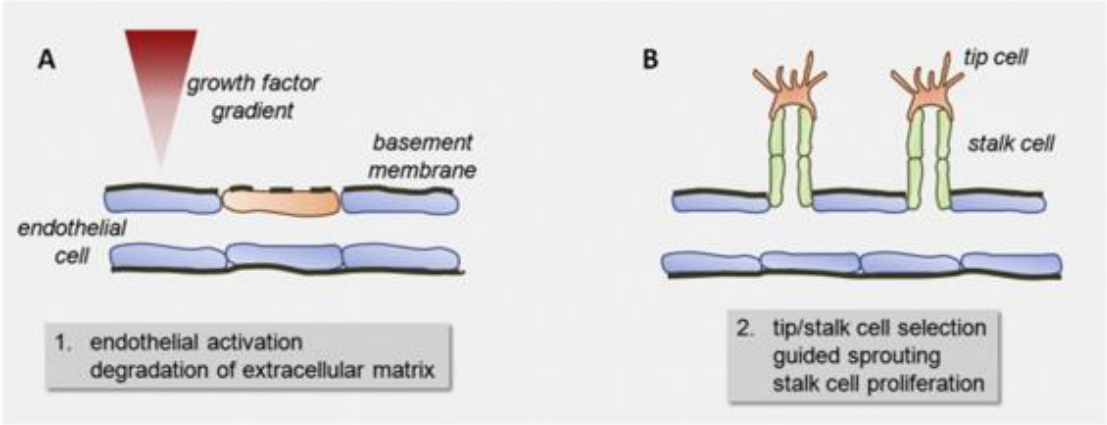

. **Figure 1**. Blood vessel formation. A) The initial stage of angiogenesis is the vessel sprouting. Growth factors trigger endothelial cells to destroy the basement membrane. (B) Tip cells migrate into the healing tissue and stalk cells proliferate.[50]

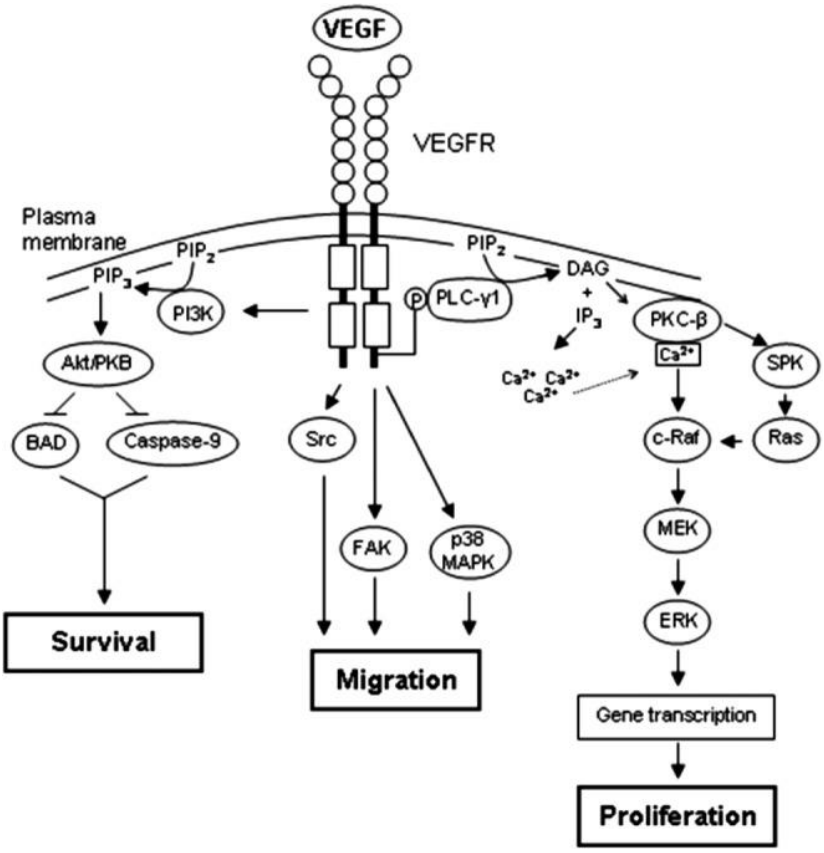

Figure 2. Schematic of VEGF activating VEGFR and down streaming angiogenic properties in endothelial cells.[60]

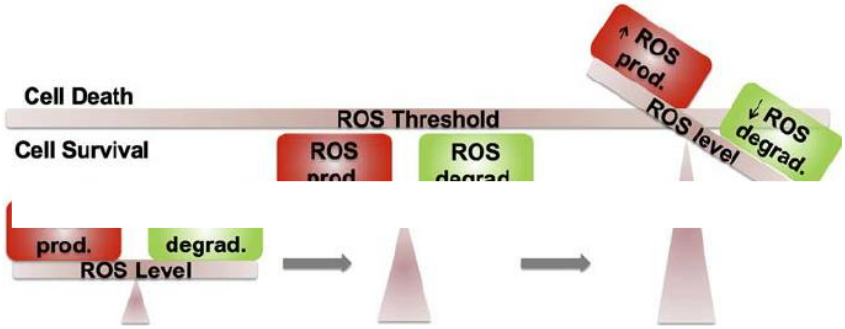

Figure 3. Schematic showing how equilibrium of between ROS production and degradation is important for normal cell physiology.[183]

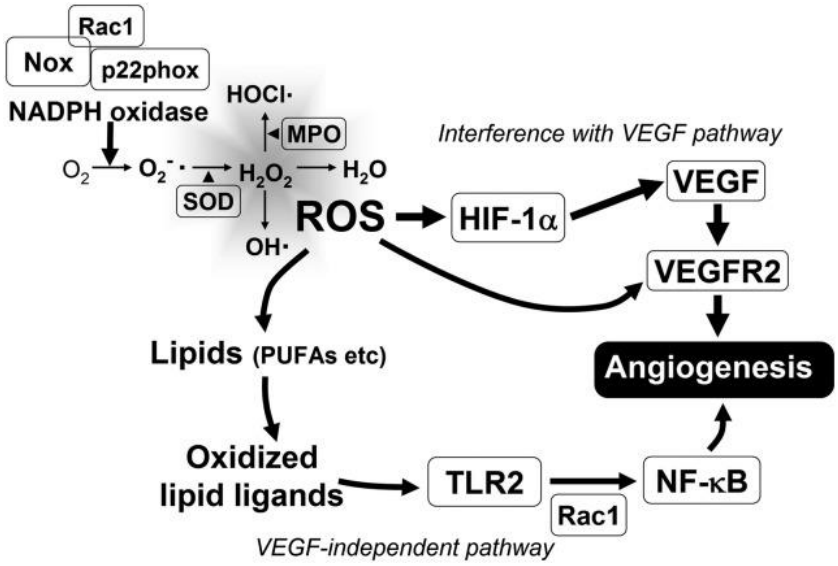

Figure 4. Shows schematic of nontoxic ROS generation and its effect on endothelial cells angiogenesis. It is shown two main mechanisms: ROS effect on HIF-VEGF/VEGFR2 signaling pathway and VEGF-independent mechanism involving generation of lipid oxidation products.[184]

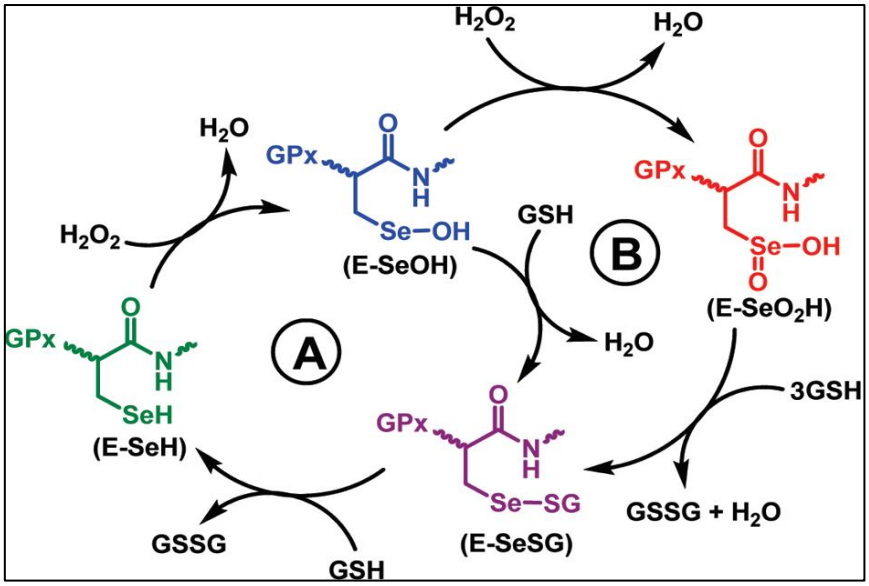

Figure 5. Schematic showing proposed mechanism for GPx antioxidant activity.[185]

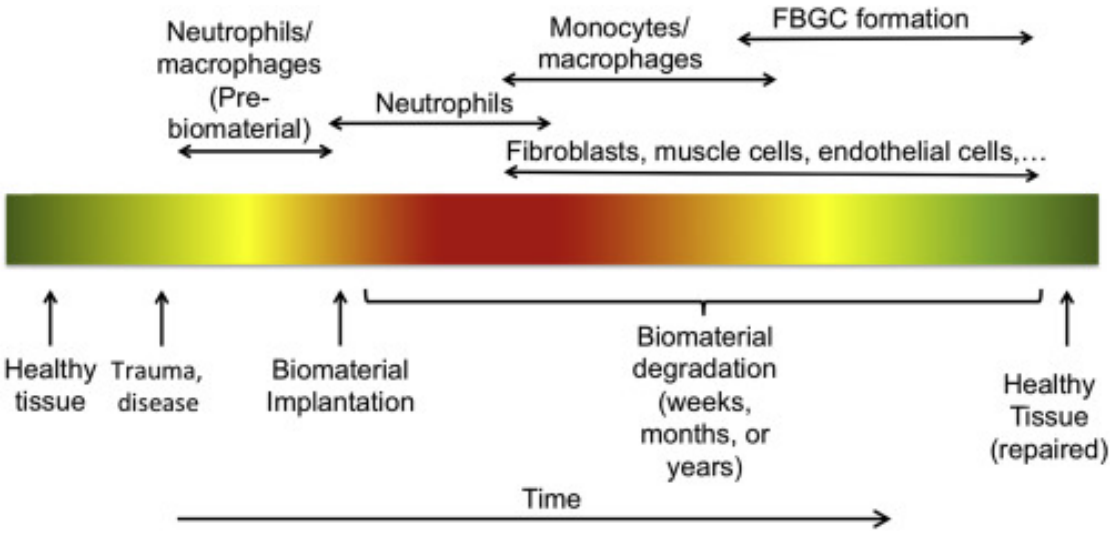

Figure 6. Oxidative stress time line before and after biomaterial implantation. process of trauma and healing with a biodegradable biomaterial (green: physiological levels of ROS and or its prodcuts, yellow: slightly elevated levels, red: high levels).[35]

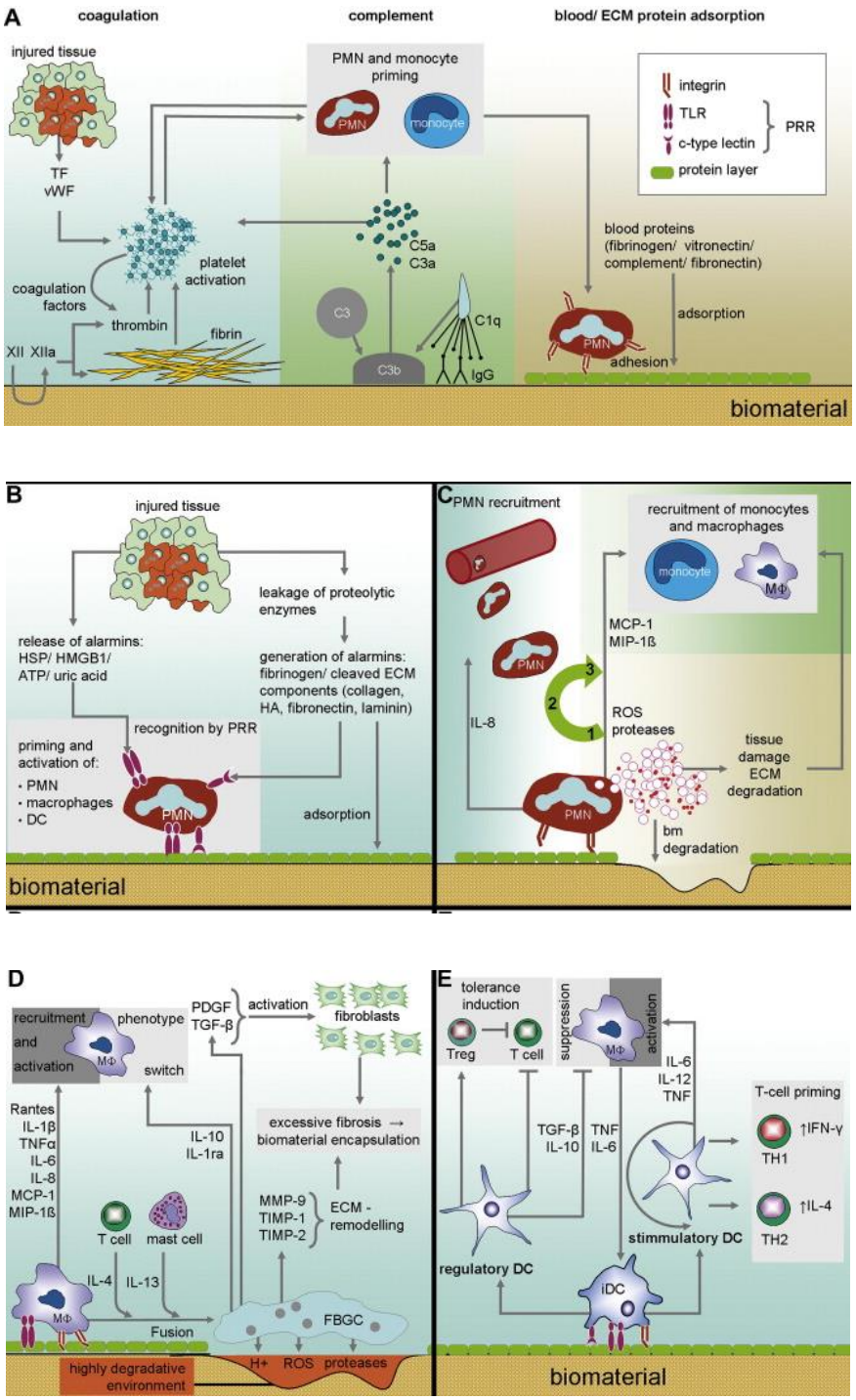

Figure 7. Immune response toward biomaterials. A) Protein adsorption and coagulation cascade activation. B) DAMPs relelased from the tissue. C) Acute inflammation and recruitment of polymorphonuclears (PMNs). In the transition to chronical stage there is immigration and activation of the monocytes and macrophages. D) Macrophages driving to chronic inflammation and release of an

inflammatory mediators and induction of macrophages fusion and formation of foreign body giant cells(FBGC). E) Activation of dendritic cells and amplification or suppression of the inflammatory response.[114]

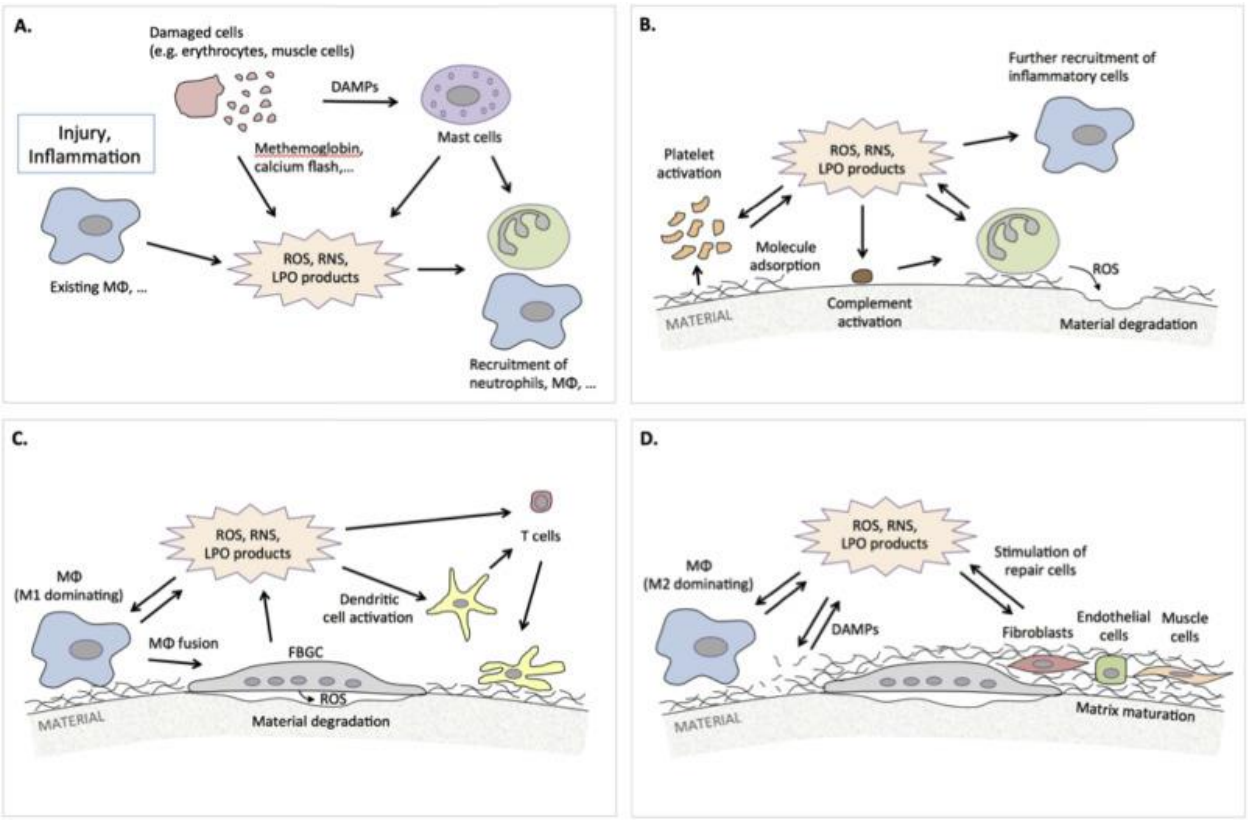

Figure 8. Role of oxidative stress in the inflammation and healing phase in the presence of biomaterials.[35]

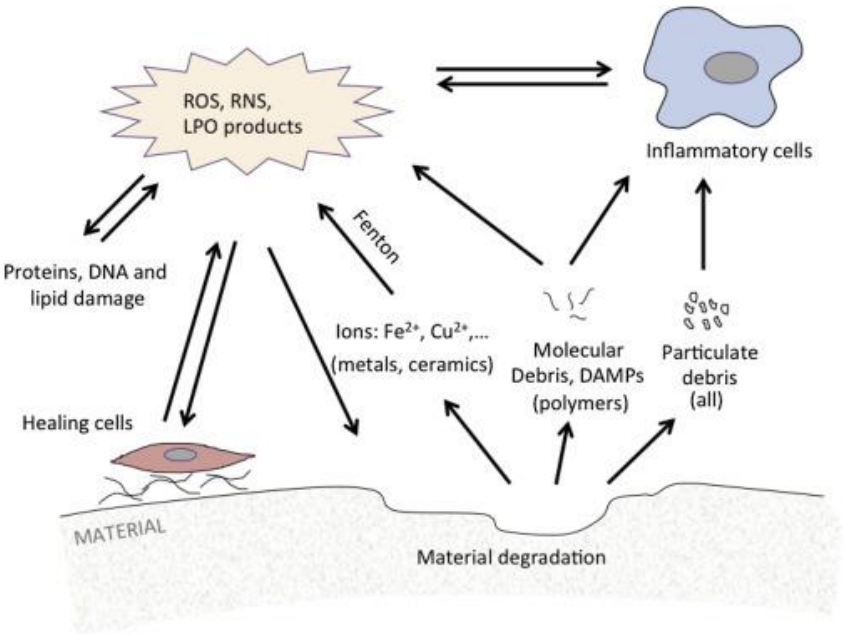

Figure 9. Schematic shows the interaction between the products of material degradation and oxidative stress.[35]

TRION ORION II

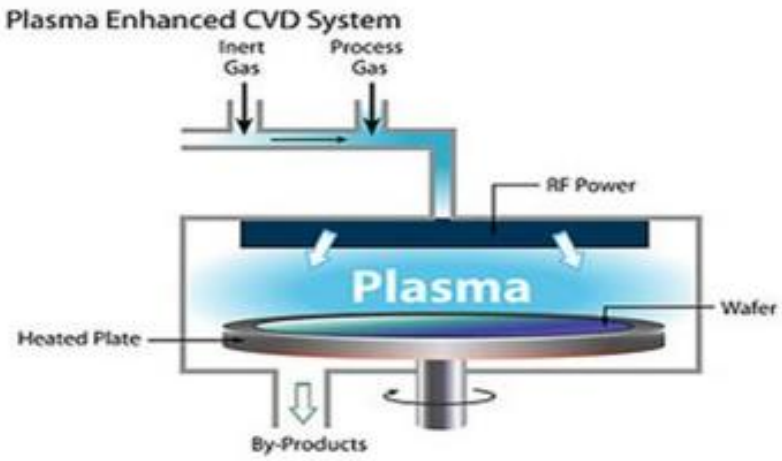

Figure 10. Picture (left) shows plasma enhanced chemical vapor deposition PECVD equipment TRION ORION, (Right) a schematic showing the mechanism.[186]

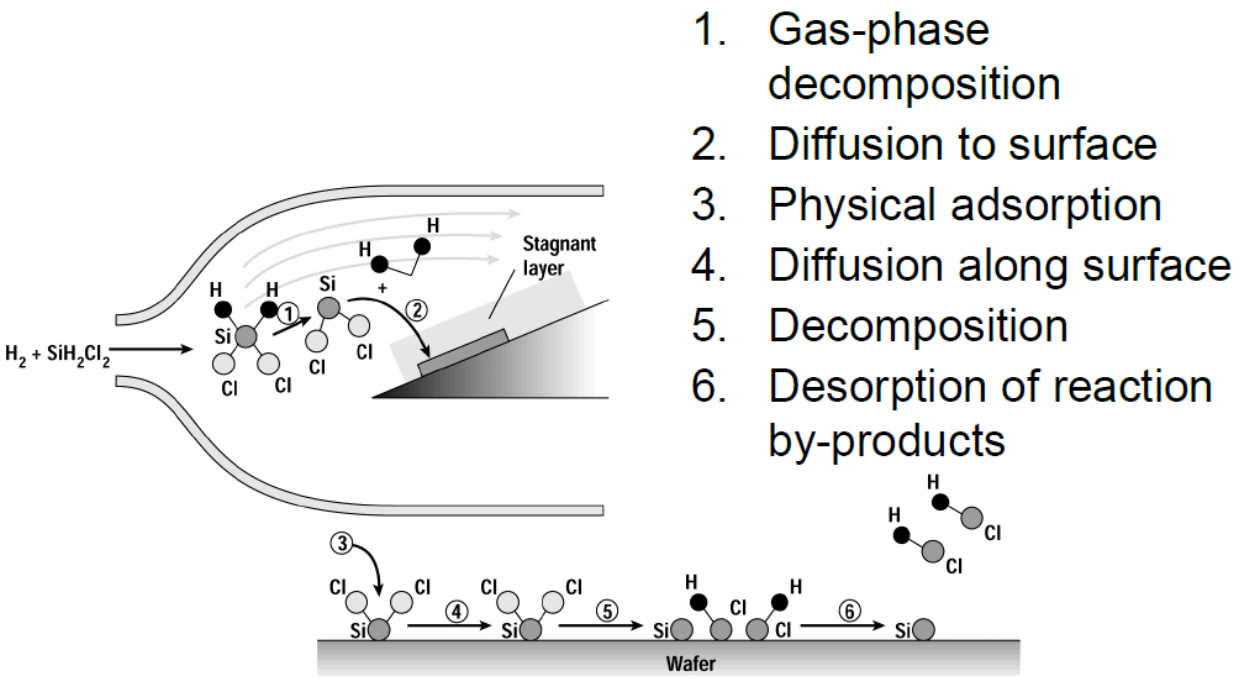

Figure 11. Schematic shows example of chemical vapor deposition (CVD) process.[177]

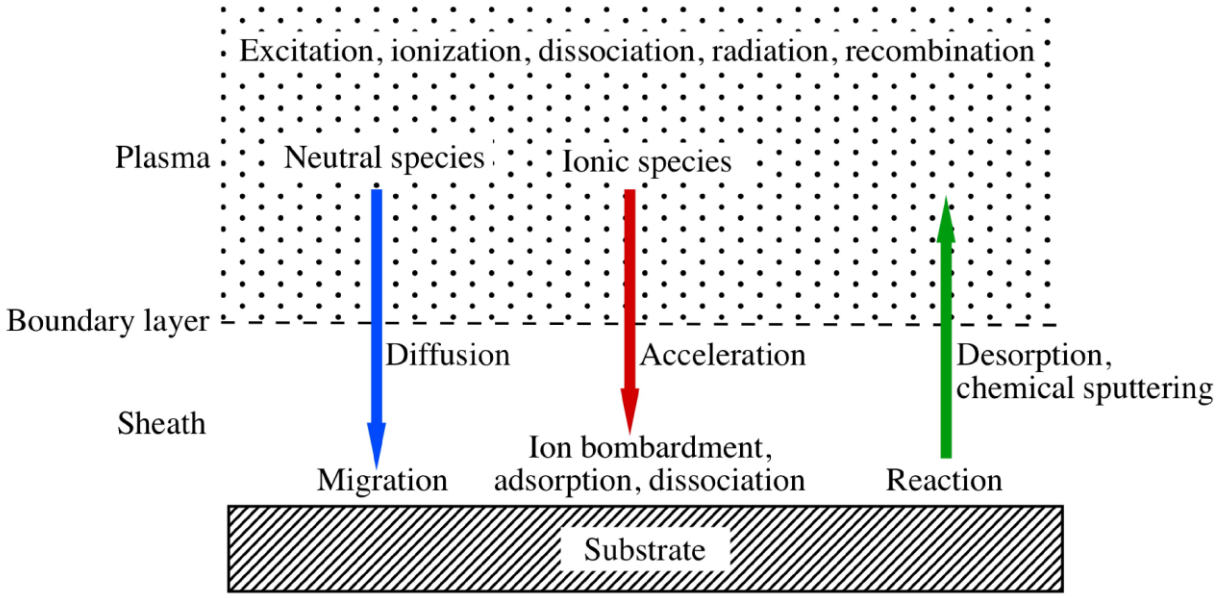

Figure 12. Shows processing steps of plasma enhanced chemical vapor deposition (PECVD) method.[182]

CHAPTER 3

IONIC SILICON IMPROVES HUMAN UMBILICAL VEIN ENDOTHELIAL CELLS' SURVIVAL UNDER HARMFUL HYDROGEN PEROXIDE CONDITIONS BY REDUCING CELL DEATH AND OVEREXPRESSING VEGFA, VEGFR-2 AND HIF-1α

Felipe Monte,[a,b] Tugba Cebe,[a] Daniel Ripperger,[c] Fareed Ighani,[c] Harry K.W. Kim,[b,d] Pranesh B. Aswath,[e] Venu G. Varanasi,[f]*

[a] Department of Bioengineering, University of Texas at Arlington, Arlington Texas 76019, USA

[b] Center for Excellence in Hip Disorders, Texas Scottish Rite Hospital, Dallas, Texas 75219, USA

[c] Department of Biomedical Sciences, Texas A&M University College of Dentistry, Dallas, Texas 75246, USA

[d] Department of Orthopedic Surgery, University of Texas Southwestern Medical Center at Dallas, Dallas, Texas 75390, USA

[e] Department of Materials Science and Engineering, University of Texas at Arlington, Arlington Texas 76019, USA

[*] To whom correspondence should be addressed:

Venu G. Varanasi, Ph.D.

3302 Gaston Avenue, Texas A&M Health Science Center, Dallas, Texas 75246, USA

Phone: +1-214-370-7006

Fax: +1-214-874-4538

E-mail: vvaranasi@tamhsc.edu

ABSTRACT

Oxidative stress, induced by harmful levels of reactive oxygen species (ROS), is a common occurrence that impairs proper bone defect vascular healing through the impairment of endothelial cell function. Ionic Silicon released from silica-based biomaterials, can upregulate hypoxia-inducible factor 1a (HIF-1a). Yet, it is unclear whether ionic Si can restore endothelial cell function under conditions of oxidative stress. Therefore, we hypothesized that silicon ion can help improve human umbilical vein endothelial cells' (HUVECS) survival under deleterious oxidative stress conditions. In this study, we evaluated the silicon ion's effect on HUVECs viability, proliferation, migration, gene expression, and capillary tube formation under normal conditions, and under harmful levels of hydrogen peroxide. Our results demonstrated that media, containing 0.5 mM Si4+, significantly enhanced cell viability and proliferation in HUVECs under normal conditions. Furthermore, 0.5 mM Si4+ enhanced cell migration more than two-fold, as compared to the control. HUVECs exposed to 0.5 mM Si4+ presented a conformational change, even without the bed of Matrigel, and tended to form significantly more tube-like structures than the control ($p<0.001$). In addition, 0.5 mM Si4+ enhanced cell viability in HUVECs under harmful hydrogen peroxide levels (0.6 mM), as well as using both live and dead fluorescent microscopy. HIF-1α, VEGFA, and VEGFR-2 were overexpressed more than two-fold in silicon-treated HUVECs, as compared to the control under harmful hydrogen peroxide concentrations (0.6mM). In conclusion, we demonstrated that 0.5 mM Si4+ can recover the HUVECs' viability under oxidative stress conditions by reducing cell death and upregulating VEGFA, HIF-1α, and VEGFR-2.

Keywords: Angiogenesis, ionic silicon, endothelial cells, oxidative stress, VEGFA, VEGFR-2, HIF-1α, cell survival.

1. Introduction

One million bone graft procedures are performed in the United States every year (Vacanti and Langer, 1999). Many of these procedures are used to correct large bone defects which are a hypoxic environment, rich in reactive oxygen species (ROS). The high levels of ROS create an oxidative stress that can damage the cells and make it difficult to enable adequate tissue regeneration (Ryter *et al.*, 2007,Tabak *et al.*, 2011). Hence, biomaterials have been used as bone substitute for treatment of these injuries. However, despite all the advances in bone tissue engineering, there are limitations in the ability to address the repair of large bone defects with a suitable biomaterial that can meet the requirements of biocompatibility and osteointegration. Moreover, there is limited understanding about the role played by these biomaterials in the healing area under oxidative stress induced by the deleterious hypoxic conditions.

There is remarkable evidence of silicon's effect in bone formation (Ryter *et al.*, 2007,Tabak *et al.*, 2011,Ilyas *et al.*, 2015,Odatsu *et al.*, 2015,Asselin *et al.*, 2004,Hench *et al.*, 1971,Renno *et al.*, 2013,Varanasi *et al.*, 2012,Wang *et al.*, 2014,Lu *et al.*, 2006). Silicon-based and Si-doped materials have been used as biomaterials to enhance bone regeneration, as they elicit mineral deposition and osteoblast differentiation(Ilyas *et al.*, 2015,Odatsu *et al.*, 2015). Currently, the biomaterials have been designed to act at a molecular level by stimulating a specific cellular response (Asselin *et al.*, 2004). Since the 1970's, with the discovery of bioactive glass 45S5 (Bioglass®) (Hench *et al.*, 1971), these Si-based materials have been shown to enhance bone healing and material-bone attachment through Si^{4+} and Ca^{2+} release, inducing deposition of a hydroxycarbonate apatite layer within a few hours (Renno *et*

al., 2013), posterior osteoblast differentiation, and collagen type I deposition (Varanasi *et al.*, 2012,Wang *et al.*, 2014) .

Angiogenesis is crucial for bone tissue repair (Lu *et al.*, 2006) and involves endothelial cell' migration, proliferation, differentiation, and tube formation (Saghiri *et al.*, 2015). The newly formed blood vessels transport the growth factors, cytokines, and progenitor cells to damaged tissue. A recent study correlated Si^{4+} release from mesoporous silica microspheres with hypoxia inducible factor 1α (HIF1-α) up regulation (Dashnyam *et al.*, 2017). Early on after trauma, tissue repair occurs in a hypoxic environment, and changes in mitochondrial activity occur, leading to reactive oxygen species' (ROS) over-production. Hypoxia can induce HIF-1α accumulation and angiogenesis downstream pathway activation (Solaini *et al.*, 2010). However, elevated levels of ROS create a cell damaging effect that can impede proper endothelial cell function (Sharma *et al.*, 2012). The threshold among physiologic, angiogenic, and hazardous levels of ROS depends on the cell type. While the mesenchymal stem cells are more sensitive to cell damage due to ROS, the endothelial cells have been shown to be more resilient (Wen *et al.*, 2013). Thus, it appears that the early effect of silicon ion released from biomaterials needs to be understood to establish the role of this element in angiogenesis under deleterious levels of oxidative stress.

Human umbilical vein endothelial cells (HUVECs) are well established for the study of the angiogenic effect of drugs and biomaterials *in vitro* (Morin and Tranquillo, 2013,Sivaraman *et al.*, 2017,Wang *et al.*, 2016). ROS are described as reactive molecules and free radicals derived from molecular oxygen; products generated from metal catalyzed oxygen reaction generated from mitochondrial activities. Under hypoxic conditions, the ROS levels can increase to concentrations that induce additional cellular damage. In particular, hydrogen peroxide is a major contributor to

oxidative damage (Solaini *et al.*, 2010). Large bone defects lead to hypoxia and production of deleterious levels of reactive oxygen species. These conditions are usually present in regions surrounding implants and biopolymers used for biological and structural support of bone defects. The studies mentioned above support the idea that silicon ion can have a positive effect on bone healing in pro-oxidant conditions by enhancing HIF-1α and improving angiogenesis. However, there is no conclusive study that evaluates the isolated effect of the silicon ion on HUVECs under harmful levels of reactive oxygen species. Thefore, this isolated effect is studied in this work.

Thus, we hypothesize that Si^{4+} at specific concentration(s) can enhance the HUVECs' viability in a toxic level of hydrogen peroxide by upregulating the gene expression of HIF-1α and, accordingly, VEGFA, and VEGFR-2. Our goal is to gain a new understanding of the ionic silicon on HUVECs under harmful oxidative stress levels and understand the element's role in angiogenesis during the early stages of tissue repair. First, the cells' viability, proliferation, tube formation, and migration in HUVECs under normal condition (culture media without H_2O_2) is verified, using three different Si^{4+} concentrations (0.1, 0.5 and 1 mM). Second, the cell viability and gene expression on HUVECs exposed to toxic levels of H_2O_2 treated with specific(s) Si^{4+} ions concentration(s) is tested.

2. Material and Methods

2.1 Silicon ion and hydrogen peroxide solutions preparation

The Si^{4+} solution was prepared by dissolving sodium meta-silicate - Na_2SiO_3 (1 mol l−1) in RNA free sterile water. After preparation, the solution was filtered using a nylon syringe filter (33mm, 0.2um, 50/PK) and followed by serial dilutions until the final dilution in endothelial cell culture media-2 (Lonza Walkersville, In) reached the desired Si^{4+} concentrations: 0.1 mM, 0.5 mM and 1.0 mM. Hydrogen peroxide (H_2O_2 30%

(w/v)) was used as the source of ROS and was diluted with sterile water followed by filtration, as mentioned above. Serial dilutions were made with sterile water until the desired H_2O_2 concentrations were reached: 0.2mM, 0.4 mM, 0.6 mM, 0.8 mM, 1.0 mM and 1.5 mM. The last dilution was made in the well-plate with the specific endothelial cell media.

2.2 Cell culture

Human umbilical vein endothelial cells (HUVECs) (Lonza Walkersville, In) were thawed and sub-cultured in 75 cm^2 Corning® cell culture flasks with canted neck and vented caps following manufacturer's protocol[4]. Endothelial cell growth media 2 (EGM-2) (Lonza Walkersville, In) was used for the HUVECs' expansion, and the media was changed every two days until the cells reached 70% confluence. The HUVECs were then sub-cultured. Cells from Passage 3 were used on all the designed experiments.

2.3 HUVECs' viability exposed to different H_2O_2 concentrations

A total of 3 x 10^4 cells/cm^2 were seeded per well in a 96 well-plate using a total volume of 100 µl of specific cell culture media (n=12/group), depending on the study. Endothelial Growth Media (EGM) was used as control, and the other six groups were formed by the H_2O_2 concentrations detailed earlier. The sterile water with H_2O_2 was placed on the bottom of the well before the reduced EGM; this was prepared by diluting EGM with Endothelial Basal Media (EBM) for a final concentration of 20% (v/v), and is labeled on this manuscript as EGM 20%, FBS concentration was corrected to 2% after dilution. Analyses were conducted after 6 and 24 hours, and 6 samples were used per time point for Calcein-AM (BD, Biosciences, CA) fluorescent staining, and 6 samples were used for CellTiter 96® AQueous One Solution Cell Proliferation Assay (MTS). First, the cells were prepared for the proliferation assay, and a solution was

prepared using 1mL of EBM per 100 µL of the reagent. After the specific time point, the cell culture media was removed from each well and 120 µl of the prepared solution was placed inside the well. After 3 hours, 60 µL of the solution was collected and placed in a new 96 well plate. This was read using a microplate reader POLARstar Omega BMG Labtech at a 490-nm wave length. Next, 50 µL of Calcein-AM 2mM was added to the other 6 wells/group and allowed to sit for 30 minutes. Fluorescent pictures were taken using the Carl Zeiss Axio Vert A1 TL/RL LED Inverted Microscope with the FITC light filter. All results presented were compared to the initial cell seeding density.

2.4 Silicon ion effect on HUVECs under normal conditions (viability and proliferation)

2.4.1 Cell viability

In all, 1.5 x10^4 cells/cm^2 were seeded per well with n=12 per group in the 5 groups: EBM + 0.1 % FBS (negative control), EGM (positive control), EBM + 0.1% FBS + Si^{4+} 0.1mM, EBM + 0.1% FBS + Si^{4+} 0.5 mM, and EBM + 0.1% FBS + Si^{4+} 1mM. After 6 and 24 hours, 6 samples per group on each time point were used for the MTS assay.

2.4.2 Cell proliferation

Totally, 1.5 x10^4 cells/cm^2 were seeded per well with n=12 per group in the 5 groups: EGM 20% (negative control), EGM (positive control), EGM 20% + Si 0.1 mM, EGM 20% + Si 0.5 mM, and EGM 20% + Si 1 mM. All groups with silicon ion were prepared with EGM 20%, with an aim to give more sensitivity to changes induced by the different Si^{4+} concentrations on HUVECs. In order to determine the best EGM dilution for this experiment, the cells were cultivated in EGM, diluted in three different concentrations. EGM at 20% dilution exhibited a significant difference ($p<0.01$) in cell proliferation, relative to control after 24 hours. The data was collected using the same methods mentioned in Section 2.3 at 6, 24, and 48 hours after cell seeding, using the MTS assay (n=6/group each time point) and Calcein-AM fluorescent staining

(n=6/group each time point) for pictures. Additionally, the fluorescent images were used for cell counting on ImageJ, v1.47 (National Institutes of Health, Bethesda, MD)(Rasband WS, 1997-2017).

2.5 Capillary-like tube formation assay under different Si^{4+} concentrations

2.5.1 HUVECs seeded on bed of Matrigel

The experimental design groups were the same as used in Section 2.4, with n=6 per group. The experiment was conducted according to previous studies (Information, 2014,Arnaoutova and Kleinman, 2010). Briefly, first, 50 µl of Matrigel® Matrix (Basement Membrane Phenol-Red Free) was placed at the bottom of each well and placed in an incubator at 37°C, with 95% relative humidity and 5% CO_2, for 30 minutes. Thereafter, 50,000/cm^2 cells were seeded per well, using 100 µL of specific media and/or Si^{4+}, as detailed above. The well plate was maintained in the incubator for 6 hours and was subsequently stained with Calcein-AM using the same method as mentioned in Section 2.3. Lastly, after 30 minutes, 3 different pictures were captured per well using Zeiss Fluorescent Microscopy FITC Filter at 5x magnification. The angiogenesis analyzer ImageJ plugin (Rasband WS, 1997-2017) was used for measuring the total tube length (pixels), number of nodes, number of meshes, and number of segments.

2.5.2 HUVECs seeded in well plates without Matrigel

Four groups were used for capillary-like tube formation without Matrigel: EGM (control) and the three silicon ion concentrations (0.1, 0.5, and 1.0 mM); 50,000 cells/cm^2 were seeded per well (n=5 per group) in a 96 well-plate using 100 µL of EGM-2. After 24 hours, the growth media from 3 of the 4 groups was changed to media with three different silicon ion concentrations, and the final group was replaced with new growth media to serve as the control. Three hours after the media change, the

cells were stained with Calcein-AM, following the protocol described. Three different 5x magnification images were captured per well using Zeiss fluorescent microscopy; FITC filter and ImageJ were used for calculations. A number of connected networks formed, indicating that conformational change of HUVECs into capillary precursor structures are presented.

2.6 Scratch wound healing assay

This experiment utilized three groups (n=3/group): EGM (positive control), EBM-2 (negative control), and Si^{4+} 0.5 mM + EBM (treatment). Initially, 50,000 cells were seeded in each well and cultured until they reached 90% cell confluence. A 200 µL pipette tip was used to make a scratch in a cross shape; the media was removed, and each well was washed two times with phosphate buffer solution (PBS). The new media was added according to the groups described above. A 5x magnification bright field image was taken just after the addition of the new media (t0). After 12 hours (t12), the wells were washed with PBS, fixed with 4% paraformaldehyde solution, and stained with toluidine blue. Images were captured from the same area as the t0 images, and the percentage of occupied area at t12 was calculated using the Wound Healing ImageJ software plugin (Rasband, 1997-2017).

2.7 Transwell migration assay

The cell migration by transwell membrane was tested in triplicate in the following groups: EGM (positive control), EBM + 2% FBS (negative control), and EBM + 2% FBS + Si^{4+} 0.5 mM (treatment). In all, 30,000 cells were seeded in the upper chamber of the 8 µM Transwell (Castor Inc) in 100 µL EBM. Thereafter, 600 µL of studied media was placed at the bottom of the well and the cells were allowed to migrate through the micropores for 12 hours; the HUVECs were fixed with 4%

paraformaldehyde solution. After fixation, the cells from the upper part of the well were removed using a cotton swab, and the remaining cells (bottom/migrated cells) were stained with DAPI (P369, Invitrogen) for nuclear visualization. Finally, three images per well were captured at 5x, 10x, 20x, and 40x magnification view using Zeiss Fluorescent Inverted Microscopy, and ImageJ software was used for cell counting.

2.8 Effect of Si on HUVECs under harmful hydrogen peroxide level

2.8.1 Cell viability

The Si^{4+} and H_2O_2 solutions and cells suspensions were prepared following the method mentioned in Sections 2.3 and 2.4. The experiment used three experimental groups: EGM, EGM + H_2O_2 0.6 mM, and EGM H_2O_2 0.6 mM + Si 0.5 mM (treatment). Both 0.6 mM H_2O_2 and Si^{4+} 0.5 mM were used, based on the results observed in the previous sections. Totally, 15,000 cells/cm^2 were seeded per well in a 96 well-plate with twelve samples per group (n=12). The data was collected after 6 and 24 hours. In all, 6 samples per group were used for the MTS assay, and 6 samples per group were used for live and dead fluorescent microscopy staining with Calcein-AM (3µM) and propidium iodite (4.5 µM) diluted in warm DPBS. Analyzed data is presented relative to control (EGM).

2.8.2 Quantitative real-time polymerase chain reaction (qRT-PCR)

In total, 500,000 cells were seeded in a 6 well-plate (n=6/group) and cultured for 24 hours. The experimental groups were the same used for viability (Section 2.8.1). First, the cells were lysed using the buffer RLT (guanidinum thiocyanate) with 10 µl β-Mercaptoethanol per 1 mL of buffer. Second, the cells were sheared using rubber scrapper under mild pressure to lyse the cells and collect mRNA (RNeasy Mini Kit, Qiagen, Valencia, CA, USA), which were then converted to cDNA using qRT-PCR method (Reverse Transcription System, Promega, Madison, WI, USA) according to

manufacturer's protocol. Both mRNA and cDNA were quantified during the process using microvolume UV-VIS spectrophotometer (Nano Drop 2000c, Thermo Fisher Scientific Inc., Watham, MA, USA). Reference gene 18S was used as housekeeping to be considered more specific to HUVEC cells (Chen *et al.*, 2013), and GAPDH was also used as housekeeping for better comparison with other studies. Lastly, relative quantification of gene expression was evaluated by comparing the cycle threshold (CT) method and fold change, calculated using $2^{-\Delta\Delta CT}$. The studied genes included VEGFA, KDR and HIF1-α (Table 1). The data was calculated relative to the housekeeping genes and compared to control (EGM 20%).

2.9 Statistical Methods

Data are expressed as means and standard deviations. Statistical analysis was performed using a one-way ANOVA with post-hoc Tukey's Pairwise for comparison amongst all groups, and Student t-test for comparison between groups. The significant level was considered when $p<0.05$. Past3 version 3.15 and OriginPro 2015 Statistical Softwares were used for calculations and graphs.

Sample size was determined based on the number of groups and standard deviation from the pilot study, and G*Power 3 version 3.0.5 Statistical Software was used for calculations.

A confidence interval of 95% and a statistical power of 80% for all required calculations were considered.

Analyzed data is presented on bar graphs, cell viability and proliferation under ROS environment, and normal condition is shown relative to initial cell seeding; cell migration assays are presented relative to positive control. The gene expression is shown relative to the housekeeping gene and compared to control. Capillary tube formation was not normalized.

3. Results

3.1 HUVECs viability exposed to different H_2O_2 concentrations

HUVECs were exposed to different concentrations of H_2O_2 to determine cell viability at 6 and 24 hours). MTS proliferation assay showed that H_2O_2 0.2 and 0.4 mM presented no significant difference compared to control (EGM without H_2O_2). However, the viable cells' number was significantly increased compared to the other H_2O_2 groups ($p<0.001$) (Figure 1A). H_2O_2 0.6 mM was the first studied level to demonstrate a significant decrease compared to control ($p<0.001$) (Figure 1A). The other groups, H_2O_2 > 0.6 mM, demonstrated to be highly toxic to HUVECs after 24 hours, with a significant decrease or absent viable cells number. H_2O_2 0.6 mM was considered and used for our experiment due to its capability of maintaining cell survival at a recoverable level, showing approximately 55% cell viability relative to initial cell seeding. Moreover, this concentration significantly reduced the viable HUVECs' number, as compared with control to 45±21%, ($p<0.001$) and 64±23% ($p<0.001$) after 6, and 24 hours, respectively (Figure 1A). The Calcein-AM fluorescent images corroborate the MTS assay results, showing the reduction of viable cells at 6 and 24 hours (Figure 1B).

3.2 Silicon ion effect on HUVECs under normal condition

3.2.1 Cell viability

The effect of the silicon ion on the HUVECs' viability was tested under normal conditions. The silicon ion had no cytotoxic effect on any concentrations used in this experiment; all groups presented an increase in cell number compared with the initial cell seeding. However, after 6 hours, the cells exposed to Si^{4+} 1.0 mM presented no significant increase. At 24 hours, Si^{4+} 0.5 mM presented a significant increase in the relative cell number (3.21 ±0.05 fold, $p<0.05$) compared with the 0.1, 1.0 mM silicon

concentrations, and negative control (EBM). The positive control (EGM) showed the most significant increase in viable cells number (3.95 ±0.07 fold, $p<0.05$) (Figure 1A).

3.2.2 Cell proliferation

Cell proliferation was tested at 6 and 24 hours. After 6 hours, the groups with silicon ion presented similarly to the 2-fold more cells than control groups ($p<0.05$). At 24 hours, the positive control (EGM) presented a significant increase (4.6 ± 0.22 fold) ($p<0.05$) among all groups. Finally, 48 hours after initial cell seeding, the positive control (EGM) had the most significant cell growth (8.04 ±0.42 fold, $p<0.01$). Nevertheless, among the silicon ion groups, the Si^{4+} 0.5 mM presented a significant increase of cell growth (4.39 ±0.28 fold, $p<0.05$) compared to the Si^{4+} 0.1 mM (3.44 ±0.25 fold) and Si^{4+} 1.0 mM (3.12 ±0.34 fold) groups (Figure 2B).

After 48 hours, the viable cell counting relative to positive control (EGM), showed that the 0.5 mM Si^{4+} group presented 2-fold more than the other silicon ion groups ($p<0.05$) and 5-fold greater than the negative control (EGM 20%, $p<0.01$) (Figures 2C and 2D).

3.3 Capillary tubule formation

3.3.1 HUVECs seeded on bed of Matrigel

Capillary tube formation of HUVECs was tested on a bed of Matrigel exposed to different silicon ion concentrations: EGM (positive control) and EBM (negative control) specific environment. Si^{4+} 0.5 mM samples showed a significant enhancement of capillary tube formation among all groups, especially on the number of meshes ($p<0.01$), which is closely related with pre-capillary structure maturity (Figures 3A and 3B).

3.3.2 HUVECS seeded without Matrigel

All silicon ion groups presented a conformational cell shape change with the cells tending to form a capillary precursor structure (circular structures labeled in Figure 3C). All silicon groups formed significantly greater number of connected networks, at least 10-fold more than control (EGM). The 0.5 mM Si^{4+} group formed 10-fold more connected networks than the 0.1 mM Si^{4+} ($p<0.05$) and 20-fold more than the 1.0 mM Si^{4+} group ($p<0.01$) (Figure 3D).

3.4 Scratch wound healing assay

A wound healing assay was used to test the amount of cell migration on a scratched surface. After fixation and staining with Toluidine blue, the bright field pictures (5x view) show the greatest amount of cell migration across the scratched area of the positive control group (EGM), followed by EBM + 0.5 mM Si^{4+}. (Figure 4A). After measurements using Wound Healing (ImageJ plug-in), the data analysis showed that the addition of 0.5 mM Si^{4+} to EBM increased the HUVEC migration almost 3-fold on the scratched area after 12 hours (Figure 4B).

3.5 Transwell migration assay

After fixation of the HUVECs, DAPI staining, and image capturing in 10x, 20x, and 40x (Figure 4C), the number of migrated cells were calculated. The data shows that the silicon treatment group presented approximately two-fold increase in migrated cell numbers, as compared to the negative control (EBM + 2% FBS, $p<0.05$) (Figures 4C and 4D).

3.6 Effect of Silicon ion on HUVECs under harmful hydrogen peroxide level

3.6.1 Cell viability

After 6 and 24 hours, the silicon treatment group presented a significant increase in the live cells number, as compared to the non-treatment group ($p<0.05$)

(Figures 5A and 5B). After 24 hours, HUVECs exposed to harmful levels of hydrogen peroxide (H_2O_2 0.6 mM), and silicon ion 0.5 mM simultaneously, presented almost 3-fold decrease in dead cell numbers, as compared to cells exposed to hydrogen peroxide without silicon treatment ($p<0.05$) (Figure 5C and 5D).

3.6.2 Quantitative real-time polymerase chain reaction (qRT-PCR)

After 24 hours of cell seeding, the cell lysate was collected and analyzed. All groups were compared with control EBM 20% and expressed relative to the housekeeping genes 18S and GAPDH. Cells exposed to 0.6 mM H_2O_2 presented a significant decrease of studied angiogenic genes expression, as compared to the control ($p<0.01$). Cells exposed to the silicon ion presented a significant increase in the expression of all angiogenic genes studied ($p<0.001$). The difference was more evident when compared to the 18S housekeeping gene: VEGF (7.13 ±0.54 fold, $p<0.01$), KDR (4.92 ±1.18 fold, $p<0.01$), and HIF-1α (5.97 ±2 fold, $p<0.01$) (Figure 6A). Similarly, but with less intensity, all genes were significantly overexpressed relative to GAPDH: VEGF (5.3 ±1 fold, $p<0.05$), KDR (4 ±0.73 fold, $p<0.05$) and HIF-1α (3 ±0.86 fold, $p<0.05$) (Figure 6B).

The results show that cells exposed to 0.6 mM H_2O_2 and treated with 0.5 mM Si^{4+} presented a significant over-expression as compared to the control, and relative to the 18S housekeeping gene: VEGFA (3.49 ±0.75 fold, $p<0.01$), KDR (2.38 ±0.58 fold), HIF-1α (2.77 ±0.45 fold) (Figure 6A). When GAPDH was considered as the housekeeping gene, there was a significant over-expression of VEGFA (4.36 ±0.68 fold, $p<0.001$) and HIF-1α (1.73 ± 0.42 fold, $p<0.05$) (Figure 6B).

4. Discussion

Our study shows the novel effect of the ionic silicon on HUVECs under harmful oxidative stress. There was significant enhancement on cell viability and reduction of

cell death on HUVECs exposed to H_2O_2 0.6 mM in the presence of Si^{4+} 0.5 mM. Furthermore, the same condition exhibited an enhancement on expression of VEGFA, VEGFR-2, and HIF-1α, which are major angiogenic markers.

The concentration of 0.6 mM hydrogen peroxide was selected for these experiments due to its significant reduction of HUVEC viability. The chosen concentration also allowed some degree of cell survival, which could be enough for cell recovery by the positive effect of the silicon ion. Other studies have used this same concept (Wen *et al.*, 2013) , but we verified the conditions for our designed experiment because, as mentioned in the material section, we have used a unique combination of cells and growth media. Superoxide is the main reactive oxygen species produced in hypoxic conditions. Nevertheless, it is highly unstable and gets converted to hydrogen peroxide (Kim and Byzova, 2014). Hence, hydrogen peroxide has been used in a variety of studies (Csordas *et al.*, 2006,Wei *et al.*, 2010,Wen *et al.*, 2013,Song *et al.*, 2014)[5–8].

Oxidative stress is a condition present at the beginning of bone regeneration after trauma, and can lead to a deleterious effect on osteoblasts and endothelial cells, impairing new bone and vascular structure and formation (Prasad *et al.*, 2003,Yeler *et al.*, 2005,Arai *et al.*, 2007). In vivo models are unable to precisely identify the reactive species levels and toxicity due to its molecular instability. Therefore, reactive oxygen species' production has been specifically studied in vitro. Some studies used hypoxic chamber (Yang *et al.*, 2014,Zhang *et al.*, 2016), but hydrogen peroxide appears to more realistically mimic the oxidative stress in an acute bone loss situation. The concentration of H_2O_2 is controversial, depending on a variety of factors, such as condition media, cell type, and passage. In our study, we used H_2O_2 0.6 mM, similar

studies have been designed with other concentrations due to usage of different condition media and cells (Csordas *et al.*, 2006,Wei *et al.*, 2010,Wen *et al.*, 2013).

Our study investigated the effect of three silicon ion concentrations (0.1, 0.5, and 1.0 mM) on the HUVECs' viability and proliferation under normal conditions (non pro-oxidant or no H_2O_2). The experimental silicon concentrations were non-toxic to the HUVECs at the concentrations tested. Thus, 0.5 mM Si^{4+} showed an increase in cell proliferation after 48 hours, potentially being a therapeutic dosage for use in unfavorable situations, such as after a trauma or injury, to combat the harmful hydrogen peroxide concentrations observed in these hypoxic environments. Contrary to our observation, a study using the same silicon ion groups showed no effect on the HUVEC's proliferation under normal conditions (Robertson, 2009). We believe that the difference observed in our experiment was due to specific changes and reductions in the growth factor used in the cell culture media of silicon ion groups, allowing the cells to be exposed to an in vitro environment with enough nutrition to demonstrate a potentially beneficial effect of the silicon ion on cell proliferation and without significant added effect from growth factors. The enhancement on cell proliferation can be associated with VEGFR2 and VEGFA upregulation, such as was described previously (Koch *et al.*, 2011), and observed in the gene expression of the present study (Figure 6).

All silicon ion concentrations used in this study induced marked conformational change, forming enhanced capillary-like structure on the HUVECs cultured in normal condition without Matrigel (Figure 3C and 3D). This observation needs further investigation to better understand silicon's effect on the cytoskeleton and cell-to-cell interaction. The tube formation on the bed of Matrigel showed the enhancement of capillary-like tube formation precursors in the presence of 0.5 mM Si^{4+}, particularly

demonstrated by the increased number of matured structures and mesh networks (Figure 3A and 3B). Some studies, which evaluated materials based on silicon, also presented a similar result; however, the effect was verified in combination with other elements, such as calcium and magnesium (Dashnyam *et al.*, 2017,Kong *et al.*, 2014). Endothelium cells' capillary tube formation is correlated with a cascade downstream of integrin ligation induced by cell matrix interaction (Davis and Senger, 2005,Davis *et al.*, 2007). Nesprin are proteins that link the cell nuclei to the cytoskeleton and are associated with the HUVECs' loop formation during angiogenesis (King *et al.*, 2014). We speculate that Si^{4+}can have some effect on the cell matrix interaction and/or nesprin activation and expression, and further investigation is necessary for clarification.

The presence of silicon ion increased the capillary tube formation structure, with, and without Matrigel. At the same time point, the three silicon groups demonstrated an enhancement of 2-fold on the cell proliferation compared to the controls (Figure 2B, 2C and 2D). However, capillary tube formation assay with Matrigel cannot be correlated with the first 6 hours' proliferation results (Figure 2B), because the cell culture condition of Matrigel is rich in endothelial cells' growth factor, and proteins are not present in the cell culture media used in the proliferation study. The same must be considered in the tube formation experiment without Matrigel, when a marked increase in the capillary-like tube structure was observed in groups with silicon and minimum cell culture condition on EBM (without growth factors) (Figures 3C and 3D).

The present study showed that 0.5 mM Si^{4+} significantly increased cell migration in the scratch assay (Figures 4A and 4B) and had a chemotactic effect on HUVECs, confirmed by the transwell cell migration, which showed significant

improvement as compared to the negative control (EBM) (Figures 4C and 4D). Cell migration is a relevant phenomenon during angiogenesis, and its enhancement would greatly impact the tissue healing process. The transwell cell migration simulated the effect of silicon ions released by the biomaterials used in bone tissue replacement and/or stabilizer. Both results were reinforced by a current publication which used mesoporous silica (Dashnyam *et al.*, 2017).

The present study demonstrates that HUVECs exposed to H_2O_2 0.6 mM (toxic levels) and treated with Si^{4+} 0.5 mM reduces cell death and enhancement of cell survival on live/dead cell fluorescent staining (Figure 5). These findings suggest that the silicon ion can limit cell death during the first 24 hours, on cells exposed to unfavorable oxidative stress present in injuries and bone loss. Recently, a few studies have been focused on effects of biomaterials/implants used on oxidative stress induced by bone defects (Ilyas *et al.*, 2016,Sansone *et al.*, 2013). These studies have focused on the long term outcome of oxidative stress and its association with implant loosening and failure (Sansone *et al.*, 2013,Pietropaoli *et al.*, 2013,Kinov *et al.*, 2006) . Yet, these studies neglected research on early time points, as the period is crucial for angiogenesis and efficient tissue repair for improved long-term implant or biomaterial attachment and potentially reduce failure rates.

The studied angiogenic genes expressed a consistent pattern with significant overexpression under harmful oxidative stress when treated with the silicon ion (Figure 6), reinforcing the observation of live/dead HUVEC microscopy and MTS proliferation assays. (Figure 5). Studies correlate silicon-based materials with a positive effect on angiogenesis and enhanced expression of VEGF and VEGFR-2 in HUVECs *in vitro* (Li and Chang, 2013,Zhai *et al.*, 2012). Nevertheless, none of these studies showed

the effect of ionic silicon in HUVECs angiogenesis in the real clinical situation of unfavorable oxidative stress.

Our study showed under-expression of VEGFA, VEGFR-2 and HIF-1α in HUVECs exposed to a harmful hydrogen peroxide concentration and recovery, with over-expression in silicon treatment groups. HIF-1α over-expression in a treatment group corroborates the fact that HUVECs have a higher survival rate and less cell death under harmful H_2O_2 concentrations. HIF-1α activation is a master event in the down-stream signaling of angiogenesis (Krock *et al.*, 2011). HIF-1α is necessary for blood vessel invasion and progenitor cell survival in hypoxic and damaged environments, especially when the blood vessels have not reached the site of injury. Downstream in the pathway, HIF-1α reduces oxygen consumption to help avoid harmful ROS accumulation (Stegen *et al.*, 2016). HIF-1α proved to be essential for new bone formation on the osteoblast progenitor cells by upregulating the angiogenic markers (Stegen *et al.*, 2016). A recent publication showed a relationship between the silicon ion released from mesoporous microcarriers and HIF1-α upregulation by HUVECs under regular cell culture media conditions without toxic levels of reactive oxygen species (Dashnyam *et al.*, 2017). Our results corroborated these findings and showed increased HIF-1α expressed in HUVECs exposed to harmful levels of hydrogen peroxide.

The present study shows that VEGFA expression is significantly increased in HUVECs exposed to 0.5 mM Si^{4+}, even when the cells were under harmful oxidative stress. The VEGFR2 followed the same pattern but with less increase. Vascular endothelial growth factor-A (VEGFA) and analogous receptor (VEGFR-2) are crucial in both angiogenesis and regulation of long term blood vessel formation (Hu and Olsen, 2016) . Moreover, VEGFA and VEGFR-2 play a significant role in the different

stages of endochondral and intramembranous ossification, having a paracrine, autocrine, and intracrine effect on osteoblast function during the bone repair (Hu and Olsen, 2016). Hence, our results support the beneficial effect of Si^{4+} under normal and deleterious levels of H_2O_2, showing overexpression of the relevant genes related with new blood vessel formation.

The effect that Si^{4+} plays on angiogenesis could be analogous to our previous work in osteogenesis. In that work (Ilyas *et al.*, 2016), it was found that osteogenic transcription was dependent on ionic Si enhancement of SOD1. It is possible that a similar link could have occurred for angiogenesis. For example, elevated superoxide dismutase activity (6-fold) under hypoxic conditions (<4% O_2) led to HIF-1α stabilization and new blood vessel formation (Wang *et al.*, 2005,Movafagh *et al.*, 2015). Other studies have noted a reduction of ROS and its products by other antioxidants such as glutathione family of antioxidants (e.g., glutathione (GSH), glutathione peroxidase (GPX1)) (MarÃ- *et al.*, 2009,Armstrong *et al.*, 2002). For example, the glutathione family of antioxidants has been linked to have a stimulatory effect on HIF-1α and VEGFA under conditions of oxidative stress (MarÃ- *et al.*, 2009,Galasso *et al.*, 2006). The study demonstrated inhibition or limitation of new blood formation in mice deficient of GPX1 (Galasso *et al.*, 2006). It may be possible that ionic Si enhances angiogenic markers as seen in this work by these antioxidant expressions. Future work will explore these important mechanisms since they play an essential role in mitigating deleterious oxidative stress and promoting angiogenesis.

5. Conclusion

This study demonstrates that ionic silicon markedly enhances HUVEC viability, even in unfavorable conditions of harmful levels of reactive oxygen species (H_2O_2). The silicon ion also induces a significant conformational change, with or without the

favorable Matrigel® condition, forming capillary precursor tube structures. Our results also show the enhancement on cells' migration in a wounded area (scratch assay) and by homing effect (transwell migration). These findings strongly support the idea that the controlled release of silicon ion by biomaterials used in bone tissue engineering can have a beneficial effect in the early stages of tissue regeneration by enhancing new blood vessel formation, a crucial step in the healing process. We believe that future studies need to focus on understanding how the silicon ion induces HUVEC cytoskeleton changes, and the specific mechanism responsible by beneficial silicon ion effect on HUVECs' survival under harmful, oxidative stress.

6. Acknowledgments

The authors would like to thank Dr. Olumide Aruwajoye, Dr. Suresh Adapala, Ila Oxendine, Yang Li, Reuel Cornelia, Amanda Mclerran and Richard Banlaygas from the Center for Excellence in Hip Disorders, Texas Scottish Rite Hospital, for their assistance. We would like to thank the Brazilian Federal Government – Coordenacao de Aperfeicoamento de Pessoal de Nivel Superior (CAPES), for sponsoring the first author.

Funding: This work was supported by a grant from the National Institutes of Health (1R03DE023872-01A1) to V. G. Varanasi and was partially supported by Departmental Startup (#304-128170, Varanasi, PI), Enhancement Grant (#24444100005, Varanasi, PI).

References

Arai M, Shibata Y, Pugdee K, Abiko Y, Ogata Y. 2007, Effects of reactive oxygen species (ROS) on antioxidant system and osteoblastic differentiation in MC3T3-E1 cells, *IUBMB Life,* **59**: 27-33.

Armstrong JS, Steinauer KK, Hornung B, Irish JM, Lecane P, Birrell GW, Peehl DM, Knox SJ. 2002, Role of glutathione depletion and reactive oxygen species generation in apoptotic signaling in a human B lymphoma cell line, *Cell Death Differ,* **9**: 252-63.

Arnaoutova I, Kleinman HK. 2010, In vitro angiogenesis: endothelial cell tube formation on gelled basement membrane extract, *Nature Protocols,* **5**: 628-35.

Asselin A, Hattar S, Oboeuf M, Greenspan D, Berdal A, Sautier JM. 2004, The modulation of tissue-specific gene expression in rat nasal chondrocyte cultures by bioactive glasses, *Biomaterials,* **25**: 5621-30.

Chen G, Zhao L, Feng J, You G, Sun Q, Li P, Han D, Zhou H. 2013, Validation of reliable reference genes for real-time PCR in human umbilical vein endothelial cells on substrates with different stiffness, *PloS one,* **8**: e67360-.

Csordas A, Wick G, Bernhard D. 2006, Hydrogen peroxide-mediated necrosis induction in HUVECs is associated with an atypical pattern of caspase-3 cleavage, *Exp Cell Res,* **312**: 1753-64.

Dashnyam K, Jin G, Kim J, Perez R, Jang J, Kim H. 2017, Promoting angiogenesis with mesoporous microcarriers through a synergistic action of delivered silicon ion and VEGF, *Biomaterials,* **116**: 145-57.

Davis GE, Senger DR. 2005, Endothelial Extracellular Matrix: Biosynthesis, Remodeling, and Functions During Vascular Morphogenesis and Neovessel Stabilization, *Circ Res,* **97**: 1093-107.

Davis GE, Kon W, Stratman AN. 2007, Mechanisms controlling human endothelial lumen formation and tube assembly in three-dimensional extracellular matrices, *Birth Defects Research Part C - Embryo Today: Reviews,* **81**: 270-85.

Galasso G, Schiekofer S, Sato K, Shibata R, Handy DE, Ouchi N, Leopold JA, Loscalzo J, Walsh K. 2006, Impaired angiogenesis in glutathione peroxidase-1-deficient mice is associated with endothelial progenitor cell dysfunction, *Circ Res,* **98**: 254-61.

Hench LL, Splinter RJ, Allen WC, Greenlee TK. 1971, Bonding mechanisms at the interface of ceramic prosthetic materials, *J Biomed Mater Res,* **5**: 117-41.

Hu K, Olsen BR. 2016, The roles of vascular endothelial growth factor in bone repair and regeneration, *Bone,* **91**: 30-8.

Ilyas A, Lavrik NV, Kim HKW, Aswath PB, Varanasi VG. 2015, Enhanced interfacial adhesion and osteogenesis for rapid "bone-like" biomineralization by PECVD-based silicon oxynitride overlays, *ACS applied materials & interfaces,* **7**: 15368-79.

Ilyas A, Odatsu T, Shah A, Monte F, Kim HKW, Kramer P, Aswath PB, Varanasi VG. 2016, Amorphous Silica: A New Antioxidant Role for Rapid Critical-Sized Bone Defect Healing, *Advanced healthcare materials,* .

Information T. 2014, Clonetics â„¢ Endothelial Cell System, : 1-15.

Kim Y, Byzova TV. 2014, Oxidative stress in angiogenesis and vascular disease, *Blood,* **123**.

King SJ, Nowak K, Suryavanshi N, Holt I, Shanahan CM, Ridley AJ. 2014, Nesprin-1 and nesprin-2 regulate endothelial cell shape and migration, *Cytoskeleton,* **71**: 423-34.

Kinov P, Leithner A, Radl R, Bodo K, Khoschsorur G, Schauenstein K, Windhager R. 2006, Role of free radicals in aseptic loosening of hip arthroplasty, *Journal of Orthopaedic Research,* **24**: 55-62.

Koch S, Tugues S, Li X, Gualandi L, Claesson-Welsh L. 2011, Signal transduction by vascular endothelial growth factor receptors, *Biochem J,* **437**: 169-83.

Kong N, Lin K, Li H, Chang J. 2014, Synergy effects of copper and silicon ions on stimulation of vascularization by copper-doped calcium silicate, *Journal of Materials Chemistry B,* **2**: 1100-.

Krock BL, Skuli N, Simon MC. 2011, Hypoxia-Induced Angiogenesis: Good and Evil, *Genes & Cancer,* **2**: 1117-33.

Li H, Chang J. 2013, Bioactive silicate materials stimulate angiogenesis in fibroblast and endothelial cell co-culture system through paracrine effect, .

Lu C, Marcucio R, Miclau T. 2006, Assessing angiogenesis during fracture healing, *Iowa Orthop J,* **26**: 17-26.

MarÃ M, Morales A, Colell A, GarcÃa-Ruiz C, FernÃ¡ndez-Checa JC. 2009, Mitochondrial Glutathione, a Key Survival Antioxidant, *Antioxidants & Redox Signaling,* **11**: 2685-700.

Morin KT, Tranquillo RT. 2013, In vitro models of angiogenesis and vasculogenesis in fibrin gel, *Exp Cell Res,* **319**: 2409-17.

Movafagh S, Crook S, Vo K. 2015, Regulation of Hypoxia-Inducible Factor-1a by Reactive Oxygen Species : New Developments in an Old Debate, *J Cell Biochem,* **116**: 696-703.

Odatsu T, Azimaie T, Velten MF, Vu M, Lyles MB, Kim HK, Aswath PB, Varanasi VG. 2015, Human periosteum cell osteogenic differentiation enhanced by ionic silicon release from porous amorphous silica fibrous scaffolds, *Journal of biomedical materials research.Part A,* **103**: 2797-806.

Pietropaoli D, Ortu E, Severino M, Ciarrocchi I, Gatto R, Monaco A. 2013, Glycation and oxidative stress in the failure of dental implants: a case series, *BMC research notes,* **6**: 296-.

Prasad G, Dhillon MS, Khullar M, Nagi ON. 2003, Evaluation of oxidative stress after fractures. A preliminary study, *Acta Orthop Belg,* **69**: 546-51.

Rasband WS. 1997-2017, ImageJ, U. S. National Institute of Helath, Bethasda, Maryland, USA, https://imagej.nih.gov/ij/, .

Renno ACM, Bossini PS, Crovace MC, Rodrigues ACM, Zanotto ED, Parizotto NA. 2013, Characterization and in vivo biological performance of biosilicate, *BioMed Research International,* **2013**.

Robertson Z. 2009, An in vitro study of the effect of silicon and magnesium ions on bone repair and angiogenesis, .

Ryter SW, Kim HP, Hoetzel A, Park JW, Nakahira K, Wang X, Choi AMK. 2007, Mechanisms of Cell Death in Oxidative Stress, *Antioxidants & Redox Signaling,* **9**: 49-89.

Saghiri MA, Asatourian A, Orangi J, Sorenson CM, Sheibani N. 2015, Functional role of inorganic trace elements in angiogenesisâ€"Part I: N, Fe, Se, P, Au, and Ca, *Critical Reviews in OncologyHematology,* **96**: 129-42.

Sansone V, Pagani D, Melato M. 2013, The effects on bone cells of metal ions released from orthopaedic implants. A review, *Clinical cases in mineral and bone metabolism : the official journal of the Italian Society of Osteoporosis, Mineral Metabolism, and Skeletal Diseases,* **10**: 34-40.

Sharma P, Jha AB, Dubey RS, Pessarakli M. 2012, Reactive Oxygen Species, Oxidative Damage, and Antioxidative Defense Mechanism in Plants under Stressful Conditions, *Journal of Botany,* **2012**: 1-26.

Sivaraman B, Swaminathan G, Moore L, Fox J, Seshadri D, Dahal S, Stoilov I, Zborowski M, Mecham R, Ramamurthi A. 2017, Magnetically-responsive, multifunctional drug delivery nanoparticles for elastic matrix regenerative repair, *Acta Biomaterialia,* **52**: 171-86.

Solaini G, Baracca A, Lenaz G, Sgarbi G. 2010, Hypoxia and mitochondrial oxidative metabolism, *BBA - Bioenergetics,* **1797**: 1171-7.

Song W, Pu J, He B. 2014, *Molecular Medicine Reports,* D.A. Spandidos.

Stegen S, Deprez S, Eelen G, Torrekens S, Van Looveren R, Goveia J, GhesquiÃ¨re B, Carmeliet P, Carmeliet G. 2016, Adequate hypoxia inducible factor 1Î± signaling is indispensable for bone regeneration, *Bone,* **87**: 176-86.

Tabak O, Gelisgen R, Erman H, Erdenen F, Muderrisoglu C, Aral H, Uzun H. 2011, Oxidative lipid, protein, and DNA damage as oxidative stress markers in vascular complications of diabetes mellitus, *Clinical and investigative medicine.Medecine clinique et experimentale,* **34**: E163-71.

Vacanti J,P., Langer R. 1999, Tissue engineering: the design and fabrication of living replacement devices for surgical reconstruction and transplantation, **1**: 32,33, 34.

Varanasi VG, Leong KK, Dominia LM, Jue SM, Loomer PM, Marshall GW. 2012, Si and Ca Individually and Combinatorially Target Enhanced MC3T3-E1 Subclone 4 Early Osteogenic Marker Expression, *J Oral Implantol,* **38**: 325-36.

Wang D, Wang G, Liu M, Sun L, Zong W, Jiang H, Zhang H, Li H, Gong J, Sun S. 2014, A novel animal model of osteonecrosis of the femoral head induced using a magnetic resonance imaging-guided argon-helium cryotherapy system, *Experimental and therapeutic medicine,* **7**: 1525-8.

Wang M, Kirk JS, Venkataraman S, Domann FE, Zhang HJ, Schafer FQ, Flanagan SW, Weydert CJ, Spitz DR, Buettner GR, Oberley LW. 2005, Manganese superoxide dismutase suppresses hypoxic induction of hypoxia-inducible factor-1alpha and vascular endothelial growth factor, *Oncogene,* **24**: 8154-66.

Wang X, Cheng F, Liu J, SmÃ¥tt J, Gepperth D, Lastusaari M, Xu C, Hupa L. 2016, Biocomposites of copper-containing mesoporous bioactive glass and nanofibrillated

cellulose: Biocompatibility and angiogenic promotion in chronic wound healing application, *Acta Biomaterialia,* **46**: 286-98.

Wei H, Li Z, Hu S, Chen X, Cong X. 2010, Apoptosis of mesenchymal stem cells induced by hydrogen peroxide concerns both endoplasmic reticulum stress and mitochondrial death pathway through regulation of caspases, p38 and JNK, *J Cell Biochem,* **111**: 967-78.

Wen YD, Wang H, Kho SH, Rinkiko S, Sheng X, Shen HM, Zhu YZ. 2013, Hydrogen Sulfide Protects HUVECs against Hydrogen Peroxide Induced Mitochondrial Dysfunction and Oxidative Stress, *PLoS ONE,* **8**.

Yang L, Zheng J, Xu R, Zhang Y, Gu L, Dong J, Zhu Y, Zhou R, Zheng L, Zhang X, Du J. 2014, Melatonin suppresses hypoxia-induced migration of HUVECs via inhibition of ERK/Rac1 activation, *International journal of molecular sciences,* **15**: 14102-21.

Yeler H, Tahtabas F, Candan F. 2005, Investigation of oxidative stress during fracture healing in the rats, *Cell Biochem Funct,* **23**: 137-9.

Zhai W, Lu H, Chen L, Lin X, Huang Y, Dai K, Naoki K, Chen G, Chang J. 2012, Silicate bioceramics induce angiogenesis during bone regeneration, .

Zhang Q, Shang M, Zhang M, Wang Y, Chen Y, Wu Y, Liu M, Song J, Liu Y. 2016, Microvesicles derived from hypoxia/reoxygenation-treated human umbilical vein endothelial cells promote apoptosis and oxidative stress in H9c2 cardiomyocytes, *BMC cell biology,* **17**: 25.

Table 1. Gene and specific TagMan assay ID. VEGFA, KDR and HIF-1α were used for angiogenesis and 18S and GAPDH as housekeeping

Gene	Assay ID
VEGFA	Hs00900055_m1
VEGFR2 (KDR)	Hs00911700_m1
HIF1-α	Hs00153153_m1
18S	Hs03003631_g1
GAPDH	Hs02786624_g1

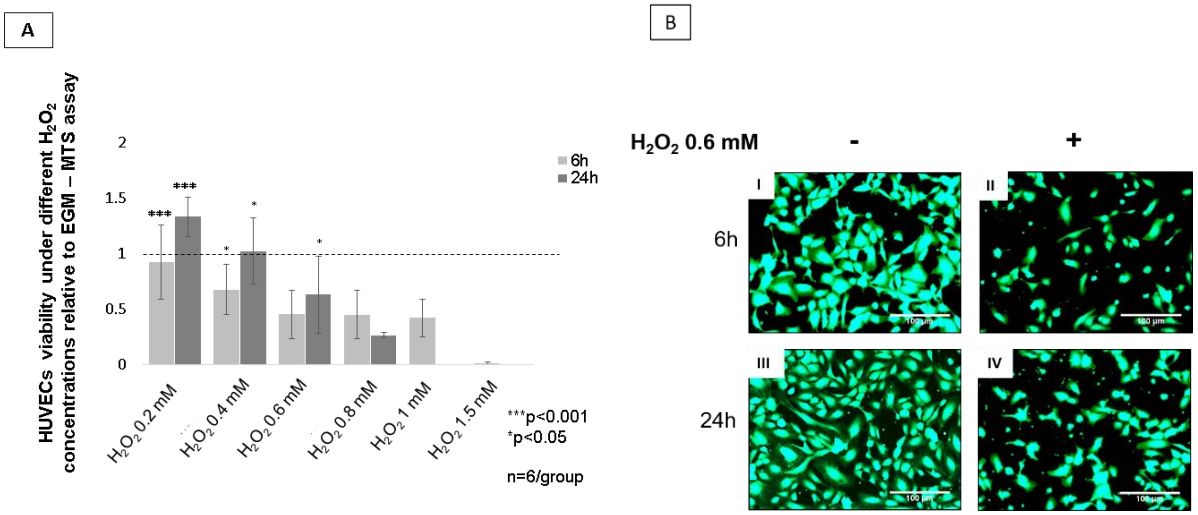

Figure 1. HUVECs viability under H_2O_2 - MTS assay and Calcein-AM staining. **A)** Shows the cells number relative to control at 6 and 24-hour time points. At 24 hours H2O2 0.6 mM was significantly lower than 0.4 mM and higher than 0.8 mM (***p<0.001, *p<0.05, n=6/group). **B)** Shows fluorescent pictures of HUVECs stained with Calcein-AM at 6 h (**I** and **III)** and 24 h (**II** and **IV**). Pictures **I** and **III** show cells exposed to endothelial cell growth media (EGM) and pictures **II** and **IV** show cells exposed to EGM and Hydrogen peroxide (H_2O_2). Scale bar = 100µm

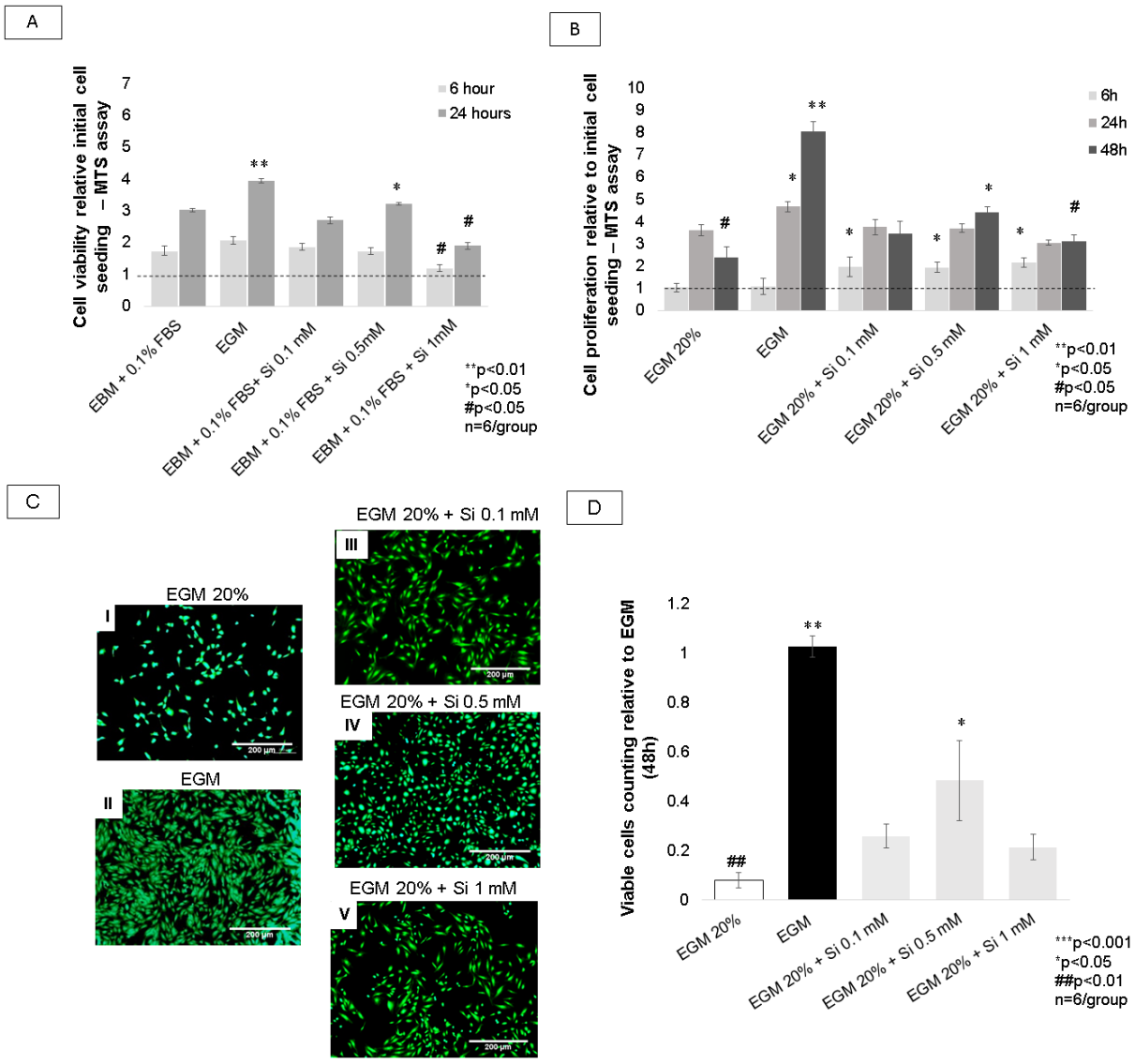

Figure 2. HUVECs viabiltity and proliferation – MTS assay and Calcein-AM. **A)** The bar graph shows the viable cells number measured by MTS assay after 6 and 24 hours. At 24 hours, Si^{4+} 0.5 mM was the most significant among the silicon groups and EBM. (**p<0.01, *p<0.05, #p<0.05) (n=6). **B)** Bar graph shows cells proliferation relative to initial cell seeding after 6, 24, and 48 hours. At 6 hours, all silicon groups similarly presented a significant enhancement in relative cell growth, as compared with controls (p<0.05). At 48 hours, among all silicon groups and EGM 20%, Si^{4+} 0.5 mM showed the most significant relative cell growth ((p<0.05). **C)** Fluorescent pictures (5x

view) of HUVECs stained with Calcein-AM after 48h, showed enhancement on cell proliferation after being exposed to silicon ion. **Picture I** shows the reduced viable cells number on negative control (EGM 20%). **Picture II** shows an outstanding increase in the cell numbers on positive control**,** followed by EGM 20% + Si^{4+} 0.5 mM group **shown in picture IV.** The other two silicon ion groups **(pictures III and V)** showed similar results with less viable cells than positive control and EBM 20% + Si^{4+} 0.5 mM. **D).** Bar graph showing viable cells number are relative to positive control (EGM). EGM 20% + Si^{4+} 0.5 mM group presented 2-fold more than the other silicon groups ($p<0.05$) and 5-fold more than negative control (EBM 20%) ($p<0.01$) (***$p<0.001$,**$p<0.01$, *$p<0.05$, ##$p<0.01$, #$p<0.05$) (n=6). EGM→ endolthelial cell growth media; EBM→ endothelail cell basal media. Scale bar = 200µm

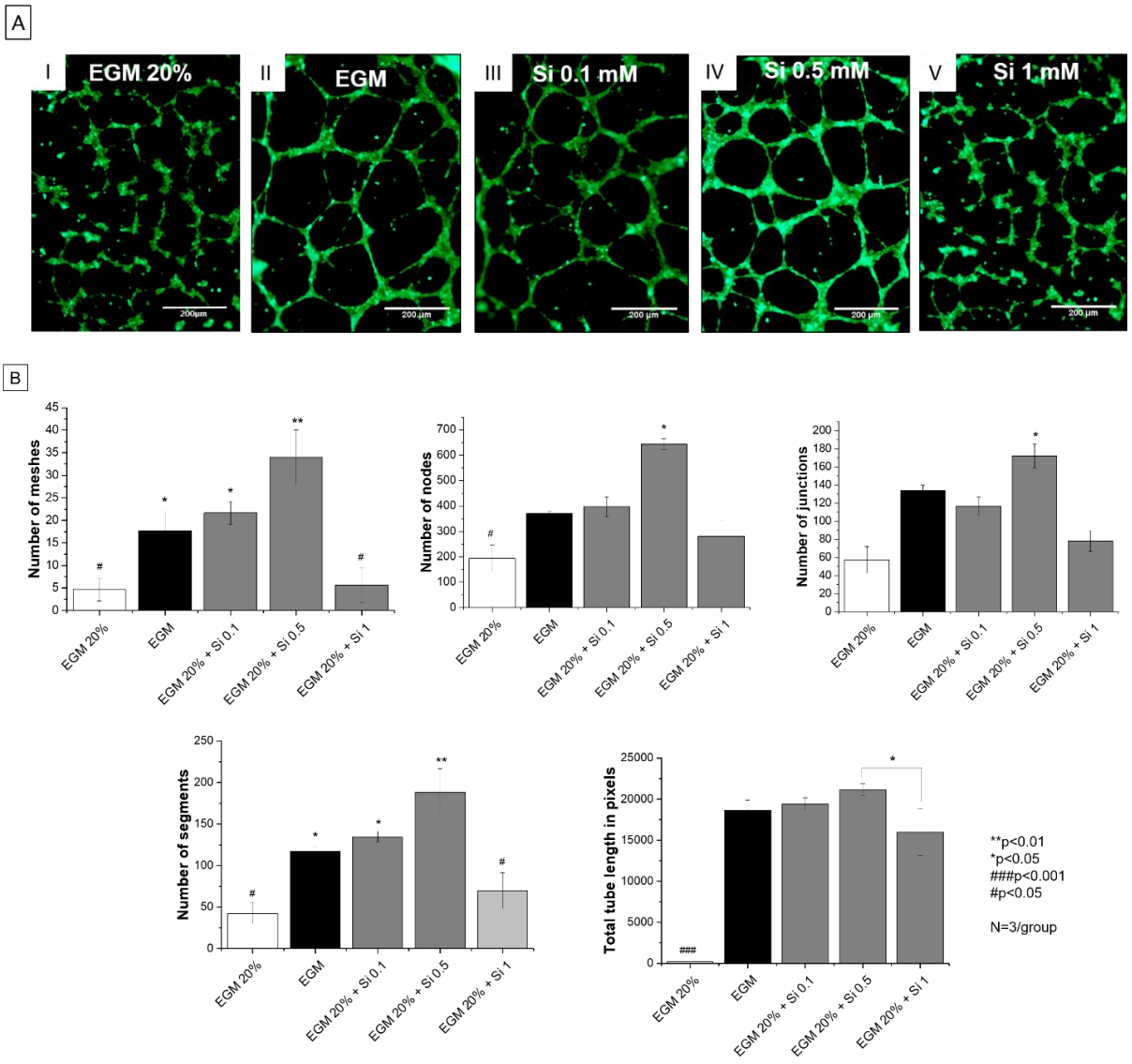

Figure 3. HUVECs capillary tube formation with and without Matrigel - Calcein-AM staining and Angiogenesis Analyzer data. **A**) **Pictures I, II, III, IV and V** show fluorescent pictures (5x view) of HUVECs stained with Calcein-AM, 6 hours after seeding on bed of Matrigel. Si^{4+} 0.5 mM presented the best parameters among all groups, especially on the number of meshes and nodes. Scale bar = 200 µm. **B)** Shows analysis of data collected from ImageJ. Si^{4+} 0.5 mM presented significantly higher number of meshes, segments, junctions and nodes when compare with other groups. **C)** Fluorescent pictures (5x view, scale bar = 200 µm; and 10x view, scale bar = 100 µm) of HUVECs stained with Calcein-AM, 3 hours after media change and 27 hours after initial cell seeding.

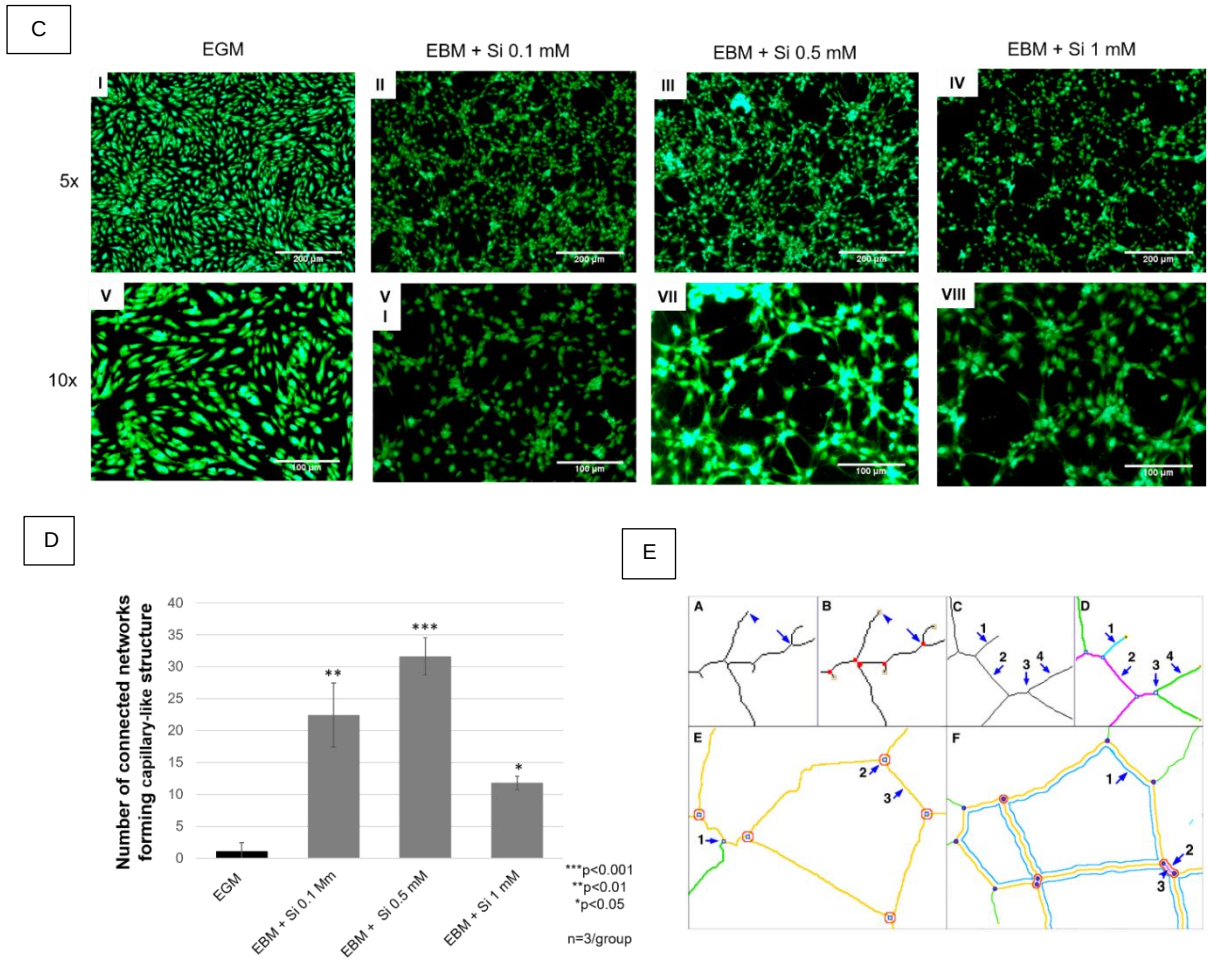

Figure 3. C Pictures I and V (control) show a low number of circles. **Pictures II, III, IV, VI, VII, and VIII** represent the cells exposed to different silicon ion concentrations and show a higher number of circular structures, similar to pre-capillary tubes. **D)** Bar graph showing the data analysis from the fluorescent pictures of number of connected networks formed according to group relative to control (EGM). EBM + Si^{4+} 0.5 mM produced the most remarkable results followed by 0.1 mM,and 1mM. **E) Angiogenesis analyzer (Image J plug-in)** (Arrow head A-B); nodes, identified as pixels that had at least 3 neighbors, corresponding to a bifurcation (arrow A-B); twig (C1, D1), segment (C2, D2) delimited by two junctions (C3, D3) (note that this pointed junction is composed of several nodes) and branches (C4, D4). E shows a junction implicated only in branch (E1) and master junctions like E2 delimiting master segments (E3). F shows the master tree composed from master segments associated by master junctions delimiting the meshes (F1). Optionally, two close master junctions can be fused into a unique master junction (F2). Note the underlying segment (F3). (***p<0.001, **p<0.01, *p<0.05###p<0.001, #p<0.05). EBM: endothelial cell basal media; EGM: endothelial cell growth media.

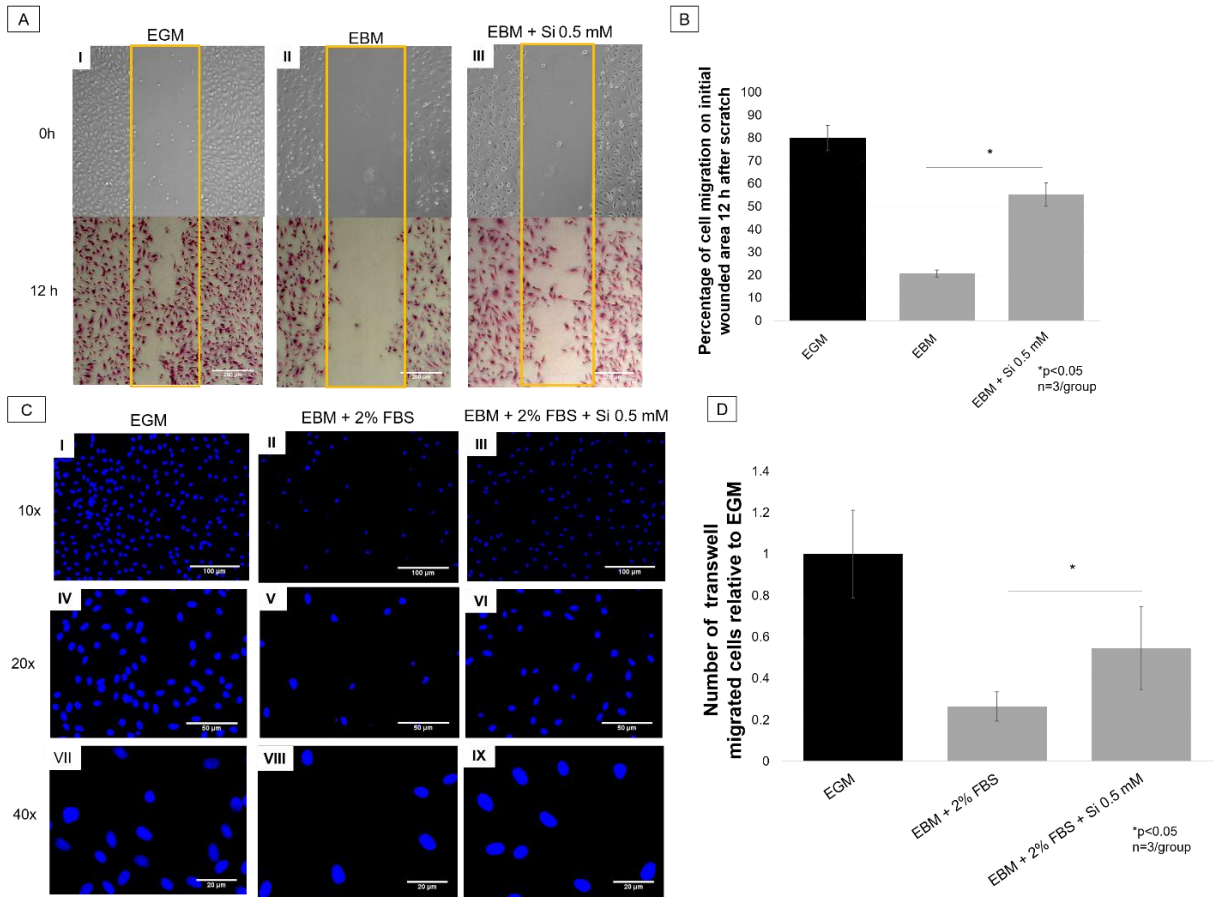

Figure 4. HUVECs migration – scratch assay (Toluidine blue) and transwell membrane (DAPI). **A)** Scratch wound healing assay. Pictures (5x view, scale bar = 200 µm) of wounded area on time 0h (no staining) and 12h (toluidine blue staining). **Picture I** shows EGM (positive control) group with higher wounded area occupied by migrated cells. **Picture II** shows EBM (negative control) group with lower number of cells on wounded area and **picture III** represents EBM treated with Si^{4+} 0.5 mM showing the increase of silicon on cell migration, as compared with EBM **(picture II)**. **B)** Graph shows percentage of occupied initial wounded area by migrated cells relative to control (EGM) 12h after scratch. EBM + Si^{4+} group presented almost 3 times more occupied area than EBM without silicon. **C)** Fluorescent pictures of HUVECs stained with DAPI 12 hours after transwell cell migration (10x , scale bar = 100 µm; 20x, scale bar = 20µm; 40X, scale bar = 20 µm). **Pictures I, IV and VII** show EGM (positive control), **Pictures II, V and VIII** EBM + 2% FBS (negative control), and **pictures III, VI and IX** silicon treatment group. **D)** Bar graph presents number of transwell migrated cells relative to EGM (positive control). Silicon treatment group showed two times more cell migration than negative control. (*p<0.05) (n=3/group). EGM: endothelial cell growth media; EBM: endothelial cell basal media. FBS: fetal bovine serum.

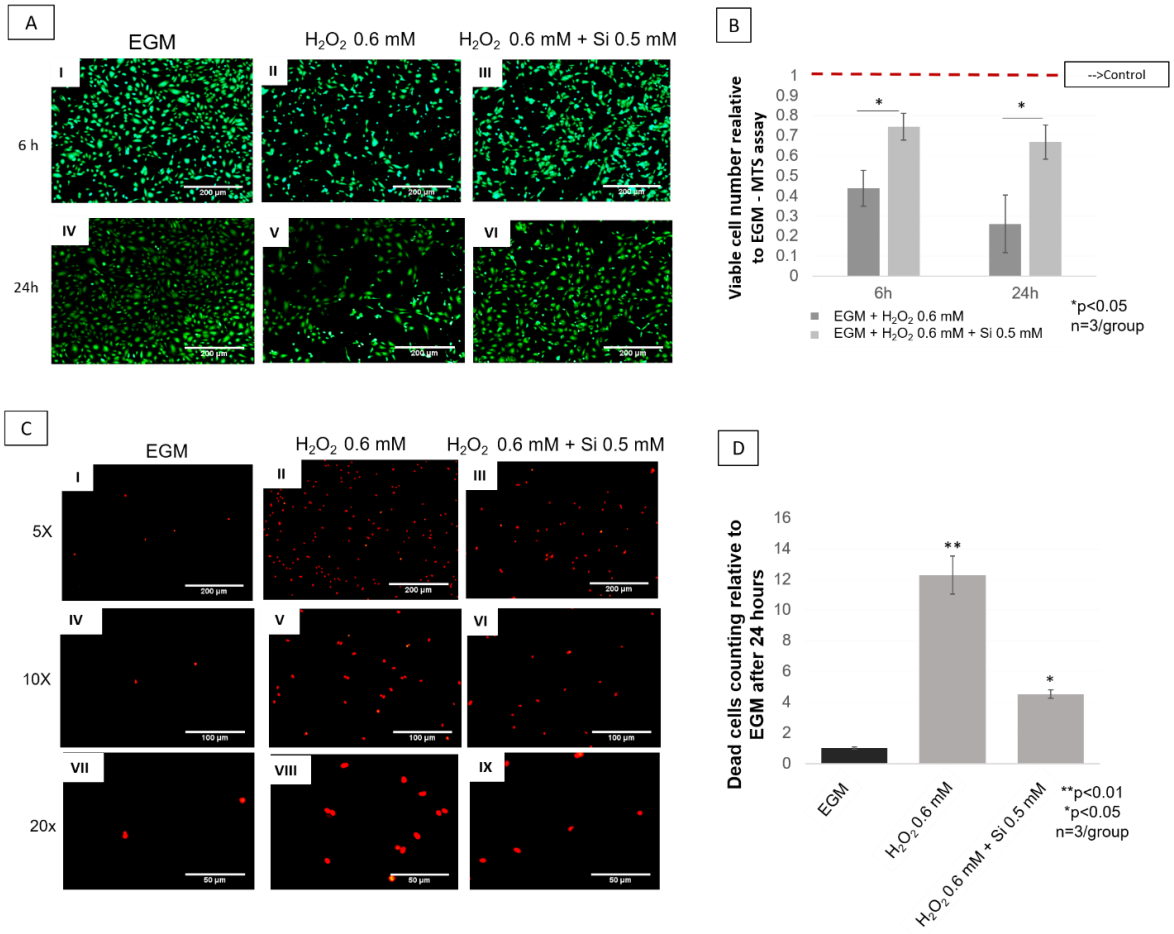

Figure 5. Live and dead assay (Calcein-AM and propidium iodide staining). **A)** Pictures (5x view, scale bar = 200 µm) of HUVECS stained with Calcein-AM under hydrogen peroxide oxidative stress with and without silicon ion treatment, as compared to control. **Pictures I and IV** show EGM (control) group. **Pictures II and V** show cells exposed to H_2O_2, and **pictures III and VI** show HUVECs under H_2O_2 environment and treated with Si^{4+} 0.5 mM**. B)** Graph presents data of comparison between treated and non-treated group relative to control (EGM). Treatment group shows twice and three times more viable cells than H_2O_2 0.6 mM group at 6 hours and 24 hours, respectively. **C)** Fluorescent pictures after propidium iodide staining 24 hours after cell seeding**. Pictures I, IV and VII** show different magnification of lowest number of dead cells on negative control (EGM**). Pictures II, V and VIII** show different magnifications of highest number of dead cells on positive control (H2O2 0.6 mM). **Pictures III, VI and IX** show lower number of dead cells than positive control. **D)** Bar graph shows that silicon treatment group (H_2O_2 + Si 0.5 mM) have three times less dead cells than positive control (H2O2 0.5 mM). (***p<0.001, **p<0.01, *p<0.05) (n=3/group). EGM: endothelial cell growth media. 5x view (scale bar = 200 µm), 10x view (scale bar = 100 µm), 20x view (scale bar = 50 µm).

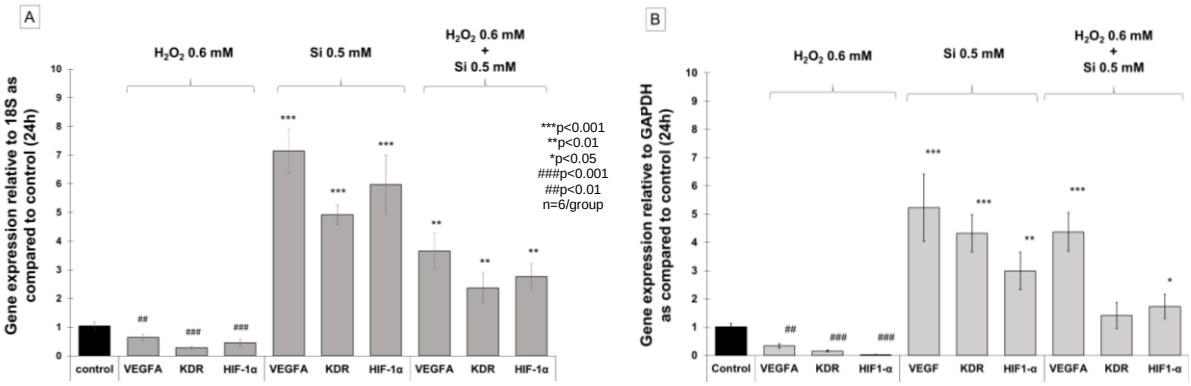

Figure 6. HUVECS Gene expression of angiogenic markers. **A)** Bar graph showing gene expression after 24 hours. VEGFA, KDR and HIF-1α were significantly under expressed when HUVECs were exposed to H_2O_2 0.6 mM ($p<0.01$), and over expressed on silicon group ($p<0.001$) and H_2O_2 treated with silicon group ($p<0.01$) relative to 18S, as compared to control (EGM 20%). **B)** Bar graph presenting gene expression of VEGFA, KDR and HIF-1α, 24 hours after cell seeding relative to GAPDH, as compared to control (EGM 20%). VEGFA, KDR and HIF-1α under expressed on H_2O_2 0.6 mM ($p<0.01$), and presented significant overexpression on silicon group ($p<0.01$). VEGFA ($p<0.001$) and HIF-1α ($p<0.05$) was significantly increased on cells exposed to H2O2 and treated with silicon. (**$p<0.01$, *$p<0.05$) (n=4/group). VEGFA: vascular endothelial growth factor A; KDR: vascular endothelial growth factor receptor 2; HIF-1α: hypoxia-inducible factor 1-alpha; GAPDH: Glyceraldehyde 3-phosphate dehydrogenase; EGM: Endothelial cell growth media.

CHAPTER 4

AMORPHOUS SILICA COATED IMPLANTS BOOST ANGIOGENIC ACTIVITIES OF ENDOTHELIAL CELLS BY STIMULATING FIBRONECTIN DEPOSITION, CAPILLARY TUBULE FORMATION, AND UPREGULATING THE EXPRESSION OF VEGFA, ANGIOPOIETIN-1 AND NESPRIN-2

Felipe A. do Monte[1,2], Kamal R. Awad[3], Ami Shah[3], Neelam Ahuja[4], Harry K.W. Kim[2,5], Pranesh Aswath[3], Venu G. Varanasi[4]*

[1] Department of Bioengineering, University of Texas at Arlington, Arlington Texas 76019, USA

[2] Center for Excellence in Hip Disorders, Texas Scottish Rite Hospital, Dallas, Texas 75219, USA

[3] Department of Materials Science and Engineering, University of Texas at Arlington, Arlington Texas 76019, USA

[4] Department of Biomedical Sciences, Texas A&M University College of Dentistry, Dallas, Texas 75246, USA

[5] Department of Orthopedic Surgery, University of Texas Southwestern Medical Center at Dallas, Dallas, Texas 75390, USA

* To whom correspondence should be addressed:

Venu G. Varanasi, Ph.D.

3302 Gaston Avenue, Texas A&M Health Science Center, Dallas, Texas 75246, USA

Phone: +1-214-370-7006

Fax: +1-214-874-4538

E-mail: vvaranasi@tamhsc.edu

ABSTRACT

Lack of osteointegration is a major cause of aseptic loosening and failure of implants used in bone replacement. Implants coated with materials that can enhance angiogenesis can improve osteointegration and potentially reduce these complications. Silicon and phosphorus based materials has been shown to upregulate gene expression of angiogenic factors in endothelial cells and improve cells migration, proliferation and capillary tube formation. In the present study we tested the hypothesis that implants coated by the plasma enhanced chemical vapor deposition (PECVD) method with amorphous silica formed by Si, O, N, and P could enhance human umbilical vein endothelial cells (HUVECs) angiogenic properties *in vitro*. The tested groups were: glass cover slip (GCS), tissue culture plate (TCP), SiON, SiONP1 and SiONP2 implants. The SiONP2 composition demonstrated the most significant enhancement on fibronectin deposition, showing 3.5 fold more than the GCS ($p<0.001$). The SiONP2 group also presented a significant improvement in capillary tubule length and thickness compared to the GCS ($p<0.01$) and the other PECVD coating amorphous silica groups ($p<0.01$). At 24 hours, we observed at least a 2 fold upregulation of vascular endothelial growth factor A (VEGFA), hypoxia inducible factor (HIF-1a), angiopoietin-1 (ang-1) and nesprin-2, more evident in the SiONP1 and SiONP2 groups. In conclusion, the studied amorphous silica coated implants, specially the SiONP2 composition, could enhance endothelial cells angiogenetic properties in vitro, and may induce faster osteointegration and healing, preventing complications such as implants loosening and failure.

Keywords: Amorphous silica, plasma enhanced chemical vapor deposition (PECVD), endothelial cells, angiogenesis, VEGF-A, Angiopoietin-1

1. INTRODUCTION

New blood vessel formation is a crucial event for adequate bone healing.[1] Large bone defects are associated with proportional vascular damage.[2] Poor vascularization reduces oxygen and nutrients that are necessary on elevated demand on sites of injured tissues under regeneration.[3] The lack of sufficient vascularization can lead to non and delayed union, and surgical intervention for bone replacement is required.[4,5] The commercially available implants, such as polyether ether ketone (PEEK), TiO_2, polymethylmethacrylate and bioceramics have been used for this purpose.[6–9] However, lack of osteointegration is still a problem of these materials, which not uncommonly, undergo to some degree of loosening and failure.[10]

Studies have been using bioceramics coating to enhance osteointegration.[11–13] Nevertheless, the frequently used materials are hydroxyapatite, that despite being the main component of natural bone does not have osteoinductive capacity[14] and bioactive glass 45S5 (Bioglass®) that is osteoinductive and osteoconductive;[15] However, the coating process requires elevated temperatures that can create cracks and lack of efficient adhesion between the coating and underlying material leading to delamination.[16]

Silica based materials have proved to enhance new bone formation by enhancing osteoblast differentiation and matrix deposition.[17–21] Moreover, these materials can induce angiogenesis in HUVECs by upregulating hypoxia inducible factor 1 alfa (HIF-1a) and vascular endothelial growth factor A (VEFGFA).[22]

Studies demonstrated that ionic phosphorus can enhance angiogenesis by upregulating VEGFA in pre- osteoblast cell line and metalloproteinase-2 (MMP-2) and fibroblast growth factor-basic (bFGF) in endothelial cells. The Nitrogen effect on

HUVECs angiogenesis is unclear and sometimes ambiguous. However, nitric oxide has an important role on angiogenesis due to its inhibiting action on angiostatin, which is an angiogenic suppressor. Moreover, inhibited endothelial cell apoptosis, enhances endothelial cells proliferation by upregulation of VEGF-A and bFGF, and induces cells migration by stimulating podokinesis overexpressing αvβ3.

PECVD coating has remarkable advantages compared to other methods. The methods require relatively lower temperatures (~300^0C) and accordingly prevent mismatch between coating and core materials. PECVD coating can efficiently form a stable coating layer of amorphous silica on an underlying metal surface. This amorphous silica coating layer formed by Si, O and N (SiON), proved to go under dissolution in an *in vitro* cell free physiologic environments, and in 6 hours can be rapidly released, interact with medium and form a hydroxycarbonate apatite layer.[21] Moreover, the same publication demonstrated that SiON coating implants can enhance osteogenesis and biomineralization.[21] Further publication, using the same coating method and composition, demonstrated that SiON implants can enhance osteogenesis by upregulating superoxidase dismutase 1 (SOD1), which is a potent antioxidant enzyme that plays a role on osteogenesis, angiogenesis and oxidative stress pathways.[17]

Previous publications demonstrated that PECVD coating SiON implants have a hydrophilic surface.[23] One study showed that a high surface energy, which is directly correlated with hydrophilicity and contact angles lower than 90^0, can improve cell attachment and proliferation.

Supported by above observations, we hypothesize that a PECVD coating amorphous silica-based materials formed by Si, O, N and P can enhance angiogenesis by

facilitating endothelial cells adhesion, proliferation, migration, matrix deposition, and capillary tubule formation. Moreover, we believe that SiONP implants can overexpress angiogenic and antioxidant markers. Our initial aim was to evaluate surfaces' contact angle and cells' adhesion making a correlation between both. Following, we evaluated the effect of SiON and SiONP implants on HUVECS viability, proliferation, fibronectin deposition, cell migration and capillary tubule formation. Lastly, we measured the gene expression of angiogenic markers (VEGFA, HIF-1a, Ang1 and Nesprin-1) and oxidative stress markers (SOD-1, CAT-1, GPX-1 and NOS3).

2. MATERIALS AND METHODS

The materials used in this study were as follows: Human umbilical vein endothelial cells (HUVECs), Endothelial cell basal medium-2 (EBM-2) and Endothelial cell growth medium (EGM-2) from Lonza®; glass cover slip (GCS), Tissue culture plate (TCP) and PECVD coating amorphous silica based implants, SiON, SiONP1 (Si= 61.8, O=7.3, N=30.5, at%) and SiONP2 (Si=58.7, O=14.2, N=26.8, at%). Alexa Fluor 488® Phalloidin actin staining, DAPI and Calcein -AM BD Biosciences® staining. Immunostaining, Anti-fibronectin (primary antibody) and mouse anti-goat with Alexa 488 (secondary). Trizol ®, isopropanol 100% and ethanol 75%. RNA purification filter from Invitrogen®, GoScript™ Reverse Transcription System for cDNA conversion and Gene expression assay from TagMan® for angiogenic and antioxidant markers. Phosphate buffered saline (PBS), fetal bovine serum (FBS) and Penicillin (10,000 units)/ streptomycin (10 mg) / per mL (P/S)mL from Sigma-Aldrich. Fluorescent pictures were captured using the Zeiss Axio Vert.A1 Inverted microscope. OrigemPro2017, Past3 and Microsoft Excel were used for graphs and data analysis. A microplate reader was used for absorbance reading, a nanodrop was used for RNA concentration and the PCR Thermo Fisher Scientific 7000 was used for Ct values on

a quantitative real time polymerase chain reaction (qRT-PCR). All experiments used HUVECs from passage 2 to 4, and the cells were all subcultured at least once after thawing and before experiments. Each experimental section used cells from the same passage. All PECVD coating samples and GCS were sterilized by dry heat applied using standard bacti-cinerator inside the biosafety cabinet.

2.1 PECVD coating amorphous silica based implants fabrication

Four inches <100> test grade P-type silicon wafers were acquired from the NOVA Electronic Materials, 1189 Porter Rd. Flower Mound, TX, USA. A standard cleaning procedure was used. First, the silicon was immersed in a piranha solution (3:1 mixture of sulfuric acid (H_2SO_4, 96%) and hydrogen peroxide (H_2O_2, 30%)). Second, they were removed and rinsed in deionized (DI) water. Third, the wafers were immersed in hydrofluoric acid to remove the native oxide layer. Finally, the wafers were rinsed in DI water for three cleaning cycles and dried with N_2 gas and placed on 200° C hot plate [8,9].

A TRION ORION II PECVD/LPECVD system (Trion Technology, Clearwater, FL) was used to deposit a 200nm uniform coating of SiON and two different compositions of SiONP (**see Table 1**). All coatings were processed at a substrate temperature of 400°C, a chamber pressure of 900 mTorr, an inductively coupled plasma ICP power of 30 W, and an applied excitation frequency of 13.56 MHz. Gase's source and flow rate can be seen on **table 1**.

The refractive indices and film's thickness were measured using an ellipsometry at a wavelength of 632.8 nm (Gaertner LS300). The results of thickness and refractive indices were also confirmed using a reflectometer (Ocean Optics NC-UV-VIS TF Reflectometer).

The elemental surface composition was verified on each PECVD coating implant group using Energy Dispersive X-Ray Analysis (EDX) from scanning electron microscopy (Hitachi S-3000N Variable Pressure SEM) at acceleration voltage of 12 KeV. The surface elemental composition can be seen on **table 2**. The SEM was also used for verifying film thickness at 20 KeV.

2.2 Surface wettability

The tested groups were as follows: GCS, TCP, SiON, SiONP1 and SiONP2. For each sample, 9 repeat drops were measured at room temperature and each coating was tested in triplicate. The hydrophilicity of the surfaces was inferred from the contact angle of water to obtain a clear image about the surface wettability. The contact angle of deionized water (DI) droplets on the wafer coated surface was measured using a sessile drop technique. The images were captured using a high-speed camera (WATEC, high resolution, NAVITAR lens) synced to (First Ten Angstrom, FTA32) software.

2.3 Cell attachment

GCS of 1.5 cm diameter and TCP were used as the negative control and the positive control, respectively. Amorphous silica implants (SiON, SiONP1 and SiONP2) measuring 1.2 x 1.2 cm, and GCS measuring 1.5 cm diameter were placed in a 12 well plate and 5 x 10^3 cell /cm^2 were seeded on top of each surface using 100 µL of EBM-2 without FBS or other growth factors (n=4/group). We allowed the cells to attach to a specific surface for 45 minutes and the amount of medium was completed up to 1 ml/well. After 4 hours the surface was gently washed 2x with PBS and then fixed with 4% paraformaldehyde prepared in PBS. The cells were permeabilized with Triton-X 100 0.1%, washed with PBS, and stained with Alexa Fluor 488 ® for actin and DAPI

for nuclei. Four fluorescent pictures were captured per group in 10x magnification and cells were counted using ImageJ Software.

2.4 Cell viability

The cells were seeded as follows: on GCS, TCP, SiON, SiONP1 and SiONP2 surfaces in a density of 5 x 10^3 cells /cm^2. EBM-2 was supplemented with 0.1% FBS and 1% P/S and used as the condition medium. This experiment used a 12 well plate and 6 samples per group. At 24 hours the medium was removed and we added a MTS reagent assay diluted 5 times in the cell culture medium. After 3 hours, 60 µL of reagent was collected in duplicate and placed in a 96 well plate, and the absorbance was read using a spectrophotometer at 570 n

m wave length. The cell number was collected using a standard curve acquired at the same moment in the same plate to maintain accuracy of the numbers. The data was calculated relative to the initial cell seeding and normalized to the surface area of each group: GCS surface area (1.767 cm^2), TCP well (3.8 cm^2), PECVD coating implants (1.44 cm^2).

2.5 Cell proliferation

Using the same cell seeding density and groups studied on the previous section (2.4) (n=6/group), the cell growth relative to the positive control was evaluated after 1, 3 and 7 days. EBM-2 supplemented with 10% FBS and 1% P/S was used as the conditioned medium and changed every 48 hours. The cell number was normalized according to the surface area and MTS assay was used for cell counting such as was mentioned on the previous section (cell viability 2.4).

2.6 Effect of eluted ions from PECVD coating amorphous silica-based implants on HUVECs proliferation

EBM-2 was supplemented with 10% FBS +1% P/S and used as the conditioned medium on the positive control, and 2 % FBS + 1% P/S was used as the negative control and for studying the elution from PECVD coating implants. Initially, EBM-2 + 1% P/S was placed in a 12 well plate with GCS, empty, SiON, SiONP1 and SiONP2 (n=6/group) without cells for 48 hours. After, eluted ions within medium from PECVD coating implants and medium in contact with GCS and TCP surfaces were collected from the 12 well plate and used for this experiment. Cells were seeded (5 x 10^3 cells /cm^2) in a 96 well plate and allowed to attach to the well for 30 minutes before adding the medium with eluted material and supplemented with 10% FBS or 2 % FBS. The cells were allowed to grow for 24 hours (n=9/group) and 48 hours (n=9/group). At each time point we added 50 µL of Calcein-AM fluorescent dye for live cells, waited 30 minutes and captured 3 pictures at 5x and 10x magnification on a Zeiss fluorescent inverted microscope per each well and used for live cells counting (n=3/group). MTS proliferation was also performed after 24 and 48 hours (n=6/group).

2.7 Effect of eluted ions from PECVD coating amorphous silica-based implants on HUVECs transwell cell migration

We used the same groups and procedures used in section 2.6 of this manuscript to prepare the medium before starting the cells experiment. Using 100 µL of EBM-2 + 1% P/S, 30,000 cells were seeded on the top surface of the transwell membrane with 8 µm pore size inserted in a 24 well plate (Castor Inc). The plate was placed in the incubator(37 ^{0}C, 5% CO_2, 90% humidity) for 30 minutes for adequate attachment. After, 600 µL of medium collected from PECVD coating implants and GCS were supplemented with 2% FBS and placed bellow to the membrane

(n=5/group), and 600 µL of medium collected from TCP group was supplemented with 10% FBS, placed bellow to the membrane and used as the positive control (n=5/group). After 24 hours the cells were fixed with 4% paraformaldehyde, diluted in PBS and a sterile cotton swab was used to remove the non-migrated cell from the upper part of the membrane. The cells were stained with DAPI and we captured 3 pictures at 10X magnification using a Zeiss fluorescent inverted microscope. The number of cells were counted using ImageJ Software.

2.8 Matrix deposition

The studied surfaces were: GCS, TCP, SiON, SiONP1 and SiONP2 (n=6/group). We seeded 5 x 10^3 cells /cm^2 using a12 well plate. The GCS and PECVD coating implant dimensions were the same used for the cell attachment, viability and proliferation. EGM-2 + 10% FBS + 1%P/S was used on the positive control (TCP), and EGM-2 + 2% FBS + 1% P/S was used as the negative control (GCS) and on amorphous silica implants (SiON, SiONP1, SiONP2). The cells were allowed to grow for 5 days. After, the surfaces were blocked with 1% bovine serum albumin prepared in PBS solution, exposed to the primary antibody anti-fibronectin, and to the secondary antibody (Goat anti-Mouse IgG Alexa Fluor™ 488) labeled with Alexa 488. We captured three pictures per sample using a Zeiss fluorescent inverted microscope at 10x and 20x magnification. Lastly, we measured by ImageJ Software the percentage of area occupied by fibronectin.

2.9 Capillary tubule formation on Matrigel® assay

Using a 12 well plate, the cells were seeded on studied surfaces (GCS, TCP, SiON, SiONP1, SiONP2) (n=4/group) at a density of 60,000 cell/cm^2 per well. Before starting the experiment, pipette tips and well plates were placed in – 20^0C per 1 hour and the Matrigel® thawed overnight at 4^0C. First, a 12 well plate was placed on an

ice block inside the cell culture hood and 200 µL of Matrigel® was placed on top of GCS, TCP or amorphous silica implants. Second, the plates with Matrigel® were placed inside the incubator (37^0C, 5% CO_2, 90% humidity) for 30 minutes. Third, the cells were seeded, and the experiment ran for 6 hours. Lastly, Calcein-AM 3µM was diluted in EBM-2, the medium was carefully aspirated and the new medium with Calcein-AM was added. After 30 minutes, we captured 3 pictures per well at 10x magnification and used for quantification of total tubule length and tubule thickness analyzed by ImageJ Software.

2.10 quantitative real-time polymerase chain reaction (qRT-PCR)

In this experiment we seeded 200,000 cells per sample (n=4/group) and EBM + 5% FBS was used as the conditioned medium for all groups (TCP, SiON, SiONP1 and SiONP2). Initially, we seeded the cells on studied surfaces using 100 µL of medium and after 30 minutes in the incubator the total medium was filled up to 1 ml per well. At each time point 1 mL of Trizol was added inside each well and mixed. The cell lysate with RNA was collected and placed in a 1.5 ml centrifuge tube and 100 µl of chloroform was added into each tube, mixed, waited 5 minutes, and centrifuged at 13,000 rpm for 15 minutes. After centrifugation, approximately 300 µl of the transparent top layer containing RNA was collected without disturbing the bottom layers (DNA and proteins) and placed in a new 1.5 ml centrifuge tube. Inside the new tubes we added 500 µl of Isopropanol 100% , used for RNA precipitation and the samples were centrifuged at 13,000 rpm for 10 minutes. The isopropanol was removed without disturbing the RNA pellet, and 1mL ethanol 70% was placed inside the tubes and centrifuged at 10,000 rpm for 5 minutes. The ethanol was carefully removed to not disturb the RNA pellet, and the tubes were maintained open at room temperature for 10 minutes for ethanol evaporation. At the end, we added 25 µl of RNA free water

in each tube for RNA resuspension. The RNA concentration was measured using a micro-volume UV-vis spectrophotometer (Nano Drop 2000c, Thermo Fisher Scientific Inc., Watham, MA, USA), and all samples were diluted to 100 ng/µL during cDNA conversion using the GoScript™ Reverse Transcription System. Gene expression assays (TagMan) were acquired from ThermoFisher Scientific and prepared in a 20 µL reaction using a 96 microplate following step-by-step company protocol. We used Applied Biosystems® 7500 Real-Time PCR Systems with a standard TaqMan set up and 50 cycles for a cycle threshold (Ct) values measurements and the samples were analyzed in duplicate. We used the delta-delta Ct method for calculations. The results were shown relative to the housekeeping gene and compared to the control. The housekeeping gene was 18S and studied genes were: VEGFA, HIF-1a, Angiopoietin-1, Nesprin-2, SOD-1, Cat-1 and NOS3.

3. RESULTS

3.1 Surface wettability

The contact angle was measured on GCS (64.81 ± 6.26^0), TCP (50.04 ± 3.32^0), SiON (40.31 ± 2.92^0), SiONP1 (47.39 ± 1.01^0) and SiONP2 (32.47 ± 1.73^0) surfaces. GCS presented the uppermost contact angle compared to other groups ($p<0.001$), showing an angle more than 2-fold higher than SiONP2 implants ($p<0.001$). (**Figure 1**)

3.2 Cell Attachment and morphology and correlation with wettability

The GCS group presented a significantly reduced attached cell number among all groups ($p<0.001$), indicated by at least 3 fold less cells than TCP, SiON and SiONP1 and 5 fold less cells than SiONP2. SiONP2 presented almost 2 fold more attached cells than TCP, SiON and SiONP1 surfaces ($p<0.001$). SiON presented a

significant enhancement on a surface cell attachment compared to SiONP1 ($p<0.05$). (**Figure 2**)

The number of cells attached on the studied surfaces was correlated with the contact angle, and we observed a significant strong inverse correlation between the parameters ($r = - 0.95$) ($p=0.0098$). (**Figure 3**)

3.3 Cell viability and proliferation

There was no cytotoxic effect of studied surfaces on HUVECs under minimal survival condition of EBM-2 and 0.1% FBS. We observed that that HUVECS exposed to SiONP groups had a significant improvement in cell number relative to controls (TCP and GCS). (**Figure 4A**)

The study of cell growth relative to TCP (positive control) demonstrated that SiONP1 implants presented a significant enhancement on cells growth among the groups after 3 ($p<0.01$) and 7 days ($p<0.001$). All amorphous silica implants presented at least 2 fold more cells than TCP ($p<0.001$) and 4 fold more than GCS ($p<0.001$) after 7 days. (**Figure 4B**)

On the study of the effect of ions released from PECVD coating implants, after 24 hours the cell growth of the medium with ions eluted from amorphous silica surfaces were comparable to the positive control (EBM + 10% FBS) ($p>0.05$) and significant more than EBM-2 + 2% FBS ($p<0.01$). After 48 hours, the positive control (EGM-2) presented the most significant cell growth compared to all other groups ($p<0.01$), and the SiONP groups presented 2 fold more cells than the GCS (**Figure 5B**). Fluorescent images show representative images of each studied group (**Figure 5A**).

3.4 Transwell membrane cell migration

The ions released from implants on conditioned medium were tested on HUVECs after 24 hours and compared to controls, EBM-2 + 2 % FBS (negative control) and EGM-2 (positive control). The only difference between medium collected from the negative control and PECVD coating implants were the presence of ions released from SiON, SiONP1 and SiONP2 groups. All amorphous silica implants coat by PECVD method presented significant improvement on cell migration compared to EBM + 2% FBS (negative control) ($p<0.001$), showing at least 3-fold more cells. Representative images of DAPI fluorescent staining can be seen in **figure 5A** and related with bar Graph seen in **figure 5B**.

3.5 Matrix deposition

The surfaces were tested for fibronectin deposition after 5 days in EBM-2 supplemented with 2% FBS on GCS (negative control) and PECVD coating amorphous silica groups, and 10 % FBS on TCP (positive control). SiON and SiONP groups presented a significant enrichment in fibronectin deposition compared to GCS ($p<0.01$). SiONP2 implants presented the most significant enhancement among all studied groups ($p<0.001$). SiONP groups showed a significant improvement compared to SiON ($p<0.01$). (**Figure 7K**). Fluorescent images demonstrated that the PECVD coating amorphous silica-based implants presented a fibronectin deposition forming a dense tubular shape network (**Figure 7E-J**).The GCS group formed a low density tubule network structure and the TCP group formed a relative dense fibronectin deposition with a poor tubular network structure. (**Figure 7A-D**).

3.6 Capillary tube formation assay

After analysis on the ImageJ Software plugin (Angiogenesis Analyzer), SiON, SiONP1 and SiONP2 groups exhibited a substantial enhancement on the tubule length compared to GCS ($p<0.05$). And the most significant difference was observed on SiONP2 ($p<0.01$) groups that presented more than 2 fold tubule length compared to GCS. The SiONP group presented 2 fold more tubule thickness among all studied groups ($p<0.001$). (**Figure 8**).

3.7 Quantitative real time polymerase chain reaction (qRT-PCR)

3.7.1 Gene expression of angiogenic markers

VEGFA, HIF-1a, Ang-1 and Nes-2 gene expression were measured after 24 and 48 hours. After 24 hours all PECVD coating amorphous silica based implants presented at least 2 fold more expression than the control group ($p<0.05$). **(Figure 9A).** After 72 hours SIONP implants expressed at least 2 fold more angiogenic markers than the control ($p<0.05$), and SiONP2 group showed a remarkable heightening ($p<0.01$), specially on 5 fold expression of Nes 2. **(Figure 9B).**

3.7.2 Gene expression of antioxidant enzymes

SOD-1, Cat-1 and NOS3 demonstrated to be significantly upregulated at 24 hours in SiON , SiONP1 and SiONP2 groups ($p<0.05$), and 72 hours in SiONP1 and SiONP2 groups ($p<0.05$). At 24 hours, Cat-1 was at least 2 fold enhanced in PECVD coating amorphous silica groups compared to the control ($p<0.01$). and SiONP2 enhanced Cat-1 expression at least 3 fold more than the control ($p<0.001$). (**Figure 9C**). At 48 hours, the most considerable upregulation can be seen on NOS3 that in SiONP2 group presented 4.5 fold more than the control ($p<0.001$), followed by SOD1

that also on the SiONP2 group was 2.5 fold more expressed than the control ($p<0.01$). (**Figure 9D**)

4. DISCUSSION

In the present study we tested the hypothesis that PECVD coating amorphous silica implants formed by silicon, oxygen and phosphorus can boost angiogenesis in endothelial cells under normal/physiological *in vitro* condition. We verified that amorphous silica coated implants can enhance angiogenic properties of HUVECS by improving cell adhesion, proliferation, migration, capillary tubule formation and gene expression of angiogenic indicators.

We could verify that the HUVECs attachment was significantly enhanced in the SiONP2 group (**figure 2**) and this observation was strongly inversed correlated with the contact angle (**figure1&3**). According to literature, surfaces with lower contact angles ($<90^0$) present high wettability and surface energy (hydrophilicity) and accordingly improve cells attachment and proliferation.[24–26,23] Hence, once the cells were exposed for a short period of time to studied surfaces (4 hours) and with no FBS or growth factors, we believe that our findings related with SiONP2 and cell attachment was mainly related with surface, energy and the surface elemental composition did not play a relevant role on these results.

As expected, the materials synthesized in our experiment did not present a cytotoxic effect on HUVECs under minimum FBS condition (**figure 4A**). Relative cell growth, indirectly evaluated by the MTS proliferation assay, verified that during the studied time frame all PECVD coating amorphous silica based implants groups presented a significant improvement in cell growth compared with GCS and TCP, especially after 7 days when SiON, SiONP1 and SiONP2 presented at least 2 fold

more cells than the positive control (TCP) (**figure 4B**). These finds corroborate previous publications when the materials based in silicon ion could enhance endothelial cells proliferation.[27] Moreover, some studies referred that high surface energy could enhance endothelial cells proliferation.

Based on the latter observation, that surface energy can have some effect on endothelial cells proliferation, we designed an experiment utilizing just the elution from studied surfaces and evaluated the cells proliferation by MTS assay and Calcein-AM staining at 24 and 48 hours. Our findings demonstrated that ions released from coated materials, mainly Si and N, could induce a significant improvement in endothelial cells growth after 24 and 48 hours. At 24 hours the elution from SiON, SiONP1 and SiONP2 showed cell growth comparable with the positive control, which clearly demonstrates the effect of released ions from PECVD coating implants once the solution used as positive control contained 5 times more FBS than elution from implants coated with amorphous silica. Furthermore, the FBS concentration used on the eluted material from SiON, SiONP1 and SiONP2 was the same used on the negative control (2 % FBS), and the implants coated with amorphous silica showed 2 fold more cells at 24 hours, and SiONP groups presented 2 fold more cells at 48 hours. We believe that the enhancement on cell proliferation at 48 hours on elution experiment (**figure 5**) can be due to the phosphorus incorporation, or higher Si and N content within the medium collected from SiONP1 and SiONP2 groups. These findings can be supported by literature, when some studies correlated the presence of ionic silicon and phosphorus with an enhancement on endothelial cells angiogenic properties.[27,28,29–31] The role of nitrogen on endothelial cells angiogenesis is still unclear, and the direct effect has been related to nitrogen compound with oxygen forming NO.[32]

The SiON, SiONP1 and SiONP2 implants showed a significant enhancement on cell migration compared to negative control (EBM + 2% FBS) (**figure 6)**, showing that the ionic content released from implants coated with amorphous silica by PECVD demonstrated some chemotactic effect on HUVECs, observation that corroborated with a previous publication. Among the amorphous silica coated implants groups, SiONP2 presented the most relevant improvement in cell migration, which can be attributed to presence of ionic phosphorus, or due to the different surface composition of Si, O and N observed on SiONP1 and SiONP2 implants, as can be seen on **table 2.**

The analysis of fibronectin deposition after 5 days shows that the amount of fibronectin was remarkably increased in the SiONP2 group, which can be attributed not just to the effect of the surface elemental composition, but to the higher surface energy observed on SiONP2 group demonstrated by the lowest contact angle (**figure 1**). Fibronectin is a extracellular glycoprotein produced by endothelial cells since the early stages of new blood vessel formation.[33,34] The presence of this protein is important for endothelial cells differentiation, migration and proliferation.[33–36] Therefore, its presence can be used as a demonstration of an efficient HUVECs matrix deposition.[34] Our results demonstrated that SiON, SiONP1 and SiONP2 (**figures 7E-J**) formed a circular structure matrix deposition, similar to the capillary tubule formation, and the SiONP2 group showed a significant enhanced deposition (**figure 7J**).

The capillary tubule formation assay on a bed of Matrigel ® used TCP and EGM-2 as the positive control, and as expected presented the longer capillary network structure (**figure 8B&F)**. The other groups, negative control (GCS) and amorphous

silica coated implants, were supplemented just with 2% FBS and 1% P/S without growth factors present on EGM-2. As we can see on fluorescent pictures (**figure 8D,E&G)**, the tubule thickness was expressively enhanced in the SiONP groups. Moreover, the total tubule length was significantly increased in the SiON and SiONP groups compared to GCS, which can be attributed to the surface energy (contact angle) and elemental composition. Study showed that silica based materials can improve capillary tubule length in HUVECs.[27] However, it was not analyzed the effect of those materials on capillary tubule thickness.

In the present research, gene expression of angiogenic markers showed a significant upregulation of VEGFA, HIF-1a, Ang-1 and Nesp-2 on HUVECS exposed to SiON and SiONP implants. VEGFA is a major angiogenesis regulator that binds and activates the vascular endothelial growth factor receptor (VEGFR) inducing endothelial cells proliferation, migration and capillary tubule formation. Recent publication verified the crucial role of ionic silicon on angiogenesis by upregulating HIF-1a and induces angiogenesis in endothelial cells. Some studies showed that phosphorus can upregulate VEGFA and induces endothelial cells migration and proliferation.[29–31] Ang-1 is a protein that can be produced by endothelial cells can induce HUVECs migration and differentiation. [33] Moreover, by activation of the tyrosine kinase 2 (Tie2-receptor) can protect endothelial cells under unfavorable survival conditions against apoptosis.[34,35] In our literature review we could not find a relationship between ang-1 and ionic silicon or silica based materials. Nes-2 is an intra-cellular protein that connects the actin filament to the endothelial cell nuclei and has been related with endothelial cell shape changing and migration.[36] As we could verify upregulation of nes-2 in our samples coat with amorphous silica by PECVD method, we believe that nes-2 could have some relationship with the enhancement in

a capillary tubule formation network and transwell cell migration observed mainly on SiONP1 and SiONP2 groups.

We also analyzed the gene expression of oxidative stress markers. In our results we could observe upregulation of enzymes that play a major role on catalysis of reactive oxygen species and its products. SOD-1 and cat-1 were significantly upregulated in cell exposed to SiON, SiONP1 and SiONP2 implants compared to control group, especially at the first 24 hours. At 24 hours SiONP2 implants presented a remarkably cat-1 upregulation among all studied groups, showing 3 fold more m-RNA levels than the control. In recent publication our group demonstrated the relevant role of ionic silicon on SOD-1 upregulation in osteoblasts.[37] We could not find publications that correlate the effect of ionic silicon or silica base materials with endothelial cells and antioxidant enzymes. SOD-1 is an enzyme that catalyze the conversion of O_2^- (superoxide) in H2O2.[38,39] And cat-1 is an enzyme responsible for catalyze the conversion H_2O_2 in H_2O and O_2.[40–42] These enzymes play a major role during physiologic and pathologic oxidative stress condition once H_2O_2 and O_2^- are the main reactive oxygen species produced during cell under oxidative stress. Further investigations are necessary for a better understanding of a possible antioxidant effect of these biomaterials on HUVECs.

In conclusion, our study demonstrated that PECVD coating amorphous silica-based materials formed by Si, O, N and P can successfully boost angiogenic properties of HUVECs, improving cell proliferation, migration, fibronectin deposition and capillary tubule formation, by upregulating VEGFA, Nesprin-2 and angiopoietin-1. The angiogenic enhancement by these implants may induce faster osteointegration and healing, preventing complications such as implants loosening and failure.

Additionally, Cat-1 and SOD-1 upregulation open some doors for further investigations of a possible antioxidant effect of these implants, which could be beneficial for improving the osteointegration and healing in the unfavorable oxidative stress environment of large bone defects.

ACKNOWLEDGMENTS

The authors would like to thank Dr. Olumide Aruwajoye, Amanda McIlaren, Dr. Suresh Adapala, Ila Oxendine, Yang Li, Reuel Cornelia, and Richard Banlaygas from the Center for Excellence in Hip Disorders, Texas Scottish Rite Hospital, for their assistance. We would like to thank the Brazilian Federal Government – Coordenacao de Aperfeicoamento de Pessoal de Nivel Superior (CAPES), for sponsoring the first author.

Funding: This work was supported by a grant from the National Institutes of Health (1R03DE023872-01A1) to V. G. Varanasi and was partially supported by Departmental Startup (#304-128170, Varanasi, PI), Enhancement Grant (#24444100005, Varanasi, PI).

REFERENCES

1. Saran, U., Piperni, S. G. & Chatterjee, S. Role of angiogenesis in bone repair. *Arch. Biochem. Biophys.* **561,** 109–117 (2014).

2. Wiese, A. & Pape, H. C. Bone defects caused by high-energy injuries, bone loss, infected nonunions, and nonunions. *Orthop. Clin. North Am.* **41,** 1–4, table of contents (2010).

3. Filipowska, J. *et al.* The role of vasculature in bone development, regeneration and proper systemic functioning. *Angiogenesis* **20,** (2017).

4. Höhne, J. *et al.* Outcomes of Cranioplasty with Preformed Titanium versus

Freehand Molded Polymethylmethacrylate Implants. *J. Neurol. Surg. Part A Cent. Eur. Neurosurg.* (2017). doi:10.1055/s-0037-1604362

5. Bone fracture healing: Cell therapy in delayed unions and nonunions. *Bone* **70,** 93–101 (2015).

6. Zanotti, B. *et al.* Cranioplasty: Review of Materials. doi:10.1097/SCS.0000000000003025

7. Parthasarathy, J. 3D modeling, custom implants and its future perspectives in craniofacial surgery. *Ann. Maxillofac. Surg.* **4,** 9–18 (2014).

8. Merolli, A. *et al.* Debris of carbon-fibers originated from a CFRP (pEEK) wrist-plate triggered a destruent synovitis in human. *J. Mater. Sci. Mater. Med.* **27,** 50 (2016).

9. Stratton-Powell, A. A., Pasko, K. M., Brockett, C. L. & Tipper, J. L. The Biologic Response to Polyetheretherketone (PEEK) Wear Particles in Total Joint Replacement: A Systematic Review. *Clin. Orthop. Relat. Res.* **474,** 2394–2404 (2016).

10. Lethaus, B., Bloebaum, M., Koper, D., Poort-Ter Laak, M. & Kessler, P. Interval cranioplasty with patient-specific implants and autogenous bone grafts e Success and cost analysis. *J. Cranio-Maxillofacial Surg.* **42,** 1948–1951 (2014).

11. Say, Y. & Aksakal, B. Effects of hydroxyapatite/Zr and bioglass/Zr coatings on morphology and corrosion behaviour of Rex-734 alloy. *J. Mater. Sci. Mater. Med.* **27,** 105 (2016).

12. Popa, A.-C. *et al.* Bioglass implant-coating interactions in synthetic physiological fluids with varying degrees of biomimicry. *Int. J. Nanomedicine* **Volume 12,** 683–

707 (2017).

13. Camilo, C. C. *et al.* Bone response to porous alumina implants coated with bioactive materials, observed using different characterization techniques. *J. Appl. Biomater. Funct. Mater.* **15,** 0–0 (2017).

14. Hoornenborg, D. *et al.* Does hydroxyapatite coating enhance ingrowth and improve longevity of a Zweymuller type stem? A double-blinded randomised RSA trial. *Hip Int.* 0–0 (2017). doi:10.5301/hipint.5000549

15. Yuan, H., de Bruijn, J. D., Zhang, X., van Blitterswijk, C. A. & de Groot, K. Bone induction by porous glass ceramic made from Bioglass (45S5). *J. Biomed. Mater. Res.* **58,** 270–6 (2001).

16. Pavón, J., Jiménez-Piqué, E., Anglada, M., Saiz, E. & Tomsia, A. P. Delamination under Hertzian cyclic loading of a glass coating on Ti6al4v for implants. in *Journal of Materials Science* (2006). doi:10.1007/s10853-006-0439-3

17. Ilyas, A. *et al.* Amorphous Silica: A New Antioxidant Role for Rapid Critical-Sized Bone Defect Healing. *Adv. Healthc. Mater.* **5,** 2199–213 (2016).

18. Saffarian Tousi, N. *et al.* Combinatorial effect of Si4 +, Ca2 +, and Mg 2 + released from bioactive glasses on osteoblast osteocalcin expression and biomineralization. *Mater. Sci. Eng. C* **33,** 2757–2765 (2013).

19. Varanasi, V. G. *et al.* Si and Ca Individually and Combinatorially Target Enhanced MC3T3-E1 Subclone 4 Early Osteogenic Marker Expression. *J. Oral Implantol.* **38,** 325–336 (2012).

20. Odatsu, T. *et al.* Human periosteum cell osteogenic differentiation enhanced by

ionic silicon release from porous amorphous silica fibrous scaffolds. *J. Biomed. Mater. Res. - Part A* **103,** 2797–2806 (2015).

21. Ilyas, A., Lavrik, N. V, Kim, H. K. W., Aswath, P. B. & Varanasi, V. G. Enhanced interfacial adhesion and osteogenesis for rapid "bone-like" biomineralization by PECVD-based silicon oxynitride overlays. *ACS Appl. Mater. Interfaces* **7,** 15368–79 (2015).

22. Dashnyam, K. *et al.* Promoting angiogenesis with mesoporous microcarriers through a synergistic action of delivered silicon ion and VEGF. *Biomaterials* **116,** 145–157 (2017).

23. Varanasi, V. G. *et al.* Role of Hydrogen and Nitrogen on the Surface Chemical Structure of Bioactive Amorphous Silicon Oxynitride Films. *J. Phys. Chem. B* **121,** 8991–9005 (2017).

24. Arima, Y. & Iwata, H. Effect of wettability and surface functional groups on protein adsorption and cell adhesion using well-defined mixed self-assembled monolayers. *Biomaterials* **28,** 3074–3082 (2007).

25. Chaiwong, S. S. and J. S. L. and S. B. J. and D. H. S. and L. D. Y. and J. G. H. and C. Wettability Effect of PECVD-SiO x Films on Poly(lactic acid) Induced by Oxygen Plasma on Protein Adsorption and Cell Attachment. *J. Phys. Conf. Ser.* **423,** 12042 (2013).

26. Terriza, A. *et al.* Osteoblasts interaction with PLGA membranes functionalized with titanium film nanolayer by PECVD. In vitro assessment of surface influence on cell adhesion during initial cell to material interaction. *Materials (Basel).* **7,** 1687–1708 (2014).

27. Dashnyam, K. *et al.* Promoting angiogenesis with mesoporous microcarriers through a synergistic action of delivered silicon ion and VEGF. *Biomaterials* **116,** 145–157 (2017).

28. Dashnyam, K. *et al.* A mini review focused on the proangiogenic role of silicate ions released from silicon-containing biomaterials. *J. Tissue Eng.* **8,** 204173141770733 (2017).

29. Camalier, C. E. *et al.* An integrated understanding of the physiological response to elevated extracellular phosphate. *J. Cell. Physiol.* **228,** 1536–1550 (2013).

30. Lin, Y., Mckinnon, K. E., Ha, S. W. & Beck, G. R. Inorganic phosphate induces cancer cell mediated angiogenesis dependent on forkhead box protein C2 (FOXC2) regulated osteopontin expression. *Mol. Carcinog.* **54,** 926–934 (2015).

31. Saghiri, M. A., Asatourian, A., Orangi, J., Sorenson, C. M. & Sheibani, N. Functional role of inorganic trace elements in angiogenesis—Part I: N, Fe, Se, P, Au, and Ca. *Crit. Rev. Oncol.* **96,** 129–142 (2015).

32. Matsunaga, T. *et al.* Angiostatin inhibits coronary angiogenesis during impaired production of nitric oxide. *Circulation* **105,** 2185–2191 (2002).

33. Hielscher, A., Ellis, K., Qiu, C., Porterfield, J. & Gerecht, S. Fibronectin deposition participates in extracellular matrix assembly and vascular morphogenesis. *PLoS One* **11,** 1–27 (2016).

34. Chiang, H. Y., Korshunov, V. A., Serour, A., Shi, F. & Sottile, J. Fibronectin is an important regulator of flow-induced vascular remodeling. *Arterioscler. Thromb. Vasc. Biol.* **29,** 1074–1079 (2009).

35. Kusuma, S., Zhao, S. & Gerecht, S. The extracellular matrix is a novel attribute

of endothelial progenitors and of hypoxic mature endothelial cells. *FASEB J.* **26,** 4925–4936 (2012).

36. Salakhutdinov, I. *et al.* Fibronectin adsorption to nanopatterned silicon surfaces. *J. Nanomater.* **2008,** (2008).

37. Harel, S., Mayaki, D., Sanchez, V. & Hussain, S. N. A. NOX2, NOX4, and mitochondrial-derived reactive oxygen species contribute to angiopoietin-1 signaling and angiogenic responses in endothelial cells. (2017). doi:10.1016/j.vph.2017.03.002

38. Jin Kwak, H., So, J.-N., Jae Lee, S., Kim, I. & Young Koh, G. Angiopoietin-1 is an apoptosis survival factor for endothelial cells.

39. Harfouche, R. *et al.* Mechanisms Which Mediate the Antiapoptotic Effects of Angiopoietin-1 on Endothelial Cells. doi:10.1006/mvre.2002.2421

40. King, S. J. *et al.* Nesprin-1 and nesprin-2 regulate endothelial cell shape and migration. *Cytoskeleton* **71,** 423–434 (2014).

41. Ilyas, A. *et al.* Amorphous Silica: A New Antioxidant Role for Rapid Critical-Sized Bone Defect Healing. *Adv. Healthc. Mater.* **5,** 2199–2213 (2016).

42. Choi, Y. J., Lee, J. Y., Chung, C. P. & Park, Y. J. Cell-penetrating superoxide dismutase attenuates oxidative stress-induced senescence by regulating the p53-p21(Cip1) pathway and restores osteoblastic differentiation in human dental pulp stem cells. *Int. J. Nanomedicine* **7,** 5091–106 (2012).

43. Fukai, T. & Ushio-Fukai, M. Superoxide Dismutases: Role in Redox Signaling, Vascular Function, and Diseases. doi:10.1089/ars.2011.3999

44. Chelikani, P., Fita, I. & Loewen, P. C. Diversity of structures and properties

among catalases. *Cell. Mol. Life Sci.* **61,** 192–208 (2004).

45. FERNÁNDEZ, C., SAN MIGUEL, E. & FERNÁNDEZ-BRIERA, A. Superoxide dismutase and catalase: tissue activities and relation with age in the long-lived species Margaritifera margaritifera. *Biol. Res.* **42,** 57–68 (2009).

46. Saxena, S. & Jamil, K. Oxidative stress and expression level of Catalase, Glutathione S Tranferase Enzyme in type 2 Diabetes Patients. *Int. J. Sci. Eng. Res.* **5,** (2014).

Table1. Shows the three steps and flow rates of the different gases used for processing SiON, SIONP1 and SiONP2 implants. Used gases→ Silane (SiH_4), Nitrous oxide (N_2O), Ammonia (NH_4), Phosphine (PH_3), Nitrogen (N_2), Argon (carrier gas).

	SiH_4/Ar (15/85%)	PH_3/SiH_4/Ar (2/15/83%)	N_2O	N_2	NH_4	Ar	Time (sec)
Step 1	0	0	0	0	0	250	30
Step 2 ($SiON_x$)	24	0	155	225	50	0	226
Step 2 ($SiONP_x$)1	0	24	**5**	225	50	0	322
($SiONP_x$)2			**16**				
Step 3	0	0	0	0	0	250	30

Table 2. Energy-dispersive X-ray spectroscopy (EDS) analysis of atomic surface composition of SION, SiONP1 and SiONP2 coating. See EDS spectra below the table.

EDS compositional data **(at%)**

Sample	Si	O	N	P
SiON	52.5	35.1	12.3	0
SiONP1	61.8	7.3	30.5	0.28
SiONP2	58.7	14.2	26.8	0.27

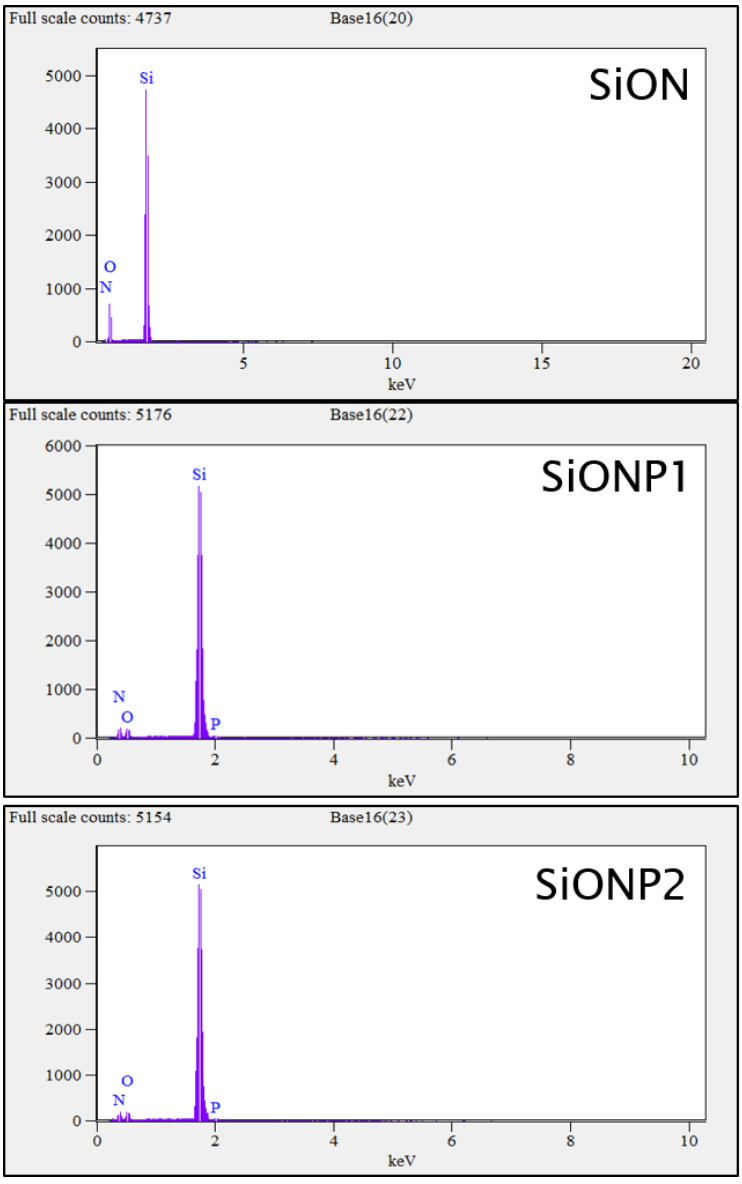

Table 3. Gene and specific TagMan assay identification

Gene	Assay identification
VEGFA	Hs00900055_m1
HIF-1a	Hs00153153_m1
Ang-1	Hs00919202_m1
Nesprin-2 (SYNE2)	Hs00794881_m1
SOD-1	Hs00533490_m1
Cat-1 (CAT)	Hs00156308_m1
e-NOS (NOS3)	Hs01574665_m1

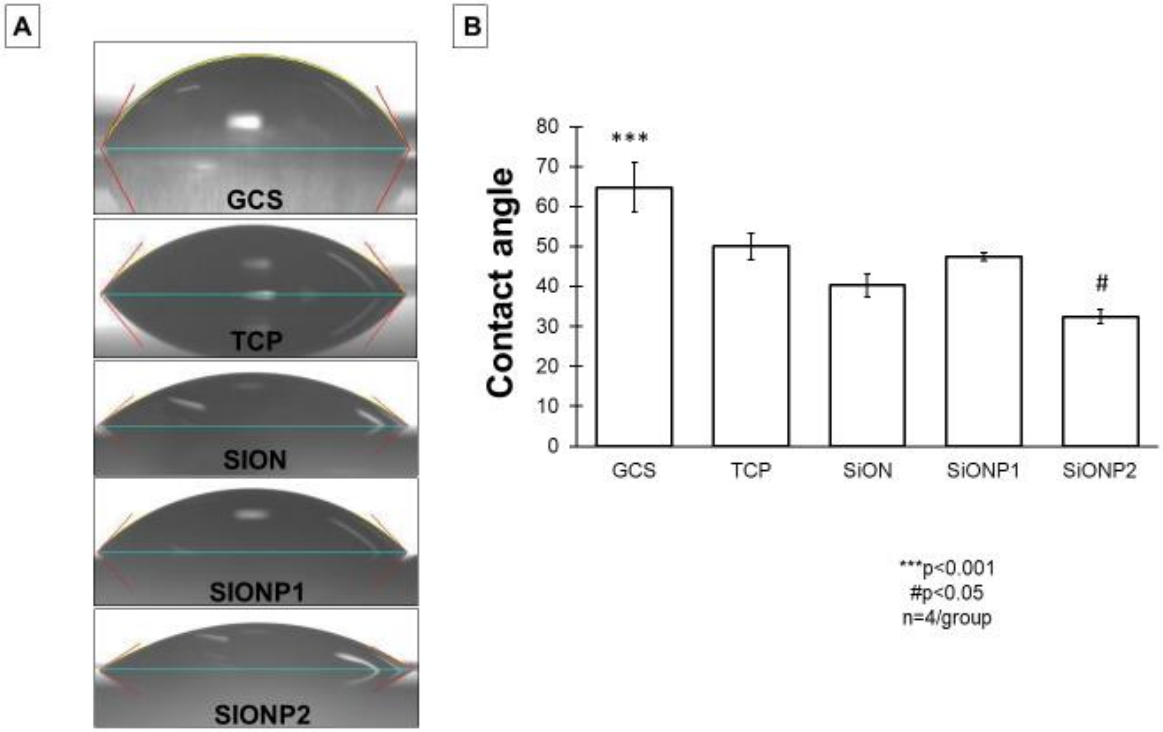

Figure 1. Contact angle (surface wettability). A) Images of water drop on studied surface and lines traced for measurements. B) Bar graph shows comparison of contact angles. (***p<0.001, #p<0.05). GCS→ glass cover slip, TCP→ tissue culture plate.

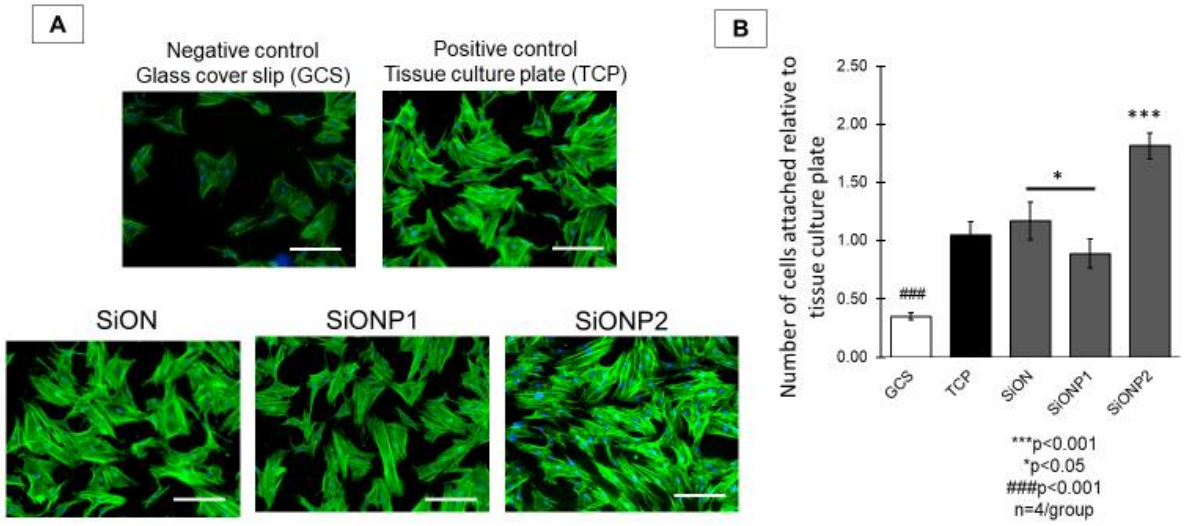

Figure 2. Cell attachment and morphology. A) Actin and DAPI fluorescent staining showing HUVECS attached to studied surfaces 4 hours after seeding in EBM-2 without FBS. Scale bar = 100 μm**.** B) Bar gpraph shows the cell attached number relative to TCP. (***p<0.001, *p<0.05, ###p<0.001). EBM-2→ endothelial cell basal media-2, GCS→ glass cover slip, TCP→ tissue culture plate.

	contact angle	Cell attachment number
GCS	64.81	18
TCP	50.04	56
SiON	40.31	62
SiONP1	47.39	47
SiONP2	32.47	97

r = - 0.95921
p= 0.009829

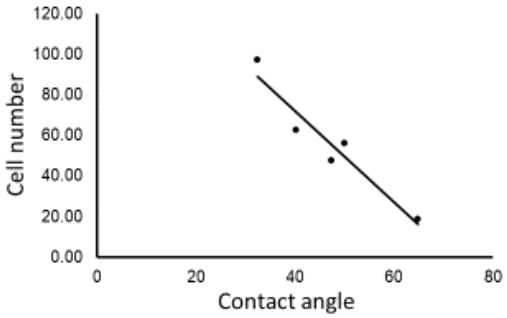

Figure 3. Correlation cell attachment number and contact angle. GCS→ glass cover slip, TCP→ tissue culture plate.

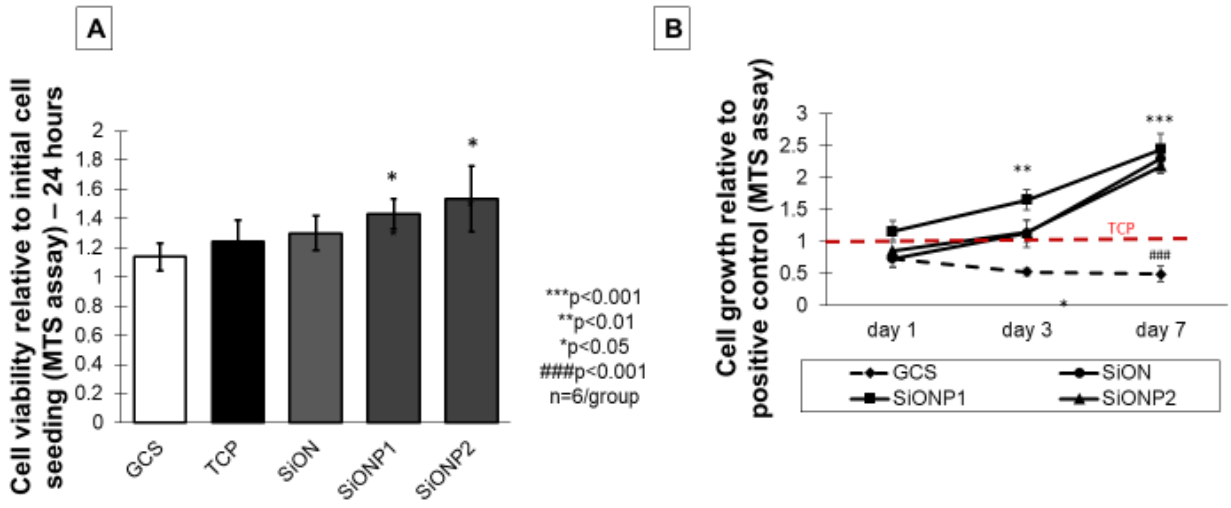

Figure 4. A) Graph shows cell viability after 24 hours (MTS-assay). B) Chart shows cell growth after 1, 3 and 7 days (MTS assay). (***p<0.001. **p<0.01, *p<0.05, ###p<0.001). GCS→ Gass cover slip, TCP→ tissue culture plate.

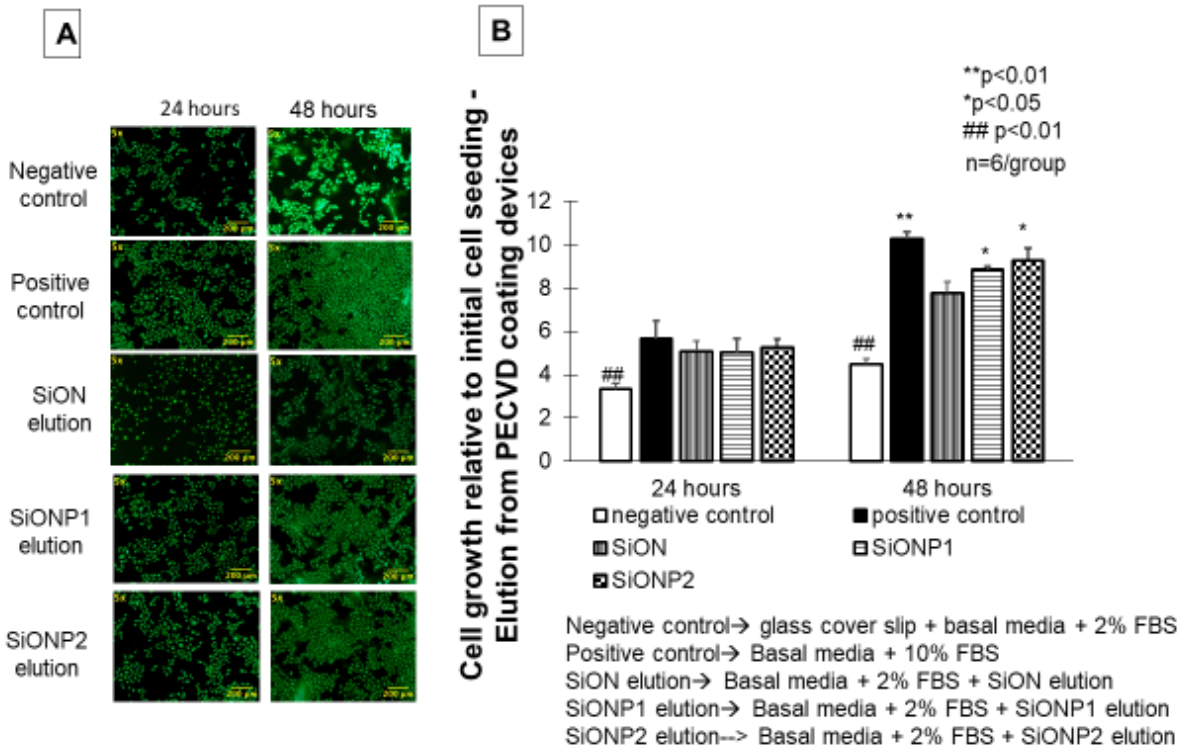

Figure 5. A) Effect of elution from amorphous silica PECVD coating scaffolds on HUVECS proliferation. A) Pictures after Calcein-AM staining (24 and 48 hours). Scale bar = 200 μm. B) Graph shows cell growth measured by MTS assay. (**p<0.01, *p<0.05), ##p<0.01.

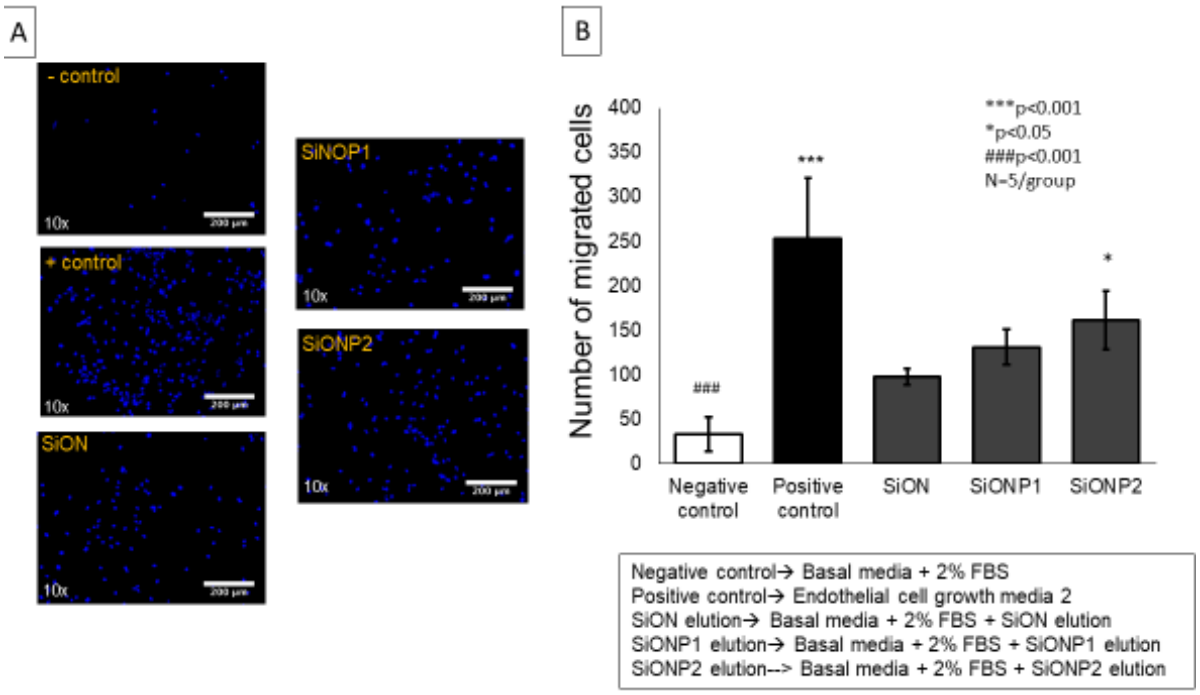

Figure 6. Effect of elution from PECVD coating implants on HUVECS membrane transwell migration (24 hours). A) Fluorescent pictures of DAPI fluorescent staining. Scale bar = 200μm. B) Bar graph shows number of migrated cells. (***p<0.001, *p<0.05, ###p<0.001).

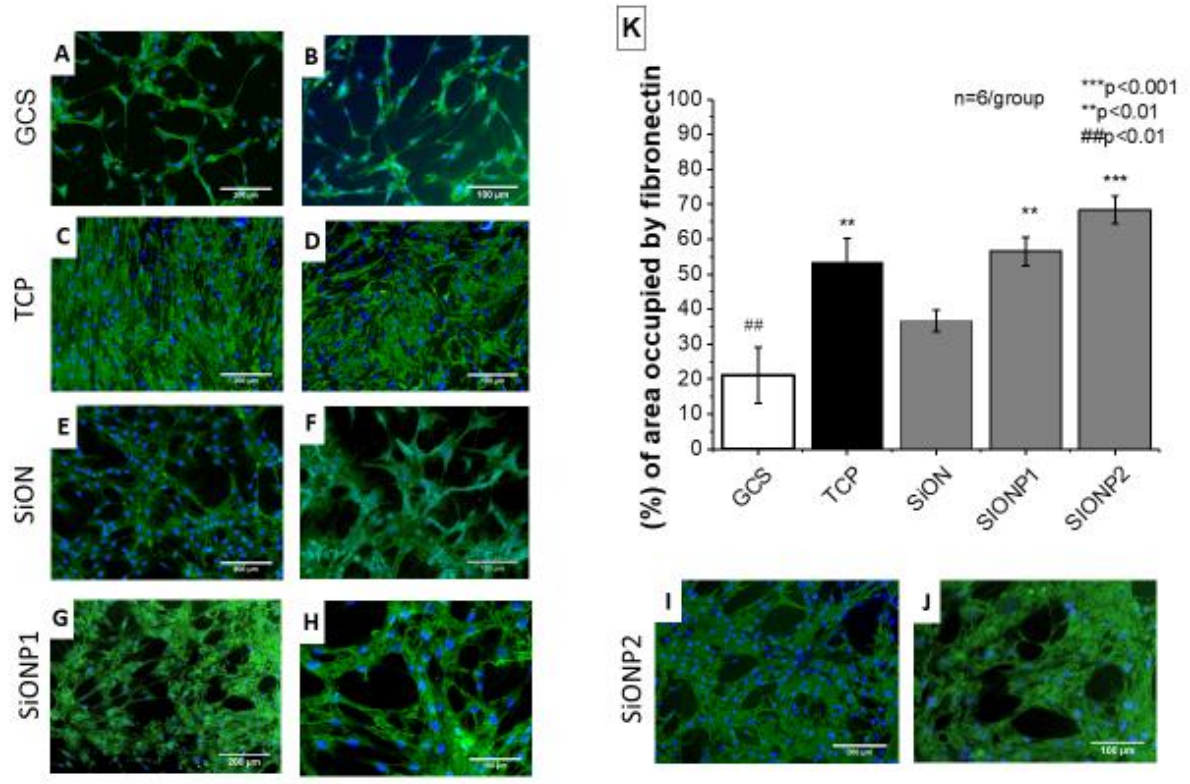

Figure 7. HUVECs matrix deposition after 5 days in cell culture. A-J) fluorescent pictures of fibronectin immunostaining and DAPI (nuclei staining). A, C, E, G and I were captured in 10x view, scale bar = 200 μm. B, D, F, H and J were captured in 20x view, scale bar=100 μm. (***p<0.001, **p<0.01, ##p<0.01). GCS→ glass cover slip, TCP→ tissue culture plate.

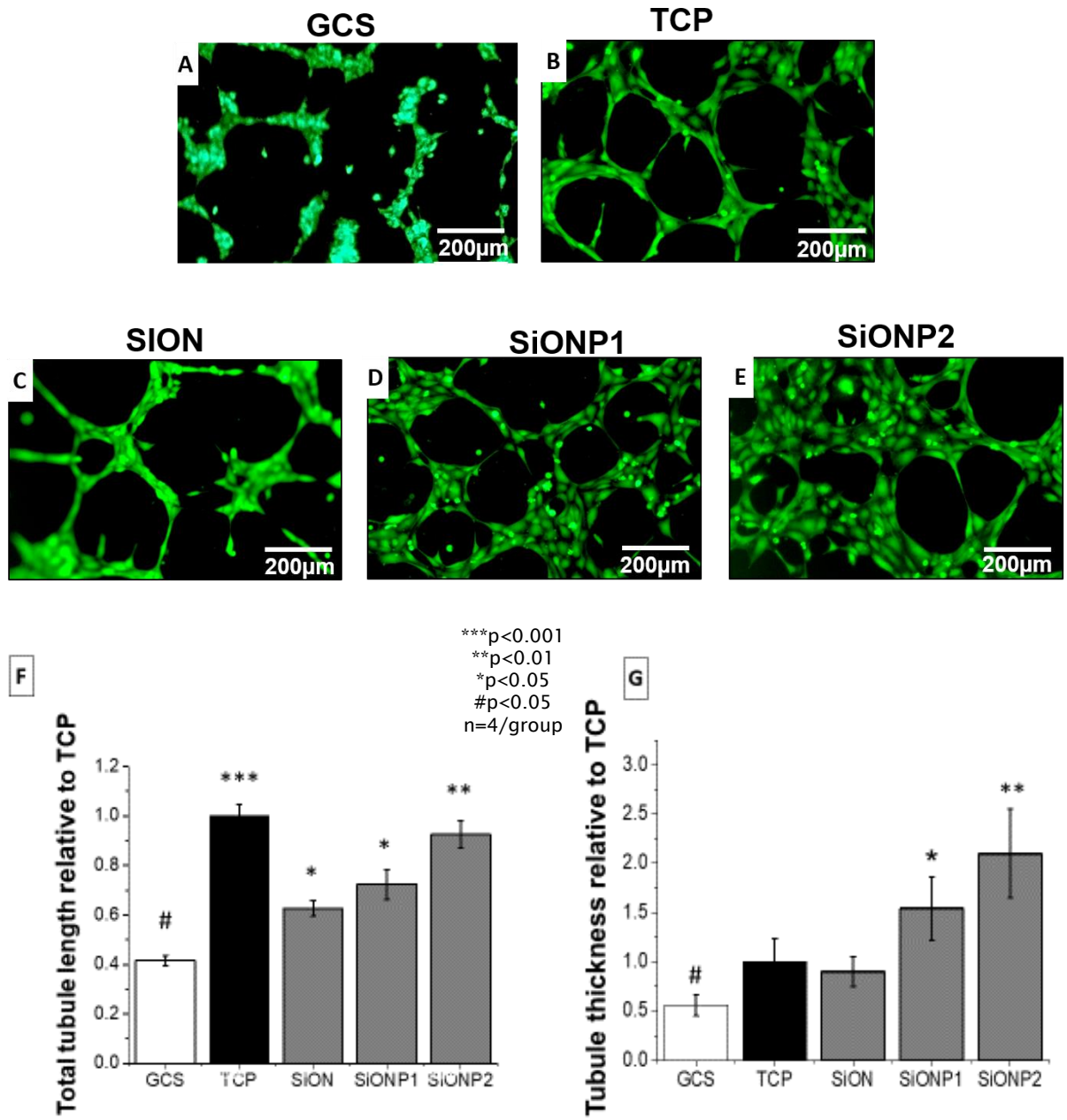

Figure 8. Capillary tubule formation 6 hours afterculture on bed of Matrigel®. A-E) Fluorescent images captured after Calcein-AM staining. Scale bar= 200 µm. F) Bar graph shows tubule length relative to TCP (positive control). G) Bar graph shows Tubules thickness relative to TCP (positive control). (***p<0.001, **p<0.01, *p<0.05, #p<0.05). GCS→ glass cover slip, TCP→ tissue culture plate.

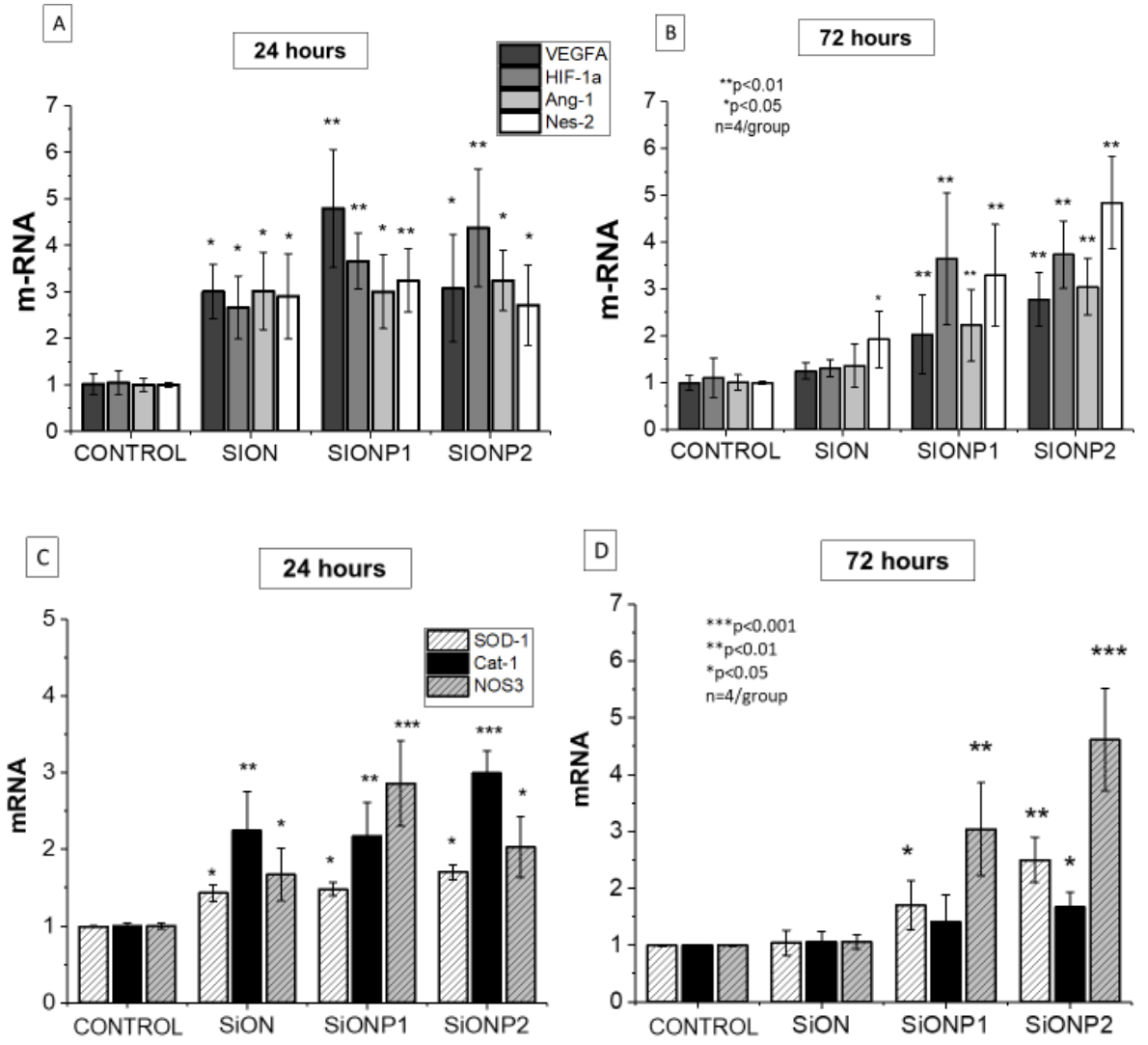

Figure 9. Gene expression angiogenic markers relative to 18S as compared to control at 24 hours (A) and 72 hours (B). Gene expression antioxidant enzymes relative to 18S as compared to control at 24 hours (C) and 72 hours (D). (***p<0.001, **p<0.01, *p<0.05). CONTROL→ endothelial cell basal medium supplemented with 2% FBS on tissue culture plate., VEGFA→ vascular endothelia growth factor A, HIF-1a→ hypoxia inducible growth factor 1 alfa, Ang-1→ angiopoietin-1, Nes-2→ Nesprin-2.

CHAPTER 5

AMORPHOUS SILICA COATING IMPLANTS IMPROVE ANGIOGENESIS AND REDUCE OXIDATIVE STRESS IN CRITICAL SIZE BONE DEFECT BY UPREGULATING VEGFA, ANGIOPOIETIN-1, AND ANTIOXIDANT ENZYMES

Felipe A. do Monte[1,2], Neelam Ahuja[3,] Kamal R. Awad[4], Ami Shah[4], Harry K.W. Kim[2,5], Pranesh Aswath[4], Venu G. Varanasi[3]*

[1] Department of Bioengineering, University of Texas at Arlington, Arlington Texas 76019, USA

[2] Center for Excellence in Hip Disorders, Texas Scottish Rite Hospital, Dallas, Texas 75219, USA

[3] Department of Biomedical Sciences, Texas A&M University College of Dentistry, Dallas, Texas 75246, USA

[4] Department of Materials Science and Engineering, University of Texas at Arlington, Arlington Texas 76019, USA

[5] Department of Orthopedic Surgery, University of Texas Southwestern Medical Center at Dallas, Dallas, Texas 75390, USA

* To whom correspondence should be addressed:

Venu G. Varanasi, Ph.D.

3302 Gaston Avenue, Texas A&M Health Science Center, Dallas, Texas 75246, USA

Phone: +1-214-370-7006, Fax: +1-214-874-4538

E-mail: vvaranasi@tamhsc.edu

ABSTRACT

Biomaterials for bone replacement need improved biocompatibility and osteointegration. Oxidative stress and decreased angiogenesis are contributing factors for poor compatibility and osteointegration. Studies demonstrated that ionic silicon released from biomaterials enhance osteogenesis and angiogenesis by upregulating superoxidase dismutase 1 and hypoxia inducible factor-1 alfa. The purpose of this study was to test angiogenic and antioxidant properties of an amorphous silica coating formed by Si, O, N and P under the toxic oxidative stress environment present in large bone defects. An in vitro experiment evaluated the effect of SiON and two different SiONP coating compositions, SiONP1and SiONP2, in human umbilical vein endothelial cells (HUVECS) under toxic oxidative stress and compared them to a tissue culture plate (TCP) and a glass cover slip (GCS). An in vivo study (n=3/group) compared a Si wafer and the SiONP2 groups using a rat critical size calvarial defect; two defects were made per animal, empty (right) and with implants (left). A group of animals was used as a sham (no bone defect, n=3). Our results showed that implants coated with amorphous silica, particularly SiONP2 coating group, significantly reduced cell death ($p<0.001$), enhanced tubule formation and matrix deposition ($p<0.01$) by upregulating VEGFA, angiopoetin-1, superoxidase dismuatse-1 and catalase-1. Animals which received SiONP2 implants presented a 4-HNE protein adduct serum concentration similar to pre-operatory 7 days after surgery ($p=0.28$). Moreover, CD31 positive cells demonstrating a tubular structure was significantly enhanced on the SIONP2 coating group compared to an empty and Si wafer ($p<0.01$). These findings suggest that an amorphous silica coating could improve implants osteointegration and reduce incidence of loosening and failure by mitigating the oxidative stress and enhancing angiogenesis.

Keywords: Oxidative stress, angiogenesis, PECVD, amorphous silica, antioxidants, matrix deposition, capillary tubule formation.

1. INTRODUCTION

Surgeons usually face loosening and failure of implants used for bone replacement. The cost of a surgical revision after these complications can be twice of the initial procedure[1]. Dental and orthopedics implants failure is defined as the inability of implants to osteointegrate to surround host tissue due to a foreign body response and/or opportunistic infection[2][3]. During the first moments of biomaterials implantation in a bone defect area, the surrounded biological tissue can undergo severe and harmful oxidative stress conditions[2–4]. High levels of oxidative stress can be deleterious to endothelial cells[5]. Endothelial cells survival and proliferation are necessary for adequate new blood vessel formation and play a major role on bone regeneration[6]. Therefore, it seems that to minimize complications, such as implants loosening and failure, and facilitate osteointegration, the materials used on bone defects reconstruction must have an antioxidant effect, as well as enhances angiogenesis. Ionic silicon has been used in combination with nitrogen and/or oxygen as implants composition and coating with the aim to enhance new bone formation and osteointegration[7–9]. Our group's recent publication showed that ionic Si is important on superoxidase dismutase activity[9]. This enzyme plays a major role on metabolism of superoxide, which is the main reactive oxygen species produced on cell metabolism. Moreover, ionic silicon can enhance angiogenesis by upregulating HIF-1a and VEGFA in HUVECs[10]. Studies demonstrated that ionic phosphorus can enhance angiogenesis by upregulating vascular endothelial growth factors A (VEGFA) and inducing cell migration, matrix deposition and capillary tubule formation in HUVECs [11–13].

In our literature review we did not find any link between the ionic silicon or angiopoietin-1 (ang-1). Preliminary experiments from our group have shown that PECVD coating amorphous silica based implants (SiON and SiONP) can upregulate ang-1 in HUVECs under normal condition (EBM-2 + FBS without H_2O_2). As the angiopoietin-1 proved to prevent apoptosis in endothelial cells under critical survival conditions by activating tyrosine kinase (Tie2)-receptor[14–17], perhaps the use of silica based materials can enhance angiogenic properties of endothelial cells under deleterious oxidative stress.

Plasma enhanced chemical vapor deposition is a coating method that showed to be useful for biomaterials manufacturing due to use a relatively low temperature processing method, to enhance interfacial adhesion and to allow surface pattern before coating, which can enhance cell attachment and matrix deposition due to a mimic nano and microstructure of an extracellular matrix[8,9].

In the present study, we hypothesize that a PECVD amorphous silica coating of SiON and SiONP overlays will enhance the angiogenesis on HUVECs exposed to toxic levels of H_2O_2. Also, these different chemistry coatings could enhance angiogenesis and reduce oxidative stress markers during the early stages of critical size bone defect healing.

To test these hypothesis, we investigated the effect of PECVD implants coating formed by Si, O, N and P on angiogenesis under a toxic oxidative stress environment induced by 0.6 mM H_2O_2. *In vitro* experiments evaluated the implants on HUVECs viability, matrix deposition, tube formation and gene expression of angiogenic and antioxidant markers. An *in vivo* study analyzed 4-Hydroxynonenal (4-HNE) levels on

the blood stream, and CD31 and 4-HNE on a histological section after implants were placed in rat critical size calvarial defect.

2. MATERIALS AND METHODS

2.1 PECVD coating amorphous silica based implants preparation and surface elemental composition

In the current study, four inches <100> test grade P-type silicon wafers were purchased from NOVA Electronic Materials, 1189 Porter Rd. Flower Mound, TX, USA. Standard cleaning procedure was used to clean the silicon wafers. Firstly, the silicon wafers were immersed for 10 minutes in a piranha solution (3:1 mixture of sulfuric acid (H_2SO_4, 96%) and hydrogen peroxide (H_2O_2, 30%)). Then, they were removed and rinsed in deionized (DI) water for 1 minute. Secondly, to remove the native oxide layer, the silicon wafers were immersed in hydrofluoric acid for 30-60 sec. Finally, the wafers were rinsed in DI water for three cleaning cycles with a continuous DI water purge and then were dried with N_2 gas and placed on 200° C hot plate for five minutes [8,9].

A TRION ORION II PECVD/LPECVD system (Trion Technology, Clearwater, FL) was used to deposit a 200nm uniform coating of SiON and two different compositions of SiONP overlays as indicated in **Table 1**. All coatings were processed at a substrate temperature of 400°C, chamber pressure of 900 mTorr, an inductively coupled plasma ICP power of 30 W, and an applied excitation frequency of 13.56 MHz. Gases source and flow rate of each gas also are indicated in **table 1**.

The refractive indices and films thickness were measured using ellipsometry at a wavelength of 632.8 nm (Gaertner LS300). The results of thickness and refractive indices were also confirmed using of a reflectometer (Ocean Optics NC-UV-VIS TF Reflectometer).

We used the scanning electron microscopy (SEM) (Hitachi S-3000N Variable Pressure) at voltage of 20 KeV for verifying film thickness. Moreover, the instrument was used to identify and measure the surface elemental composition of the PECVD coating implants using Energy Dispersive X-Ray Analysis (EDX) apparatus at voltage of 12 KeV. The surface elemental composition can be seen in **table 2**.

In vitro study

Using HUVECs from passage 2 to 4 acquired from Lonza®, endothelial cell growth medium 2 (EGM-2) was used for cell growth and subculture, and endothelial cell basal media 2 (EGM-2) was used for the experiments, acquired from Lonza®. The experiments were divided into 5 groups: I- glass cover slip (GCS), II- tissue culture plate (TCP), III- SiON, IV- SiONP1, and V- SIONP2. Calcein-AM was used as fluorescent dye for live cells, and actin staining 488 and DAPI Nuclei staining on fixed samples. Purified mouse anti-fibronectin from BD Bioscience was used as a primary antibody and Goat anti mouse with Alexa 488 was used as secondary for fibronectin immune staining. ImageJ Software was used for quantitative data on pictures analysis. The hydrogen peroxide concentration used for mimicking an oxidative stress environment was 0.6 mM, the stock solution was acquired from Sigma-Aldreich 30% w/w in H_2O_2 with stabilizer. Based in preliminary experiments, this specific H_2O_2 concentration demonstrated to be toxic . Moreover, we used a phosphate buffered saline (PBS) from Sigma-Aldrich and Trypsin, a buffer and trypsin neutralizer from Lonza ® . Angiopoietin 1 Human ELISA Kit from Invitrogen®, and HNE competitive ELISA kit from Cell Biolabs, Inc.

2.2 Cells viability under toxic H_2O_2

Using a 12 well plate, PECVD amorphous silica coating implants (squared shape) measured 1.2x1.2 cm and GCS measured 1.5 cm diameter. HUVECS were

seeded on a studied surface (5000 cell/cm^2) in 100µL of EGM-2 and allowed to attached on a specific surface for 1 hour. After, we added 900 µL of EBM-2 + 10% FBS + H_2O_2 0.6 mM. The experiment ended 24 hours after the initial cell seeding and 4 samples/group was used for measuring the number of cells by MTS proliferation assay, and 3 samples per group was used for Calcein-AM staining and fluorescent pictures.

2.3 Matrix deposition under toxic H_2O_2

Using 4 samples per group, the cells were seeded as mentioned above on section 2.2 and the same media was used for mimicking an oxidative stress environment. After 48 hours under oxidative stress, the medium was changed for EBM-2 + 10% FBS without H_2O_2. Five days after the initial cell seeding the cells were fixed with 4% paraformaldehyde and immunostaining for fibronectin. Three pictures from different areas were captured per sample using 10x magnification on a Zeiss Axion cell culture fluorescent microscope, and the ImageJ was used for quantifying the area occupied by fibronectin.

2.4 Capillary tubule formation under toxic H_2O_2

Using 4 samples per group, PECVD implants and GCS were cut to 0.5x0.5 cm. Using a 48 well plate, PECVD coating amorphous silica based implants, GCS, and pipette tips were placed in 4 degrees Celsius 12 hours before the start of the experiment. Matrigel® without growth supplement was slowly thawed at 4 degrees Celsius for 12 hours. First, 100 µL of Matrigel® was placed on the implants, GCS and TCP, and the well plate was placed inside the cell culture incubator at 37ºC, 95% humidity and 5% CO_2 for 30 minutes. Second, 100µL of EBM-2 + H_2O_2 was used to seed 60,000 cell/cm^2 on bed of Matrigel®. Finally, six hours after the initial cell seeding, 50 µL of Calcein AM 2µM diluted in EBM-2 was added in each well, and after

30 minutes 3 pictures from different areas in 10x magnification were captured per well. The total tube length was calculated using the Angiogenesis Analyzer Software (ImageJ plug-in).

2.6 Gene expression of angiogenic and oxidative stress markers on HUVECS under toxic hydrogen peroxide levels.

The groups used on this experiment were as follows: TCP , SiON, SIONP1 and SiONP2. The cells were seeded on TCP and scaffolds (200,000 cells per well) in a 12 well plate, n=4/group and EBM-2 + 10% FBS + H_2O_2 0.6mM was used as a conditioned medium. After 24 hours the cells were lysed using the Tryzol method and after RNA collection and precipitation in 70% ethanol, and the RNA solution was purified using a miRNAeasy MINI KIT (50) from QIOGEN ®. RNA samples concentration were normalized to 100µg/mL and cDNA conversion was made using a Goscript™ Reverse transcriptase from Promega Corporation. It was prepared a 20µL reaction for reverse transcription polymerase chain reaction (RT-PCR) using the TagMAn® Gene Expression Assays and the PCR machine from life technology was set up for a standard protocol adjusted for 50 cycles. The results were expressed relative to the housekeeping gene 18S and compared to the control (TCP), and delta delta Ct method was used for calculations. Studied angiogenic markers: Vascular endothelial growth factor A (VEGFA, Nesprin-2 (SYNE2) and Angiopoietin 1 (Agpt-1). Studied oxidative stress markers: superoxidase dismutase 1 (SOD-1), Catalase-1 (Cat-1), nitric oxide synthase 3 (NOS-3), and Gluthathione peroxidase 1 (GPX-1) **(table 3)**.

2.7 Angiopoietin-1 and 4-HNE levels in conditioned medium using enzyme-linked immunosorbent assay (ELISA)

Using the same groups, sample size and conditioned medium used for PCR (section 2.6), the medium was collected before lysing the cells for RNA extraction, and placed in a 1.5 ml centrifuge tube with protease inhibitor (1:1000 dilution) and stored at – 20^0C. The samples were used for quantification of the protein concentration by bicinchoninic acid (BCA) assay. The BCA assay results were used to measure the amount of ang-1 per µg of protein per sample. The data and comparison among groups were expressed in a bar graph showing the values relative to control (TCP). The 4-HNE was measured by competitive ELISA and expressed in a bar graph in µg/ml.

In vivo study

Materials used on the procedure: disposable surgical blades n 15, gauze, dental bur n 1 and 2, PBS, templates made of silicon wafer (6x4mm), Isoflurane and Nalbuphine. In addition, we used suture (Vicryl 4-0) and accessories surgical tools.

Adult males Sprague Daley rats (~450 g) were used on this experiment for measuring local and systemic levels of oxidative stress markers and local angiogenesis. The study was approved by Institutional Animal Care and Use Committee (IACUC). The animals were randomly assigned for specific treatment. The animal study had 3 groups (n=3/group): I - sham, II – silicon wafer and III - SiONP2. In group I (sham), the surgical procedure was the same as the other groups without the bone defect. Groups II and III, had two critical size calvarial defects measuring 6x4 mm on each side of median sagittal suture following the same technique used on the previous publication. [9] The right side was empty (internal control) and the left side

was implanted with SIONP2 samples or silicon wafer samples (negative control). All the animals were sacrificed in CO_2 chamber 2 weeks after the surgical procedure.

Summary of the surgical procedure: Immediately before surgery, 0.1-0.12 ml of painkiller/sedative nalbuphine was injected subcutaneously. With the animal under anesthesia (2-3% isoflurane), we made an incision of approximately 2.5 cm on an imaginary line traced over the sagittal suture, from between eyes to posterior. The cut was from the skin to the periosteum. Then, the periosteum was carefully elevated and spread to expose the two parietal bones. The two bone defects were created using a dental bur number 1 and/or 2 and the implant was placed in the left side. At the end the skin was sutured with Vicryl 4.0.

2.8 Systemic detection of oxidative stress marker

Blood samples were collected from the animal tail vein (n=4/group), placed in a centrifuge tube and centrifuged at 5000 rpm for 10 minutes. The supernatant formed by the serum was storage at - 80^0C up to measuring 4-HNE by a competitive enzyme-linked immunosorbent assay (ELISA) kit acquired from Cell Biolabs, Inc. Time points: just before surgery, 1 week, and 2 weeks (just before sacrifice the animals). After 1 week and 2 weeks, the animals were anesthetized using 2-3% isoflurane for samples collection.

2.9 Local detection of angiogenic and oxidative stress markers (histological analysis)

After sacrifice, the calvarial samples were harvested using a diamond saw and preserving at least 5 mm of the original defect limits and implanted samples. All sham samples had a sagittal suture and parietal bones preserved. The samples were fixed in 4% paraformaldehyde at 4^0C during 5 days, and decalcified by

ethylenediaminetetraacetic acid (EDTA) for 1 week. Half of each sample was used for frozen section and half for plastic.

Sanderson's Staining

The samples in plastic were polished and cleaned using polishing cloth and washed with tap water and ultrasound cleaner. Afterward, the samples were stained with Sanderson's stain and counterstain with acid Fuchsin. Digital images were acquired using 10x objective of BIOQUANT OSTEOIMAGER (BIOQUANT Image Analysis Corp, Nashville, TN). These images were used to show anatomic relation between the bone defects and the implants and demonstrates the analyzed area on immunofluorescence staining.

Immunostaining (CD31 and 4-HNE)

The samples used for frozen sections were perfused with sucrose and imbedded in an optimal cutting temperature compound for a frozen section and further immunostaining for CD31 (endothelial cell marker) and 4-HNE (oxidative stress marker). After frozen the samples were cut 10 µm thickness in a coronal plane in a way to maintain the bone defects with and without implant in the same slide. The staining procedure was as follows: first, the slides were washed with PBS and blocked with 10% goat serum. Second, washed with PBS and the primary antibodies were placed on the slides and incubated overnight at 4 ^{0}C, Rabbit polyclonal to 4-HNE (ab46545) 1:8000 and Rabbit polyclonal CD-31 (M20)^{TM} 1:500. Lastly, we placed in the slides the secondary antibodies Alexa Dye 594 Goat anti Rabbit in 1:200 dilution, washed twice with PBS and mount with cover slip for microscope evaluation. One slide per group was used as negative control and was not exposed to the primary anti-body. The pictures were captured from the central area just above the implant or central

fibrotic tissue (empty) of the defect in other to minimize presence of neovascularization from surrounded bone. We used a 20x objective from a Zeiss Axion cell culture fluorescent microscope for images acquisition. We captured 3 images per slide, and the slides were obtained from thee different areas (anterior, medium and posterior). ImageJ software was used to calculate the amount of fluorescence in relation to the total area.

2.10 Statistical Methods

The results were presented in charts showing the mean, standard deviation and symbols demonstrating significance levels. Student *t*-test was used for comparing a difference between means from the two groups for a significance level $p<0.05$. One-way ANOVA (Tukey's Pairwise) was used when it was compared means from more than two groups for a significance level $p<0.05$. OrigenPro 2017, Past3 and Microsoft Excel 2016 Software were used for graphics and calculations. G-power software was used for sample size calculation for 80% power, $\alpha = 0.05$, and effect size = 0.30.

3. RESULTS

3.1 Cell Viability under toxic H_2O_2

GCS and TCP showed a significant reduction of approximately 20% and 40%, respectively, in a viable cells number compared to initial cell seeding ($p<0.001$). TCP group presented almost 50% lower number of cells compared to SiON, SiONP1 and SiONP2 ($p<0.01$). There was no significant difference among PECVD coating amorphous silica based implants groups. **(Figure 1)**

3.2 Matrix deposition after exposed to toxic H_2O_2 environment

The GCS group presented 3 times lower fibronectin deposition (21.35 ± 10.19 %) than SiON (71.46 ± 4.58 %) and SiONP1 (72.59 ± 3.84 %) groups ($p<0.05$), and

4 times lower than SiONP2 (90.11 ± 7.06 %, $p<0.01$). The TCP group showed a significant reduction of fibronectin deposition (48.64 ± 12.29) compared to SION, SiONP1 ($p<0.05$) and SiONP2 ($p<0.01$). (**Figure 2B**).

Fluorescent pictures showed that the GCS group presented a decreased fibronectin deposition, despite the tubular network structure. The TCP group showed more fibronectin deposition than the GCS group, however, with a minimum tubular arrangement of the fibers. SION, SIONP1 and SIONP2 groups presented an enhancement on fibronectin deposition compared to GCS and TCP. There was a remarkable enhancement in a tubular structure network on all amorphous silica based implants, and SIONP2 group demonstrated more dense structure. (**Figure 2A)**

3.3 Capillary tubule formation under toxic H_2O_2

Fluorescent images and tubule network lines traced on ImageJ software demonstrated the improvement of tubule structure formation and length on HUVECS placed on PECVD coating amorphous silica based materials compared to GCS and TCP. (**Figure 3A**).

All amorphous silica groups presented a significant enhancement on total tubule length compared TCP. SION implants showed 30% improvement ($p<0.05$), SIONP1 43% improvement ($p<0.05$) and SIOPN2 65% improvement ($p<0.01$). GCS presented a significant reduction in total tubule length compared to all other groups ($p<0.01$). (**Figure 3B**).

3.4 Angiopoietin-1 and 4-HNE protein adduct levels in conditioned medium after oxidative stress (ELISA)

After 24 hours, our results demonstrated that compared to control (TCP), amorphous silica groups induced a remarkable increase in ang-1 production by

HUVECs under toxic oxidative stress. The SION group increased 2 fold, the SiONP1 more than 6 fold, and the SIONP2 almost 5 fold. (**Figure 4A**)

There was no significant difference in 4-HNE protein adduct levels among the implants coated with amorphous silica. However, all of the amorphous silica coating groups presented a significant reduction compared to TCP (control) ($p<0.05$). **(Figure 4B)**

3.5 Gene expression of angiogenic and oxidative stress markers on HUVECS under toxic hydrogen peroxide levels.

All angiogenic makers (VEGFA, NES-2 and ang-1) were significantly overexpressed on amorphous silica implants compared to the control. VEGFA was at least 2 times overexpressed in HUVECs seeded on PECVD coating implants ($p<0.05$). Nesprin-2 was overexpressed in SiON (1.64 ± 0.11 times, $p<0.01$), SIONP1 (1.44 ± 0.1 times , $p<0.01$) and SIONP2 (1.67 ± 0.2 times, $p<0.01$). Ang-1 was overexpressed in SION (1.47 ± 0.12 times, $p<0.05$), SiONP1 (1.79 ± 0.35 times, $p<0.05$) and SIONP2 (2.71 ± 0.98 times, $p<0.05$). (**Figure 5)**

Among all studied oxidative stress markers (cat-1, SOD-1, GPX and NOS3), GPX presented no significant difference compared to the control group. Catalase 1 was significantly overexpressed in SiON (1.49 ± 0.12 times, $p<0.05$), SIONP1 (1.69 ± 0.11 times, $p<0.05$), and SIONP2 (1.75 ± 0.23 times, $p<0.05$). SOD1 was significantly overexpressed in SiON (2.91 ± 0.24, times, $p<0.01$), SIONP1 (2.76 ± 0.14, $p<0.05$), and SiONP2 (2.16 ± 0.42, $p<0.05$). NOS3 was significantly overexpressed in SION (1.22 ± 0.09 fold, $p<0.05$), SiONP1 (1.46 ± 0.21 times, $p<0.05$), and SiONP2 (1.64 ± 0.27 times, $p<0.05$). (**Figure 6**)

In vivo

The surgical procedure with biomaterial's implantation can be seen on **figure 7A**. During the samples' harvesting there was no macroscope evidence of inflammation and all the samples were well placed inside the defect as can be verified on X-ray images in **figure 7B**.

3.6 Serum levels of 4-HNE protein adduct (ELISA)

At 7 days (57.81±6.4 µg/ml) after surgery, there was a significant elevation in the 4-HNE serum concentration compared to the pre-operatory (42.64±1.72 µg/ml) and 15 days (37.32±4.11 µg/ml) after surgery in the Si wafer group ($p<0.05$). The other groups did not show significant difference among the three time points inside the same e group ($p>0.05$).

At 7 days after surgical procedure there was a significant elevation in 4-HNE serum concentration to the same timepoint of the sham group (39.67±1.28 µg/ml) ($p<0.05$). (**Figure 8**)

3.8 Histology

Sanderson's Staining

The slide was used the show areas used to capture fluorescent images after CD31 and 4-HNE immunostaining. The sham sample is demonstrated on figure 9A and the black rectangular box represents the analyzed area. The bone defect sample in showed on figure 9B. The green rectangular box represents the empty, the red rectangular box represents the new tissue formed on the implants, and the red circle represents the rat calvarial muscle area.

Immunostaining (CD31 and 4-HNE)

Our results showed that rats implanted with SiONP demonstrated a statistically significant enhancement in CD31 positive cells, with at 2 fold more than empty and Si wafer ($p<0.01$). There was no significant difference among SiONP2, muscle (positive control) and sham groups ($p>0.05$). (**Figure 10**)

There was no difference among the groups in percentage of area occupied by 4-HNE tissue fluorescence signal ($p>0.05$). (**Figure11**)

DISCUSSION

In the present study we tested the hypothesis that amorphous silica based materials could enhance angiogenesis in an oxidative stress environment. Here we distinctively demonstrated that implants PECVD coated with amorphous silica could enrich angiogenesis under deleterious oxidative stress conditions as could be seen on an *in vitro* experiment and an *in vivo* critical size bone defect.

Initially, we demonstrated that SiON and SIONP groups could reduce HUVECs' death and improve cells proliferation such as can be seen on **figure 1.** The ions released and/or surface energy are somehow having a protective effect on HUVECs exposed to 0.6 mM H_2O_2. We could not find studies that correlate silica based materials with a reduction of endothelial cells' death, particularly in experiments that use oxidative stress conditions. Studies reported that ionic silicon and silica based materials improve endothelial cells' proliferation by upregulating HIF-1a and VEGFA.[10,18–20] These findings suggested that these biomaterials could accelerate tissue regeneration and accordingly the angiogenesis and the new bone formation even under unfavorable conditions, such as hypoxia and elevated reactive oxygen species present in large and complex bone defects.

In the following *in vitro* experiments we detected a relevant improvement in the length of the capillary tubule network and the fibronectin deposition in all PECVD coated amorphous silica implants, particularly the SiONP2 group, which clearly formed more matrix with an evident circular structure (**Figure 2A)**. Some studies demonstrated that silica based materials can improve endothelial cells' capillary tubule formation properties.[10,21] However, none of those showed this effect under oxidative stress conditions as we observed in our experiments. This fact could facilitate the interaction between the biomaterial and the host tissue and improve angiogenesis under a toxic oxidative stress environment. Fibronectin is a glycoprotein that is produced by HUVECs and plays a major role in an extracellular matrix formation during angiogenesis. This protein regulates vascular remodeling, endothelial cell migration, survival and elongation.[22–24] In our experiment we can see on **figures 2C, 2D and 2E** that SiON, SiONP1 and SiONP2 groups presented a fibronectin deposition in a circular shape with significantly increased density in the SiONP groups. We could not find studies that associate fibronectin deposition and silica based biomaterials under normal or oxidative stress conditions.

We measured the concentration of ang-1 and 4-HNE in conditioned media collected from the HUVECs' culture after 24 hours under oxidative stress induced by H_2O_2. We demonstrated that ang-1 production was enhanced in HUVECs exposed to SiON, SiONP1 and SiONP2 (**Figure 4A**). In addition, all PECVD coating implant groups presented a significant reduction of 4-HNE adduct (**Figure 4B**). Ang-1 has been related to protection of endothelial cells against apoptosis when they are under unfavorable survival condition.[14,16] Moreover, this protein is important for endothelial cells migration, proliferation and differentiation.[17,25] Another pertinent aspect is that ang-1 can induce osteoblast differentiation, bone matrix deposition and

enhance bone mineral density [26,27]. The 4-HNE protein adduct is a product of lipid peroxidation and has been used to demonstrate the oxidative stress level *in vivo* and *in vitro*. Other molecules, such as Malondialdehyde (MDA) has been used to measure oxidative stress levels; however, MDA is less stable with a shorter half-live. Our results showed that the PECVD coating implants reduced oxidative stress and enhanced ang-1 production, which could be acting on prevention of HUVECs' death, such as was observed in our initial *in vitro* experiment (**Figure 1**).

The evaluation of the angiogenic markers gene expression demonstrated that the mRNA levels of ang-1 was at least 2.5 fold enhanced in the SiONP2 group, and that find corroborates with the protein level in the conditioned medium. VEGFA and Nesprin-2 mRNA levels were also enhanced in all implants coated with amorphous silica. The VEGFA is a well known major regulator of angiogenesis and can be stimulated by multiple factors.[28,29] Studies demonstrated that the ionic silicon released from the mesoporous silica and bioactive glasses can enhance angiogenesis by upregulating VEGFA.[10,30] As it was already mentioned above, ang-1 has its relevance in angiogenesis and osteogenesis.[14,16,17,26,27] Nesprin-2 is a large multi-domain protein that plays a dominant role regulating endothelial cell shape and migration. This protein connects the nuclei to the cytoskeleton and regulates the architecture of both structures, controlling the angiogenic loop formation during the pre-capillary tubule network organization.[31]

At the end of in vitro experiments, we measured the mRNA level of antioxidant enzymes and nitric oxide synthase. Our results showed that SOD-1 and cat-1 were significantly up regulated by PECVD coating surfaces. Moreover, the NOS3 level was significantly elevated in SiONP groups. SOD-1 is an enzyme which catalyzes the conversion of superoxide, the main reactive oxygen species produced during cell

metabolism to hydrogen peroxide. Cat-1 is a potent antioxidant protein that accelerates the conversion of H_2O_2 in H_2O and O_2. Thus, the enhancement of SOD-1 and cat-1 activity and production can reduce oxidative stress and accordingly improve biocompatibility ad osteointegration.[32] NOS3 is an enzyme that participates of nitric oxide (NO) synthesis and is important for angiogenesis and tissue regeneration.[33] Our group has reported the important role of ionic silicon in the SOD-1 regulation in osteoblasts differentiated from MC3T3 cells.[9] However, we could not find publications that correlated the effect of products of dissolution of silica based materials on endothelial cell regulation or production of SOD-1 and cat-1.

Previously, a study reported that products of dissolution of calcium silicate can stimulate angiogenesis by inducing nitric oxide synthase upregulation [34]. The NO can have an ambiguous role in angiogenesis under oxidative stress conditions. On one hand, high levels of superoxide can neutralize the angiogenic effect of NO by forming peroxydonitrite, which is a highly toxic molecule.[35] On the other hand, authors reported that NO suppresses angiostatin, which is an inhibitor of angiogenesis.[36] Lastly, NOS3 and NO are associated with fracture healing modulation and showed to be necessary for adequate bone formation,[37,38] which enforces the use of amorphous silica in bone defects.

In the *in vivo* experiments we measured the angiogenesis by CD31 and oxidative stress by 4-HNE immunofluorescent staining. In addition, the 4-HNE was measured from blood samples collected before and after surgery. The SiONP2 implant was used on the *in vivo* study due to present t the most relevant outcome in the *in vitro* experiments. SiONP2 implants presented CD31 positive cells comparable to sham and muscle samples. This supports our *in vitro* observations and demonstrates that these implants can support and enhance angiogenesis in critical size bone defects. 4-

HNE immune staining could not detect a difference between groups, probably because after 15 days the products of lipid peroxidation were already eliminated or adducted to other molecules. Studies shows that 4-HNE is unstable and can be difficult to detect after 10 days from the initial oxidative stress cause.[39,40]. After 7 days, the serum levels of 4-HNE adduct showed that animals implanted with SiONP2 in the left calvarial bone defect presented no difference compared to pre-operatory levels. This observation suggests that the implants coated with amorphous silica by the PECVD method can reduce oxidative stress and possibly improve and accelerate the biomaterial's osteointegration.

In general, all elements used in our study for the PECVD surface coating have been reported to facilitate angiogenesis.[13,41,42]. Among Si, N and P, silicon is the most studied and supported in enhancing angiogenesis.[10,43–46] As we can see in the **table 2**, the EDX analysis shows that the difference between SiON, SiONP1 and SiONP2 groups is mainly represented by Si, O and N at%, once the P represent less than 1 at% of surface composition. However, the addition of phosphorus and the different N_2O flow rate between SiONP1 and SiONP2 **(see table 1)** is playing the role of elemental surface composition of these two implants. It seems that the elevated silicon at% can be responsible for the SiONP1 and SiONP2 outcome in enhancing angiogenesis and reducing the oxidative stress demonstrated in our *in vitro* studies. In terms of ionic surface composition, the different results observed in the SiONP1 and SiONP2 groups can be attributed to oxygen content. The SiONP2 group presented twice more oxygen than the SiONP2. Furthermore, despite its to not being part of this study, we demonstrated in a concurrent manuscript that SiONP2 presented a significantly reduced wettability compared to SIONP1, which also can justify the most relevant angiogenic effect of implants coated with SiONP2, once more hydrophilic

surfaces could enhance angiogenesis by improving cell attachment and proliferation. [47,48]

We could notice that there was an antioxidant effect of the amorphous silica implants at different levels, once we observed an upregulation of SOD-1 and cat-1. The nuclear factor (erythroid-derived 2)-like 2 (Nfr2) is a latent protein that is a major transcriptional activator of genes coding for enzymatic antioxidants, such as catalase, Glutathione peroxidase and superoxidase dismutase.[49] One study showed that a diet rich in silicon could reduce oxidative stress in liver of old rat by upregulating Nfr2 and antioxidant enzymes production.[50] Perhaps this major regulator is playing a role in the antioxidant effect of amorphous silica in HUVECs.

The superoxidase dismutase has a cationic site formed by zinc and/or cooper that by electrostatic interaction facilitates the bond between the enzyme and the superoxide (O_2^-).[51–53] Using the same rational, maybe the Si^{+4} released from the implants coated with amorphous silica can reduce oxidative stress by interacting with the superoxide and preventing its interaction with lipids, DNA and proteins.

In conclusion, our study showed that implants coated with amorphous silica reduced cells' death, enhanced matrix deposition and capillary tube formation in HUVECs under toxic oxidative stress. In addition, we demonstrated under the same conditions that these implants upregulated ang-1, VEGFA and antioxidant enzymes. An *in vivo* experiment showed that the implants coated with amorphous silica, mainly SiONP2, enhanced new blood vessel formation and reduced oxidative stress. These findings support the use of implants coated with amorphous silica formed by Si (58.7 at%), O (14.2 at%), N (26.8 at%) and P (0.27 at%) in bone replacement due to create

a favorable environment for biomaterials osteointegration, and accordingly mitigation of implants loosening and failure.

ACKNOWLEDGMENTS

The authors would like to Dr. Olumide Aruwajoye, Dr. Suresh Adapala, Dr. Gen Kuroyanagi, Ila Oxendine, Yang Li, Reuel Cornelia, and Richard Banlaygas from the Center for Excellence in Hip Disorders, Texas Scottish Rite Hospital, for their assistance. We would like to thank the Brazilian Federal Government – Coordenacao de Aperfeicoamento de Pessoal de Nivel Superior (CAPES), for sponsoring the first author.

REFERENCES

[1] I.S. Vanhegan, A.K. Malik, P. Jayakumar, S. Ul Islam, F.S. Haddad, A financial analysis of revision hip arthroplasty: the economic burden in relation to the national tariff., J. Bone Joint Surg. Br. 94 (2012) 619–23. doi:10.1302/0301-620X.94B5.27073.

[2] D. Pietropaoli, E. Ortu, M. Severino, I. Ciarrocchi, R. Gatto, A. Monaco, Glycation and oxidative stress in the failure of dental implants: a case series., BMC Res. Notes. 6 (2013) 296. doi:10.1186/1756-0500-6-296.

[3] J. Lindhe, J. Meyle, Group D of European Workshop on Periodontology, Peri-implant diseases: Consensus Report of the Sixth European Workshop on Periodontology., J. Clin. Periodontol. 35 (2008) 282–5. doi:10.1111/j.1600-051X.2008.01283.x.

[4] C. Szpalski, J. Barr, M. Wetterau, P.B. Saadeh, S.M. Warren, Cranial bone defects: current and future strategies, Neurosurg. Focus. (2010).

doi:10.3171/2010.9.FOCUS10201.

[5] Z. Liu, Y. Liu, Q. Xu, H. Peng, Y. Tang, T. Yang, Z. Yu, G. Cheng, G. Zhang, R. Shi, Critical role of vascular peroxidase 1 in regulating endothelial nitric oxide synthase Endothelial nitric oxide synthase Nitric oxide Asymmetricdimethylarginine Angiotensin II Oxidative stress, Redox Biol. 12 (2017) 226–232. doi:10.1016/j.redox.2017.02.022.

[6] U. Saran, S.G. Piperni, S. Chatterjee, Role of angiogenesis in bone repair, Arch. Biochem. Biophys. 561 (2014) 109–117. doi:10.1016/j.abb.2014.07.006.

[7] R.M. Bock, B.J. McEntire, B.S. Bal, M.N. Rahaman, M. Boffelli, G. Pezzotti, Surface modulation of silicon nitride ceramics for orthopaedic applications, Acta Biomater. 26 (2015) 318–330. doi:10.1016/j.actbio.2015.08.014.

[8] A. Ilyas, N. V Lavrik, H.K.W. Kim, P.B. Aswath, V.G. Varanasi, Enhanced interfacial adhesion and osteogenesis for rapid "bone-like" biomineralization by PECVD-based silicon oxynitride overlays., ACS Appl. Mater. Interfaces. 7 (2015) 15368–79. doi:10.1021/acsami.5b03319.

[9] A. Ilyas, T. Odatsu, A. Shah, F. Monte, H.K.W. Kim, P. Kramer, P.B. Aswath, V.G. Varanasi, Amorphous Silica: A New Antioxidant Role for Rapid Critical-Sized Bone Defect Healing, Adv. Healthc. Mater. 5 (2016) 2199–2213. doi:10.1002/adhm.201600203.

[10] K. Dashnyam, G.-Z. Jin, J.-H. Kim, R. Perez, J.-H. Jang, H.-W. Kim, Promoting angiogenesis with mesoporous microcarriers through a synergistic action of delivered silicon ion and VEGF, Biomaterials. 116 (2017) 145–157. doi:10.1016/j.biomaterials.2016.11.053.

[11] C.E. Camalier, M. Yi, L.R. Yu, B.L. Hood, K.A. Conrads, Y.J. Lee, Y. Lin, L.M. Garneys, G.F. Bouloux, M.R. Young, T.D. Veenstra, R.M. Stephens, N.H. Colburn, T.P. Conrads, G.R. Beck, An integrated understanding of the physiological response to elevated extracellular phosphate, J. Cell. Physiol. 228 (2013) 1536–1550. doi:10.1002/jcp.24312.

[12] Y. Lin, K.E. Mckinnon, S.W. Ha, G.R. Beck, Inorganic phosphate induces cancer cell mediated angiogenesis dependent on forkhead box protein C2 (FOXC2) regulated osteopontin expression, Mol. Carcinog. 54 (2015) 926–934. doi:10.1002/mc.22153.

[13] M.A. Saghiri, A. Asatourian, J. Orangi, C.M. Sorenson, N. Sheibani, Functional role of inorganic trace elements in angiogenesis—Part I: N, Fe, Se, P, Au, and Ca, Crit. Rev. Oncol. 96 (2015) 129–142. doi:10.1016/j.critrevonc.2015.05.010.

[14] R. Harfouche, H.M. Hasséssian, Y. Guo, V. Faivre, C.B. Srikant, G.D. Yancopoulos, S.N.A. Hussain, Mechanisms Which Mediate the Antiapoptotic Effects of Angiopoietin-1 on Endothelial Cells, (n.d.). doi:10.1006/mvre.2002.2421.

[15] N.A. Abdel-Malak, M. Mofarrahi, D. Mayaki, L.M. Khachigian, S.N.A. Hussain, Early growth response-1 regulates angiopoietin-1-induced endothelial cell proliferation, migration, and differentiation., Arterioscler. Thromb. Vasc. Biol. 29 (2009) 209–16. doi:10.1161/ATVBAHA.108.181073.

[16] H. Jin Kwak, J.-N. So, S. Jae Lee, I. Kim, G. Young Koh, Angiopoietin-1 is an apoptosis survival factor for endothelial cells, (n.d.). https://ac.els-cdn.com/S0014579399003786/1-s2.0-S0014579399003786-main.pdf?_tid=8344d804-ae19-11e7-a15d-

00000aacb35e&acdnat=1507681205_7508a055f34ac8d044c0a7573b0878fb (accessed October 10, 2017).

[17] S. Harel, D. Mayaki, V. Sanchez, S.N.A. Hussain, NOX2, NOX4, and mitochondrial-derived reactive oxygen species contribute to angiopoietin-1 signaling and angiogenic responses in endothelial cells, (2017). doi:10.1016/j.vph.2017.03.002.

[18] A. Hoppe, N.S. Guldal, A.R. Boccaccini, A review of the biological response to ionic dissolution products from bioactive glasses and glass-ceramics., Biomaterials. 32 (2011) 2757–2774. doi:10.1016/j.biomaterials.2011.01.004.

[19] H. Li, J. Chang, Bioactive silicate materials stimulate angiogenesis in fibroblast and endothelial cell co-culture system through paracrine effect., Acta Biomater. 9 (2013) 6981–6991. doi:10.1016/j.actbio.2013.02.014.

[20] K. Dashnyam, A. El-Fiqi, J.O. Buitrago, R.A. Perez, J.C. Knowles, H.-W. Kim, A mini review focused on the proangiogenic role of silicate ions released from silicon-containing biomaterials, J. Tissue Eng. 8 (2017) 204173141770733. doi:10.1177/2041731417707339.

[21] W. Zhai, H. Lu, L. Chen, X. Lin, Y. Huang, K. Dai, K. Naoki, G. Chen, J. Chang, Silicate bioceramics induce angiogenesis during bone regeneration., Acta Biomater. 8 (2012) 341–349. doi:10.1016/j.actbio.2011.09.008.

[22] A. Hielscher, K. Ellis, C. Qiu, J. Porterfield, S. Gerecht, Fibronectin deposition participates in extracellular matrix assembly and vascular morphogenesis, PLoS One. 11 (2016) 1–27. doi:10.1371/journal.pone.0147600.

[23] H.Y. Chiang, V.A. Korshunov, A. Serour, F. Shi, J. Sottile, Fibronectin is an

important regulator of flow-induced vascular remodeling, Arterioscler. Thromb. Vasc. Biol. 29 (2009) 1074–1079. doi:10.1161/ATVBAHA.108.181081.

[24] H. Kiyonaga, Y. Doi, Y. Karasaki, K. Arashidani, H. Itoh, S. Fujimoto, H. Kiyonaga, H. Itoh, Y. Doi, S. Fujimoto, Y. Karasaki, K. Arashidani, Expressions of endothelin-1, fibronectin, and interleukin-1α of human umbilical vein endothelial cells under prolonged culture, Med Electron Microsc. 34 (2001) 41–53.
http://download.springer.com.ezproxy.uta.edu/static/pdf/392/art%253A10.1007%252Fs007950100003.pdf?originUrl=http%3A%2F%2Flink.springer.com%2Farticle%2F10.1007%2Fs007950100003&token2=exp=1490272151~acl=%2Fstatic%2Fpdf%2F392%2Fart%25253A10.1007%25252Fs00795 (accessed March 23, 2017).

[25] N.A. Abdel-Malak, C.B. Srikant, A.S. Kristof, S.A. Magder, J.A. Di Battista, S.N.A. Hussain, Angiopoietin-1 promotes endothelial cell proliferation and migration through AP-1-dependent autocrine production of interleukin-8., Blood. 111 (2008) 4145–54. doi:10.1182/blood-2007-08-110338.

[26] T. Suzuki, T. Miyamoto, N. Fujita, K. Ninomiya, R. Iwasaki, Y. Toyama, T. Suda, Osteoblast-specific Angiopoietin 1 overexpression increases bone mass, (2007). doi:10.1016/j.bbrc.2007.08.099.

[27] S.-H. Park, J. Lee, M.-A. Kang, Y.J. Moon, S. Il Wang, K.M. Kim, B.-H. Park, K.Y. Jang, J.R. Kim, Potential of L-thyroxine to differentiate osteoblast-like cells via Angiopoietin1, (2016). doi:10.1016/j.bbrc.2016.08.137.

[28] N. Ferrara, H.-P. Gerber, J. LeCouter, The biology of VEGF and its receptors., Nat. Med. 9 (2003) 669–676. doi:10.1038/nm0603-669.

[29] M. Shibuya, Vascular endothelial growth factor and its receptor system: physiological functions in angiogenesis and pathological roles in various diseases., J. Biochem. 153 (2013) 13–19. doi:10.1093/jb/mvs136.

[30] S. Zhao, L. Li, H. Wang, Y. Zhang, X. Cheng, N. Zhou, M.N. Rahaman, Z. Liu, W. Huang, C. Zhang, Wound dressings composed of copper-doped borate bioactive glass microfibers stimulate angiogenesis and heal full-thickness skin defects in a rodent model., Biomaterials. 53 (2015) 379–391. doi:10.1016/j.biomaterials.2015.02.112.

[31] S.J. King, K. Nowak, N. Suryavanshi, I. Holt, C.M. Shanahan, A.J. Ridley, Nesprin-1 and nesprin-2 regulate endothelial cell shape and migration, Cytoskeleton. 71 (2014) 423–434. doi:10.1002/cm.21182.

[32] P.A. Mouthuy, S.J.B. Snelling, S.G. Dakin, L. Milković, A.Č. Gašparović, A.J. Carr, N. Žarković, Biocompatibility of implantable materials: An oxidative stress viewpoint, Biomaterials. 109 (2016) 55–68. doi:10.1016/j.biomaterials.2016.09.010.

[33] A. Aicher, C. Heeschen, C. Mildner-Rihm, C. Urbich, C. Ihling, K. Technau-Ihling, A.M. Zeiher, S. Dimmeler, Essential role of endothelial nitric oxide synthase for mobilization of stem and progenitor cells, Nat. Med. 9 (2003) 1370–1376. doi:10.1038/nm948.

[34] M.Y. Chou, C.T. Kao, C.J. Hung, T.H. Huang, S.C. Huang, M.Y. Shie, B.C. Wu, Role of the P38 pathway in calcium silicate cement-induced cell viability and angiogenesis-related proteins of human dental pulp cell in vitro, J. Endod. 40 (2014) 818–824. doi:10.1016/j.joen.2013.09.041.

[35] U. Förstermann, W.C. Sessa, Nitric oxide synthases: regulation and function.,

Eur. Heart J. 33 (2012) 829–37, 837a–837d. doi:10.1093/eurheartj/ehr304.

[36] T. Matsunaga, D.W. Weihrauch, M.C. Moniz, J. Tessmer, D.C. Warltier, W.M. Chilian, Angiostatin inhibits coronary angiogenesis during impaired production of nitric oxide, Circulation. 105 (2002) 2185–2191. doi:10.1161/01.CIR.0000015856.84385.E9.

[37] A.D. Diwan, M.I.N.X. Wang, D. Jang, W.E.I. Zhu, G.A.C. Murrell, Nitric Oxide Modulates Fracture Healing, J. Bone Miner. Res. 15 (2000) 342–351. doi:10.1359/jbmr.2000.15.2.342.

[38] W. Zhu, a D. Diwan, J.H. Lin, G. a Murrell, Nitric oxide synthase isoforms during fracture healing., J. Bone Miner. Res. 16 (2001) 535–40. doi:10.1359/jbmr.2001.16.3.535.

[39] J.S.C.& B.-M. Dong Hyun Kim, Seung Jun Kwack, Kyung Sik Yoon, Lee, 4-Hydroxynonenal: A Superior Oxidative Biomarker Compared to Malondialdehyde and Carbonyl Content Induced by Carbon Tetrachloride in Rats, (n.d.). file:///C:/Users/falve/Desktop/752208.pdf (accessed October 7, 2017).

[40] C.M. Spickett, The lipid peroxidation product 4-hydroxy-2-nonenal: Advances in chemistry and analysis, Redox Biol. 1 (2013) 145–152. doi:10.1016/j.redox.2013.01.007.

[41] M.A. Saghiri, A. Asatourian, J. Orangi, C.M. Sorenson, N. Sheibani, Functional role of inorganic trace elements in angiogenesis—Part II: Cr, Si, Zn, Cu, and S, Crit. Rev. Oncol. Hematol. 96 (2015) 143–155. doi:10.1016/j.critrevonc.2015.05.011.

[42] M.A. Saghiri, J. Orangi, A. Asatourian, C.M. Sorenson, N. Sheibani, M.A. Saghiri, Functional Role of Inorganic Trace Elements in in Angiogenesis Part III: (Ti, Li, Ce, As, Hg, Va, Nb and Pb) HHS Public Access, Crit Rev Oncol Hematol. 98 (2016) 290–301. doi:10.1016/j.critrevonc.2015.10.004.

[43] L.A. Haro Durand, G.E. Vargas, R. Vera-Mesones, A. Baldi, M.P. Zago, M.A. Fanovich, A.R. Boccaccini, A. Gorustovich, In vitro human umbilical vein endothelial cells response to ionic dissolution products from lithium-containing 45S5 bioactive glass, Materials (Basel). 10 (2017). doi:10.3390/ma10070740.

[44] H. Keshaw, A. Forbes, R.M. Day, Release of angiogenic growth factors from cells encapsulated in alginate beads with bioactive glass., Biomaterials. 26 (2005) 4171–4179. doi:10.1016/j.biomaterials.2004.10.021.

[45] R.M. Day, Bioactive glass stimulates the secretion of angiogenic growth factors and angiogenesis in vitro., Tissue Eng. 11 (2005) 768–777. doi:10.1089/ten.2005.11.768.

[46] A. Hoppe, N.S. Güldal, A.R. Boccaccini, A review of the biological response to ionic dissolution products from bioactive glasses and glass-ceramics., Biomaterials. 32 (2011) 2757–74. doi:10.1016/j.biomaterials.2011.01.004.

[47] S.S. and J.S.L. and S.B.J. and D.H.S. and L.D.Y. and J.G.H. and C. Chaiwong, Wettability Effect of PECVD-SiO x Films on Poly(lactic acid) Induced by Oxygen Plasma on Protein Adsorption and Cell Attachment, J. Phys. Conf. Ser. 423 (2013) 12042. doi:10.1088/1742-6596/423/1/012042.

[48] Y. Arima, H. Iwata, Effect of wettability and surface functional groups on protein adsorption and cell adhesion using well-defined mixed self-assembled monolayers, Biomaterials. 28 (2007) 3074–3082.

doi:10.1016/j.biomaterials.2007.03.013.

[49] M. Gallorini, C. Petzel, C. Bolay, K.-A. Hiller, A. Cataldi, W. Buchalla, S. Krifka, H. Schweikl, Activation of the Nrf2-regulated antioxidant cell response inhibits HEMA-induced oxidative stress and supports cell viability., Biomaterials. 56 (2015) 114–128. doi:10.1016/j.biomaterials.2015.03.047.

[50] J.A. Santos-López, A. Garcimartín, P. Merino, M.E. López-Oliva, S. Bastida, J. Benedí, F.J. Sánchez-Muniz, Effects of Silicon vs. Hydroxytyrosol-Enriched Restructured Pork on Liver Oxidation Status of Aged Rats Fed High-Saturated/High-Cholesterol Diets, PLoS One. 11 (2016) e0147469. doi:10.1371/journal.pone.0147469.

[51] E.D. Getzoff, J.A. Tainer, P.K. Weiner, P.A. Kollman, J.S. Richardson, D.C. Richardson, Electrostatic recognition between superoxide and copper, zinc superoxide dismutase., Nature. 306 (1983) 287–290.

[52] C.L. Fisher, R.A. Hallewell, V.A. Roberts, J.A. Tainer, E.D. Getzoff, Probing the structural basis for enzyme-substrate recognition in Cu,Zn superoxide dismutase., Free Radic. Res. Commun. 12–13 Pt 1 (1991) 287–296.

[53] Y. Shi, R.A. Mowery, B.F. Shaw, Effect of metal loading and subcellular pH on net charge of superoxide dismutase-1., J. Mol. Biol. 425 (2013) 4388–4404. doi:10.1016/j.jmb.2013.07.018.

Tables and Illustrations

Table 1. Shows the three steps and flow rates of the different gases used for processing SiON, SIONP1 and SiONP2 implants. Used gases→ Silane (SiH_4), Nitrous oxide (N_2O), Ammonia (NH_4), Phosphine (PH_3), Nitrogen (N_2), Argon (carrier gas).

	SiH_4/Ar (15/85%)	PH_3/SiH_4/Ar (2/15/83%)	N_2O	N_2	NH_4	Ar	Time (sec)
Step 1	0	0	0	0	0	250	30
Step 2 ($SiON_x$)	24	0	155	225	50	0	226
Step 2 ($SiONP_x$)1 ($SiONP_x$)2	0	24	5 16	225	50	0	322
Step 3	0	0	0	0	0	250	30

Table 2. Energy-dispersive X-ray spectroscopy (EDS) analysis of atomic surface composition of SION, SiONP1 and SiONP2 coating. See EDS spectra below the table.

EDS compositional data (at%)

Sample	Si	O	N	P
SiON	52.5	35.1	12.3	0
SiONP1	61.8	7.3	30.5	0.28
SiONP2	58.7	14.2	26.8	0.27

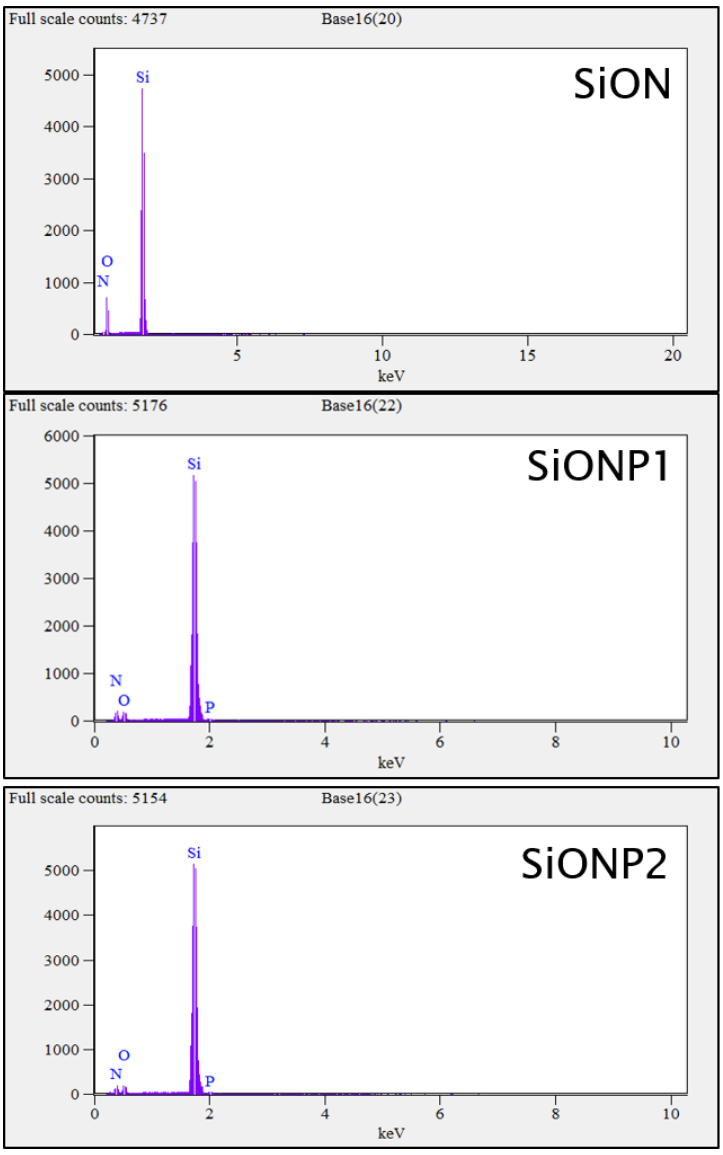

Table 3. Gene expression assay TaqMan® identification.

Gene	Assay identification
VEGFA	Hs00900055_m1
Ang-1	Hs00919202_m1
Nesprin-2 (SYNE2)	Hs00794881_m1
SOD-1	Hs00533490_m1
Cat-1 (CAT)	Hs00156308_m1
e-NOS (NOS3)	Hs01574665_m1

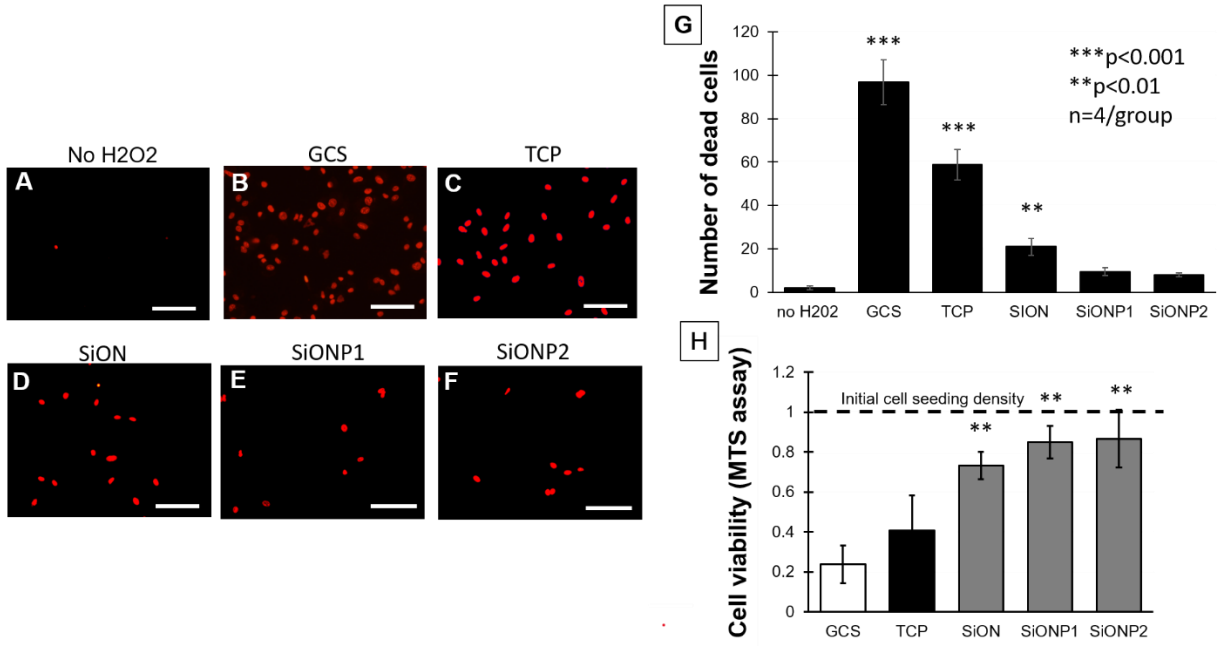

Figure 1. Effect of amorphous silica PECVD coating implants on HUVECs under toxic levels of H_2O_2 (24h). Scale bar = 100 µm. Figures A-F show propidium iodide (PI) staining. G) Bar graph of analysis after ANOVA (Tukey's pairwise) shows data from PI counting according to group. H) Bar graph shows comparison of cell viability among groups after MTS assay, the data was analyzed by ANOVA (Tukey's pairwise). (***p<0.001, **p<0.01). GCS→ Glass cover slip, TCP→ Tissue culture plate.

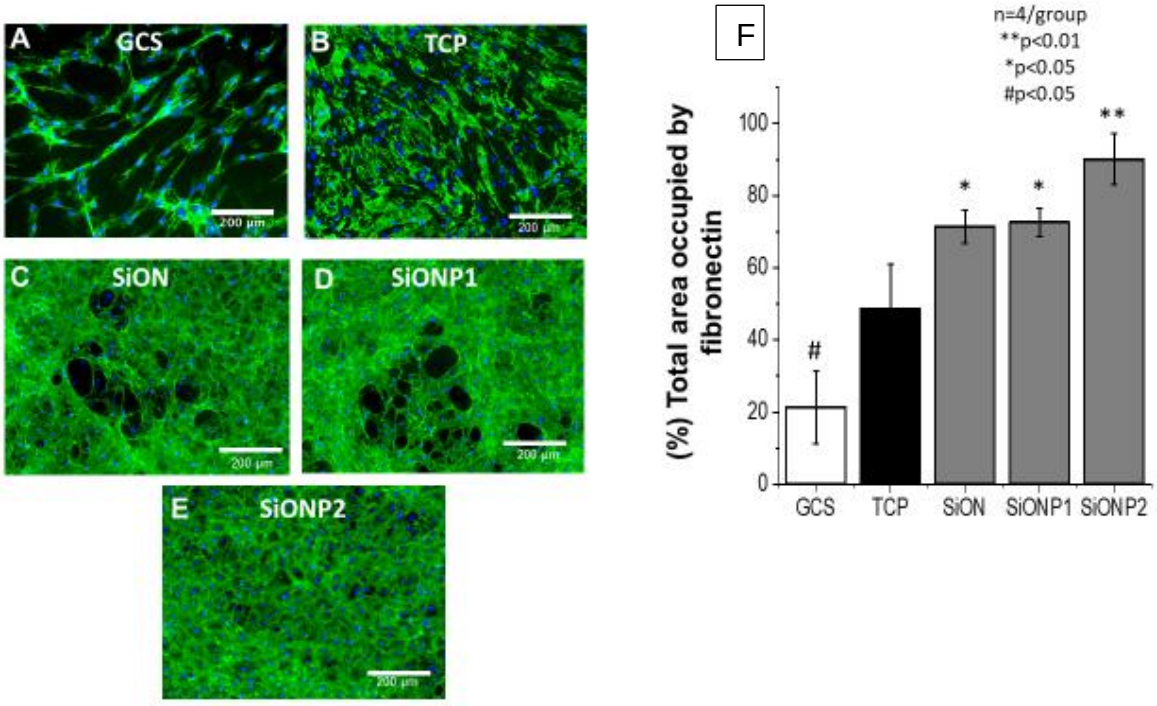

Figure 2. Shows fibronectin deposition. Pictures (A-E) show fluorescent images after immunostaining for fibronectin deposition 5 days after HUVECs were exposed to toxic oxidative stress (H_2O_2 0.6 mM). Scale bar = 200 µm. F) Bar graph of data analysis after ANOVA (Tukey's pairwise) shows of percentage of area occupied by fibronectin after data collection using ImageJ. (**p<0.01, *p<0.05, #p<0.05). GCS→ glass cover slip, TCP→ tissue culture plate.

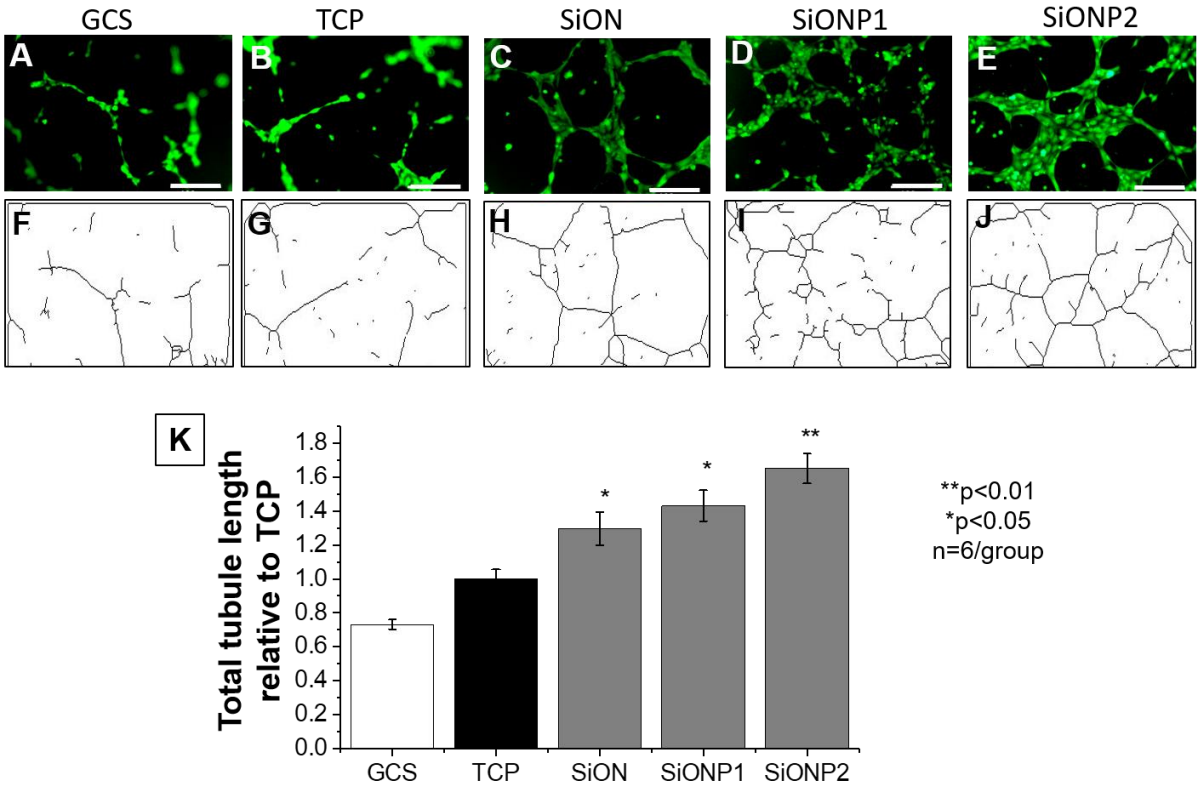

Figure 3. Representative Pictures (A-E), showing fluorescent images after Calcein-AM staining of HUVECs capillary tubule formation under toxic oxidative stress (H_2O_2 0.6 mM). Scale bar = 200 µm. Pictures (F-J) show tree capillary network traced lines after analysis by Angiogenesis analyzer (ImageJ plugin) software. K) Bar graph of data analysis after ANOVA (Tukey's pairwise), shows comparison of total tubule length. (**p<0.01, *p<0.05). GCS→ glass cover slip, TCP→ tissue culture plate.

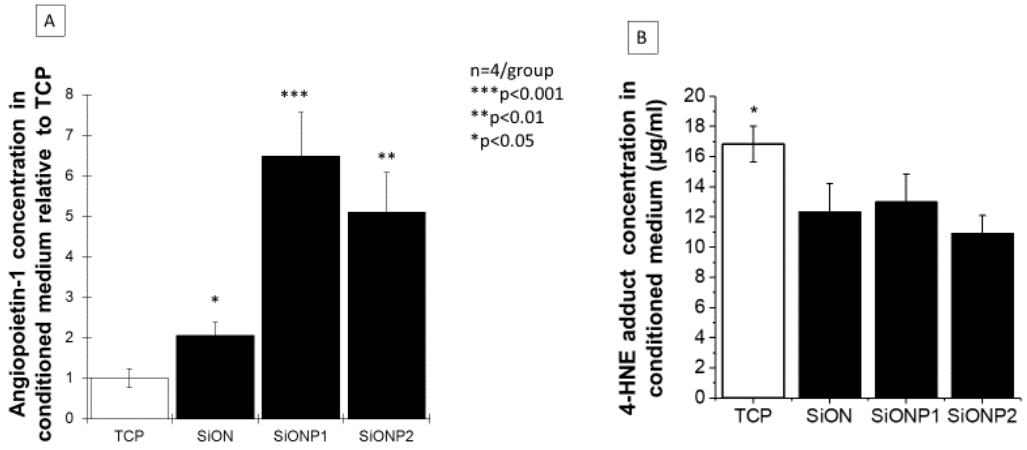

Figure 4. A) Bar graph comparing ang-1 concentration in conditioned medium relative to TCP (control). ANOVA (Tukey's pairwise) was used for analysis and BCA assay was used to quantify the amount of ang-1 per µg of total protein on each sample. B) Bar Graph shows 4-HNE protein addcuts concentration. The conditioned medium was obtained from HUVECs cell culture after 24 hours in toxic oxidative stress induced by 0.6mM H_2O_2. (***p<0.001, **p<0.01, *p<0.05). TCP→ tissue culture plate, ang-1→ angiopoietin 1, BCA→ bicinchoninic acid, 4-HNE→ 4-Hydroxynonenal.

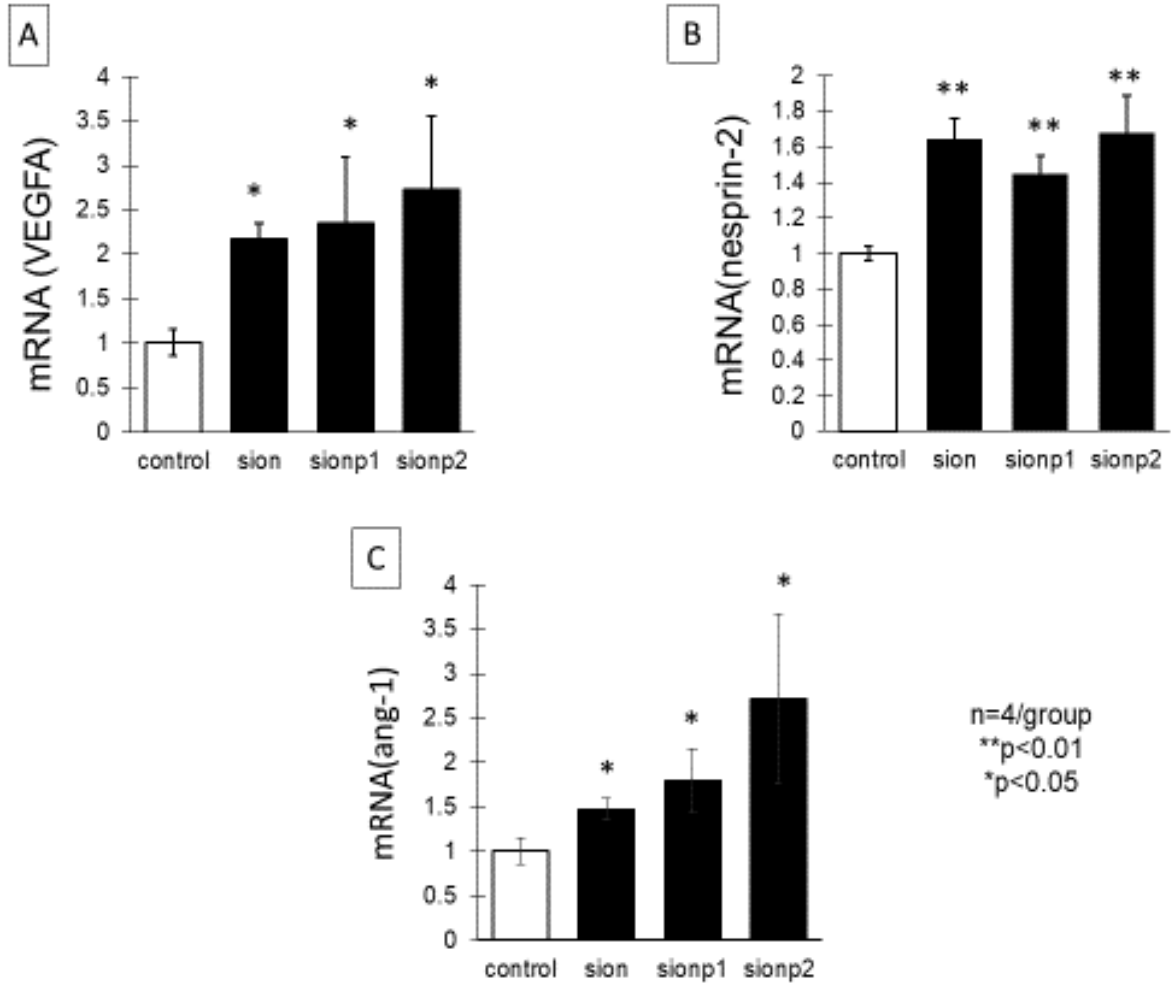

Figure 5. Bar graphs showing HUVECs gene expression angiogenic markers relative to 18S as compared to control 24 hours under toxic oxidative stress (H_2O_2 0.6mM). A) mRNA VEGFA. B) mRNA Nesprin-2. C) mRNA angiopoeietin-1. (**p<0.01, *p<0.05). VEGFA→ vascular endothelial growth factor A, ang-1→ angiopoietin 1.

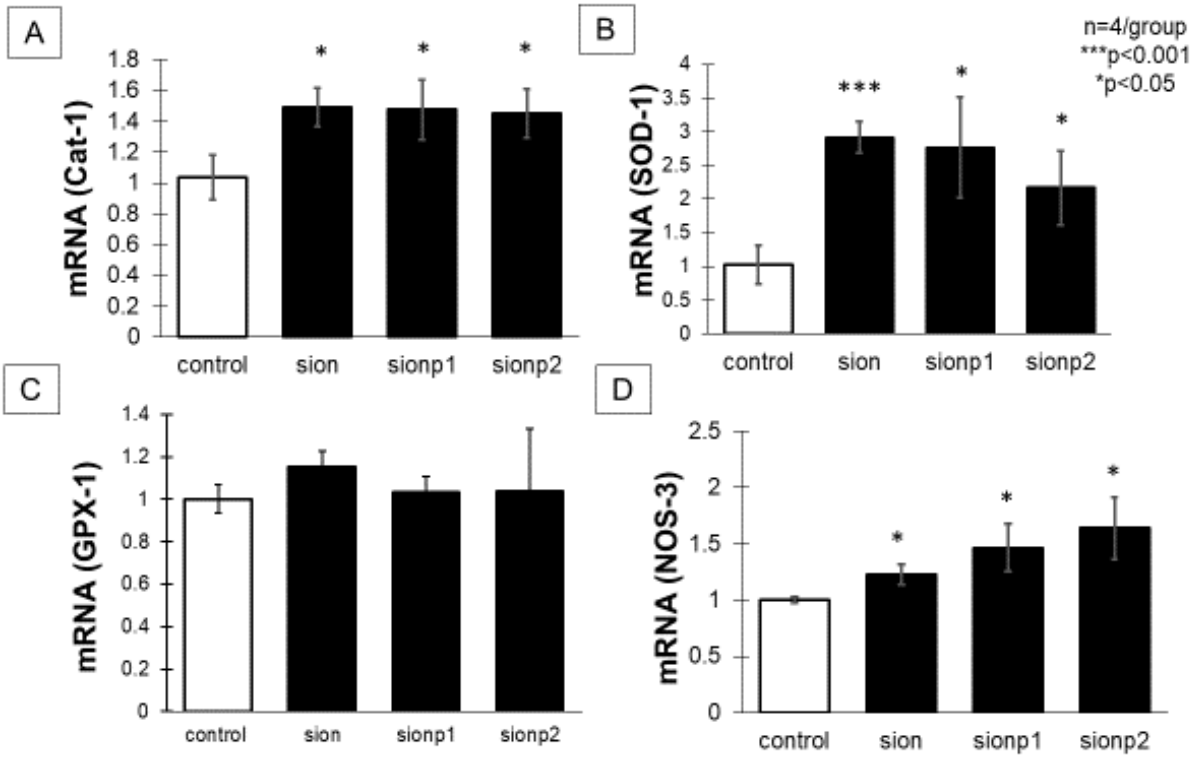

Figure 6. Bar graphs showing HUVECs gene expression of antioxidant enzymes relative to 18S as compared to control 24 hours under toxic oxidative stress (H_2O_2 0.6mM). A) mRNA Cat-1. B) mRNA SOD-1. C) mRNA GPX. D) NOS3 (***p<0.01, *p<0.05). Cat-1→ Catalase 1, SOD-1→ Superoxidase dismutase 1, GPX-1→ Glutathione peroxidase 1.

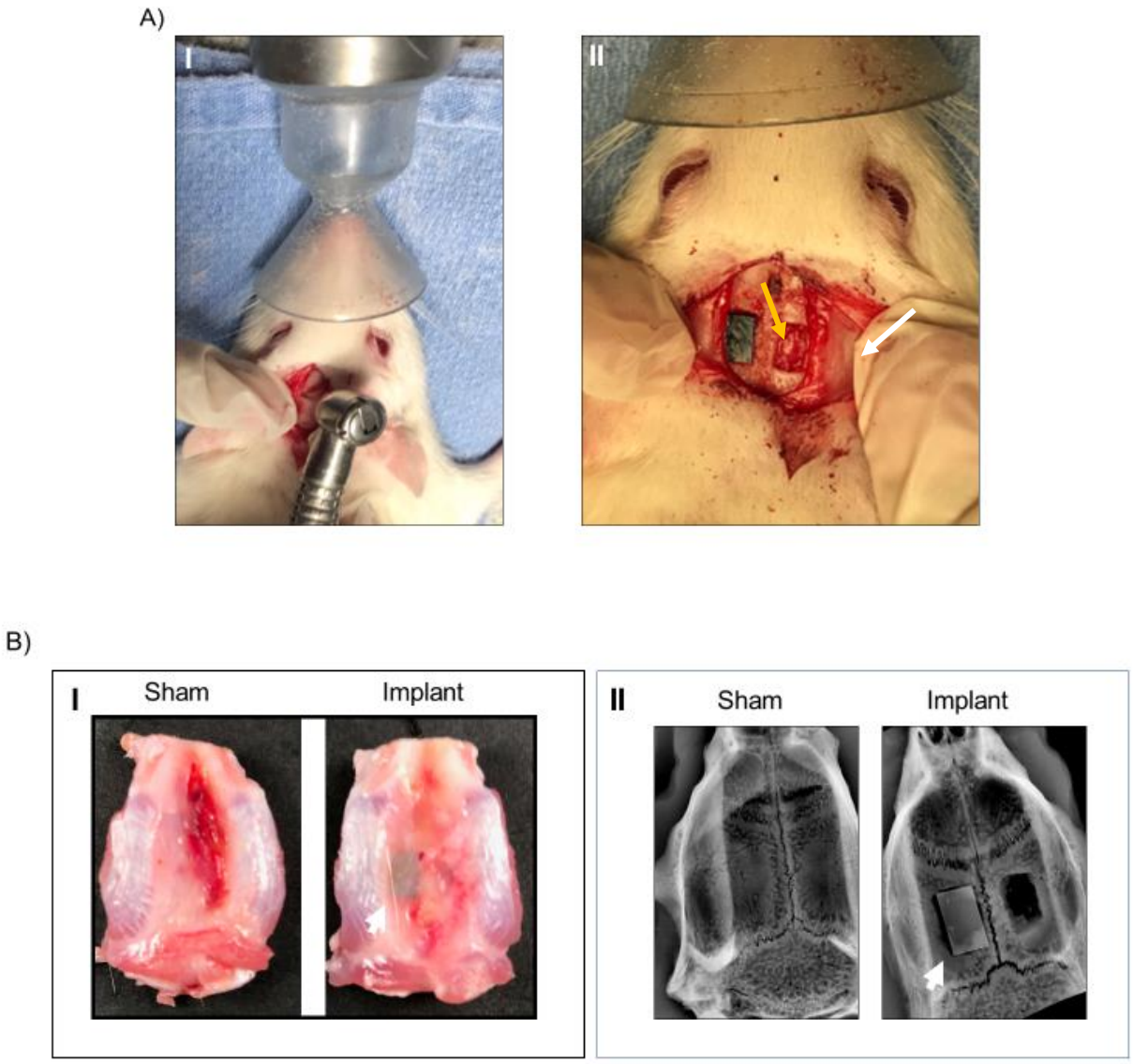

Figure 7. A) Surgical procedure for material implantation. I) Gross image of calvarial defect surgery with dental bur. II) Gross image of the parietal bone bilateral calvarial defect (6x4 mm), implant on the left (yellow arrow) and empty on the right (white arrow). B) Samples harvest from rat calvarial 15 days after surgery. I) Gross image shows the macroscopic superior view of the calvaria. II) shows an X-ray image with the sham (left) and calvarial defects and implant (right).

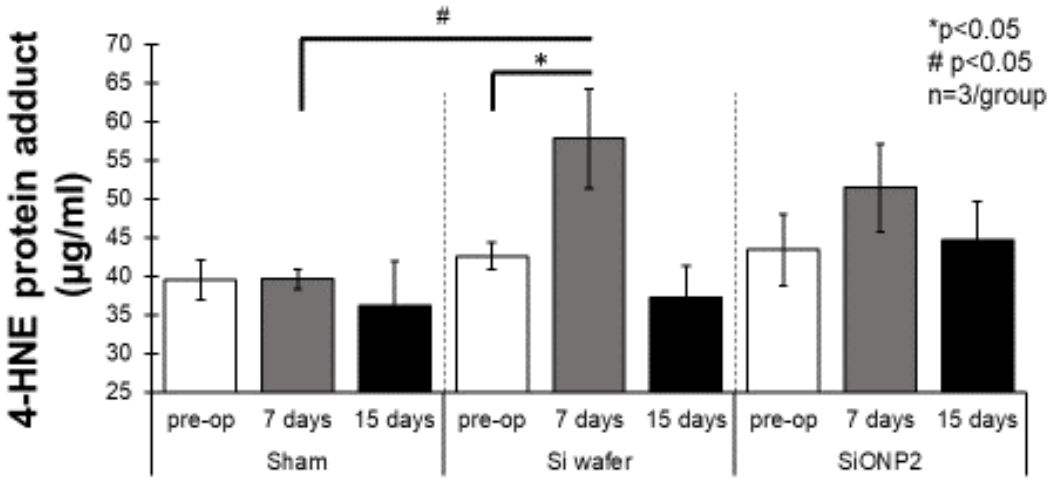

Figure 8 . Bar graph shows 4-HNE protein adduct concentration in the rat serum before surgery, 7 days after surgery and 15 days after surgery (competitive ELISA). *p<0.05 (One-way ANOVA – Tukey's pairwise within the Si wafer group), #p<0.05 (One-way ANOVA – Tukey's pairwise, same time point different groups).

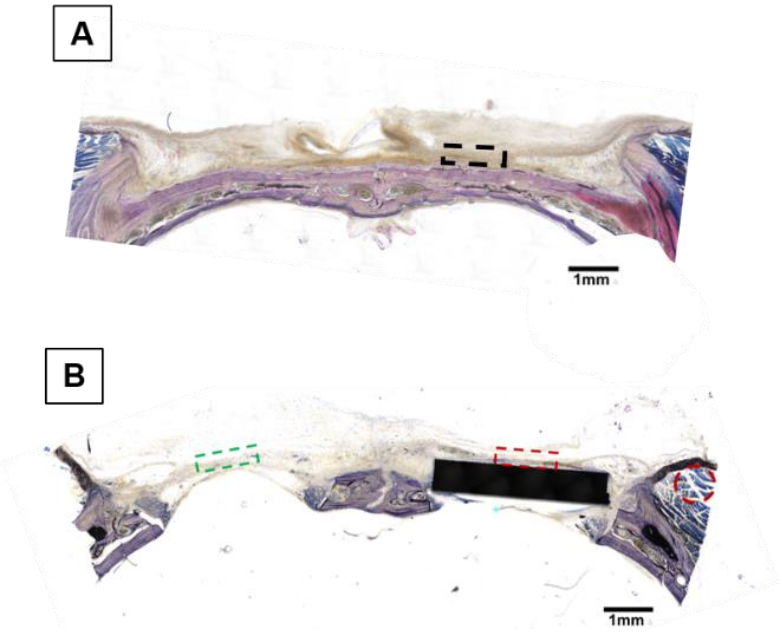

Figure 9. Bright field image acquired using the BIOQUANT OSTEOIMAGER. Coronal section of rat calvarial after Sanderson's staining representing the areas used for capturing immunofluorescent images. A) The black rectangular box is representative of a sham B) The green rectangular box indicates the location assessed for the empty critical calvarial defect, while the red rectangular box indicates the location of the assessed implant-filled critical calvarial defect. The muscle is traced with a red circle. Scale bar = 1mm.

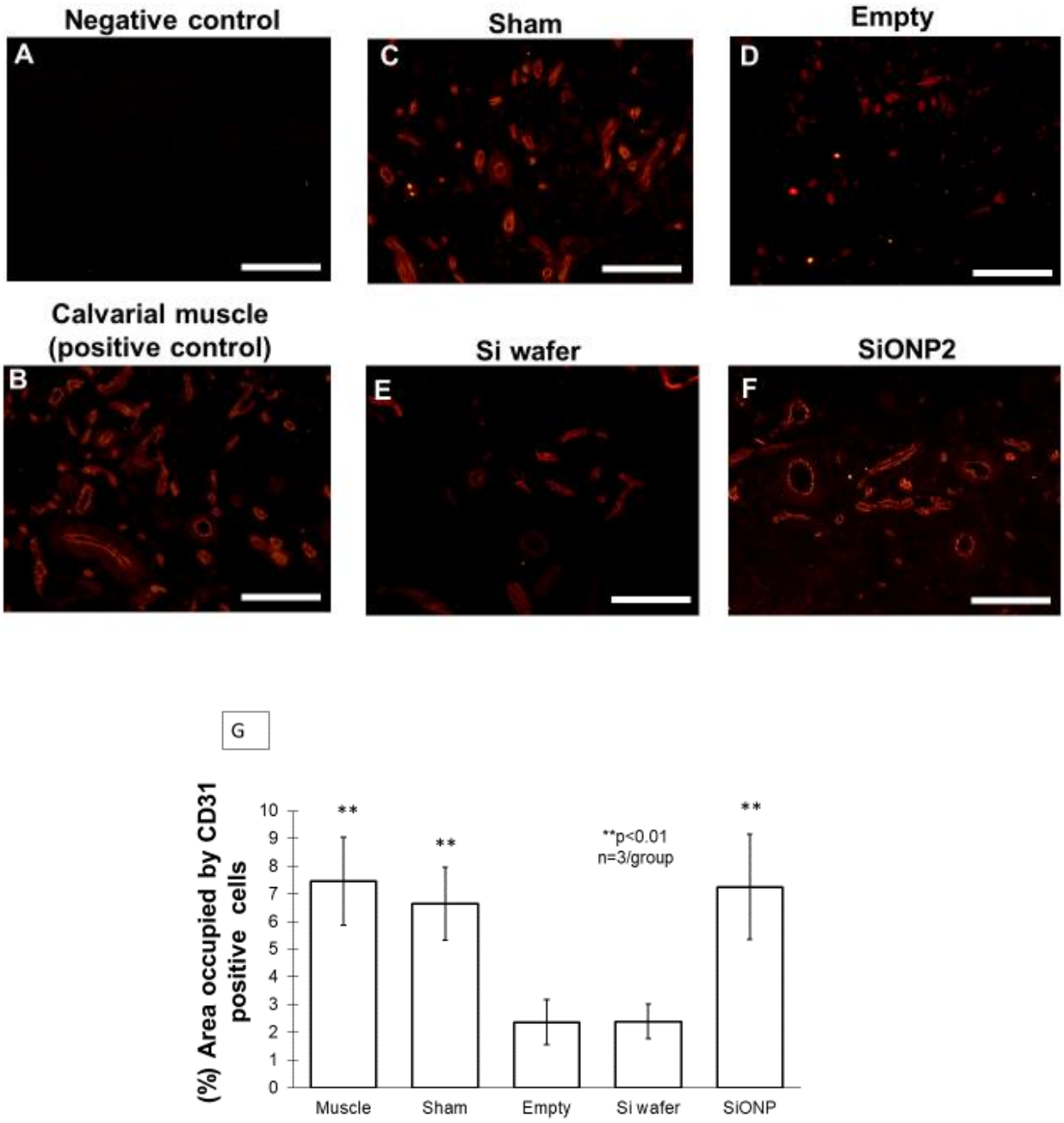

Figure 10. Immunofluorescence staining (Alexa Fluor 594 dye) for CD31 15 days after implantation. Scale bar = 100 µm. A) negative control (no secondary antibody was used on cavarial bone from sham samples. B) Calvarial muscle (positive control) C) Sham (surgical procedure, no bone defects). D) right side (empty implant). E) Si wafer. F) SiONP2. G) Bar graph shows (%) area occupied by blood vessels and capillary network relative to sham. (**p<0.01).

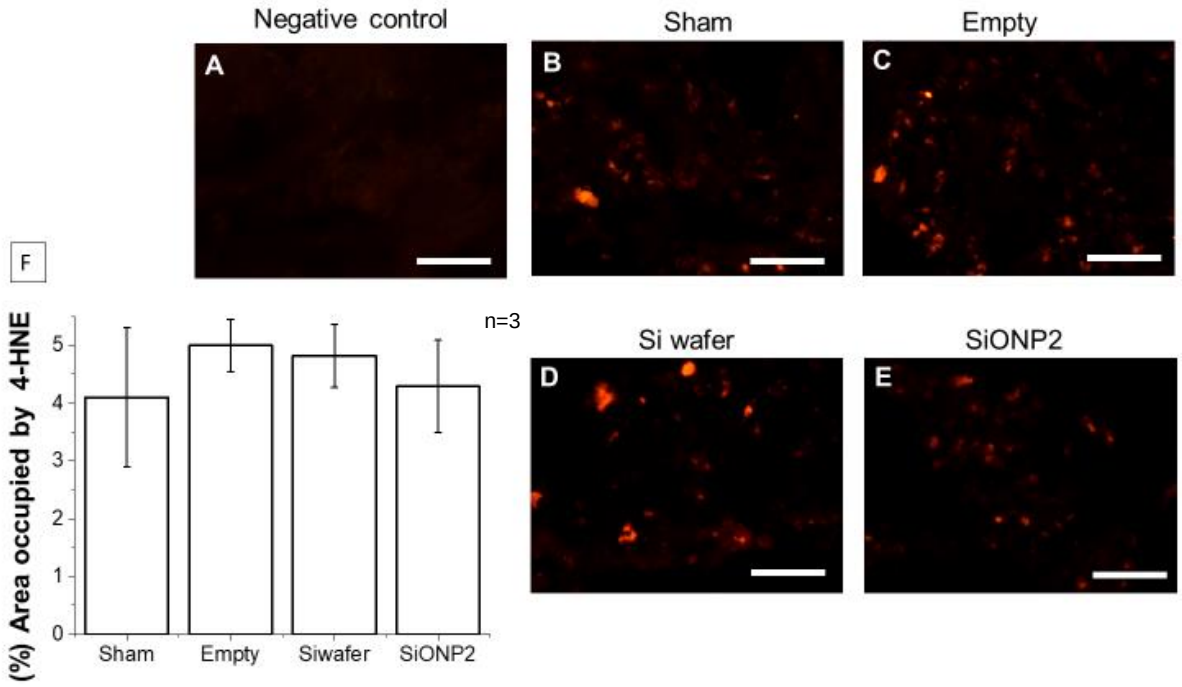

Figure 11. Immunofluorescence staining (Alexa Fluor 594 dye) for 4-HNE, 15 days after implantation. Scale bar 50 µm. A) Negative control. B) Sham. C) Empty. D) Si wafer, E) SiONP2. F) Shows bar graph with (%) of area occupied by 4-HNE. 4-HNE→ 4-Hydroxynonenal.

CHAPTER 6

CONCLUSION

Understanding and managing oxidative stress before materials implantation seems to be an appropriate strategy to reduce inflammatory response and promote implant osteointegration. In our research work we demonstrated that the Implants coated with amorphous silica by plasma enhanced chemical vapor deposition (PECVD) method, and incorporated with nitrogen and phosphorus, can reduce the oxidative stress and enhance the angiogenesis by upregulating VEGFA, angiopoietin-1, superoxidase dismutase-1 and catalase-1. Here we studied the effect of ionic silicon released from biomaterials on HUVECs under normal and oxidative stress conditions. We supported our hypothesis by performing in vitro experiments in human umbilical vein endothelial cells (HUVECs) and evaluating its angiogenic properties as follows: cells migration, proliferation, matrix deposition, capillary tubule formation, angiogenic markers, oxidative stress markers and antioxidant enzymes. In addition, a well-known animal model, rat critical size calvarial defect, was used to demonstrate the effect of implanted materials on angiogenesis and oxidative stress.

Initially, we studied the isolated effect of ionic silicon on HUVECs under normal and oxidative stress condition. We identified that the 0.5 mM silicon in endothelial cell basal medium showed the most relevant results. We observed significant enhancement in cell survival and upregulation of HIF-1a and VEGFA on cells under toxic oxidative stress induced by 0.6 mM hydrogen peroxide. These findings suggested that ionic silicon released from biomaterials can have an antioxidant effect in HUVECs.

After, we tested in an *in vitro* experiment the effect of PECVD coating amorphous silica-based materials in HUVECs angiogenesis. We evaluated three different coating compositions: SiON, SiONP1, and SiONP2, and compared them to glass cover slip and plasma treated tissue culture plate. We demonstrated that SIONP2 implants presented the most hydrophilic surface, which significantly enhanced cell attachment. Moreover, SiONP2 surfaces remarkably improved HUVECs' matrix deposition, and the ions released from SIONP2 surface significantly enhanced cell proliferation and migration. In addition, we verified enrichment in angiopoietin-1 mRNA expression, which was proved to prevent apoptosis in HUVECs. Finally, we observed upregulation of superoxidase dismutase-1 and catalase-1, which suggested that perhaps these implants can reduce oxidative stress and prevent cell apoptosis and death.

Lastly, we analyzed the effect of implants coated with amorphous silica in angiogenesis and oxidative stress *in vitro* and *in vivo*. In the *in vitro* study we observed that the coated implants can improve the matrix deposition and the capillary tubule formation in HUVECs under toxic oxidative stress. Furthermore, there was a relevant upregulation of angiopoietin-1, eNOS, Cat-1 and SOD-1. The *in vivo* study showed that the SIONP2 implants can reduce oxidative stress, demonstrated by reduction of 4-HNE systemic levels. Moreover, the SIONP2 coating enhanced angiogenesis during the first 2 weeks after being placed in a rat critical size calvarial defect.

Here we show for the first time the antioxidant effect of ionic silicon and silica based materials in endothelial cells under toxic oxidative stress. Mainly, we believe that the upregulation of angiopoitin-1, superoxidase dismutase-1 and catalase-1 are playing a major role on HUVECs survival . However, it is not completely clear how the silica based materials are acting, once multiple molecules seems to be activated and

stimulated during the process. Nuclear factor (erythroid-derived 2)-like 2 (Nfr2) is a potent latent protein that when activated upregulates genetic expression of the antioxidant enzymes. Therefore, maybe this major regulator is playing a role in the antioxidant effect of amorphous silica in the HUVECs. Another aspect that can be explored in the future is a possible neutralization effect of superoxide by the ionic silicon. Perhaps the positive charge of ionic silicon can interact with superoxide anode. Hence, the Si^{+4} could neutralize O^{-} availability, avoiding or reducing the superoxide binding with protein, DNA, and lipids, and accordingly preventing cell death.

Altogether, our findings strongly support the use of the amorphous silica based materials as an alternative to reduce inflammation, improve biocompatibility and biomaterial's osteointegration. The augmentation of these properties can reduce the incidence of implants loosening and failure, improve patient quality of life, and reduce costs. Further investigation needs to evaluate the specific effect of ionic silicon and Nfr2 activation pathway and the direct effect and a possible interaction between the ionic silicon and the superoxide predominant in oxidative stress environment.

BIOGRAPHICAL INFORMATION

Felipe Alves do Monte graduated from medical school (Faculdade de Medicina de Pernambuco, Recife-PE, Brazil) in 1999. He made residence in Orthopedics surgery in Hospital Ipiranga, Sao Paulo-SP, Brazil (2000-2002). After residence he made 1 year fellowship in orthopedic pediatric surgery in Escola Paulista de Medicina, Sao Paulo-SP, Brazil (2003). He acquired his master's degree in Health Science from Universidade de Pernanbuco in 2012. He started his PhD course at the University of Texas at Arlington in 2014 under the supervision of Dr. Pranesh Aswath. His current research focus is in biomaterials used for bone tissue engineering. He is studying the effect of silica based and infiltrated biomaterials in angiogenesis and its relationship with oxidative stress environments. He is presenting his defense in December 2017.